1979

Optimal integration of Omega and local timing signals

Kim Strohbehn
Iowa State University

7924273

STROHBEHN, KIM
OPTIMAL INTEGRATION OF OMEGA AND LOCAL TIMING SIGNALS.

IOWA STATE UNIVERSITY, PH.D., 1979

University Microfilms International 300 N. ZEEB ROAD, ANN ARBOR, MI 48106

Optimal integration of Omega

and local timing signals

by

Kim Strohbehn

A Dissertation Submitted to the

Graduate Faculty in Partial Fulfillment of

The Requirements for the Degree of

DOCTOR OF PHILOSOPHY

Major: Electrical Engineering

Approved:

Signature was redacted for privacy.

In Charge of Major Work

Signature was redacted for privacy.

For the Major Department

Signature was redacted for privacy.

For the Graduate College

Iowa State University
Ames, Iowa

1979

TABLE OF CONTENTS

INTRODUCTION

A precise timing scheme

Consider the precise timing scheme shown in Figure 1. A local timing signal is available, but time as given by this signal contains errors. An independent timing signal is also available, and time as generated by it also contains errors; however, these errors are independent of the errors due to the local signal. By combining these two independent signals, it should be possible to obtain an improved timing signal.

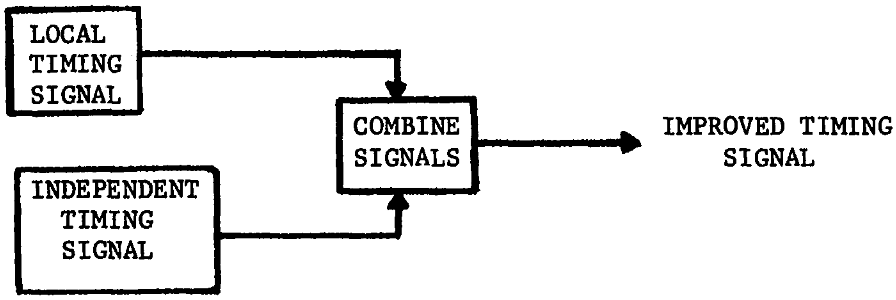

Figure 1. A precise timing scheme

In the case considered in this work, time as generated by a high quality quartz oscillator is updated using a composite timing signal derived from Omega navigation system broadcasts. Before discussing the manner in which the two timing signals are combined, i.e., the manner in which the updating is done, a more detailed discussion of the two timing signals is in order.

<u>The composite Omega signal</u>

The Omega navigation system consists of several broadcasting stations located throughout the world. Each station transmits three very low frequency (VLF) signals. These signals are each phase-locked to a cesium beam reference which is, in turn, aligned with the cesium beam references at the United States Naval Observatory (USNO). Since these signals are available throughout the world due to the long-range propagation characteristics of VLF, and since they are aligned with the references at the USNO, the Omega navigation system is attractive for purposes of precise time dissemination. Indeed, the Omega system has been used in several such applications (1, 2, 3).

The motivation for using a composite Omega signal derived from all three frequencies of an Omega station's signals rather than a single frequency signal will be evident after examining the propagation characteristics of VLF signals.

At very low frequencies the earth and the ionosphere act as a concentric spherical-shell waveguide. This makes possible world wide coverage of the Omega broadcasts with just eight transmitters judiciously placed throughout the world. See Figure 2.

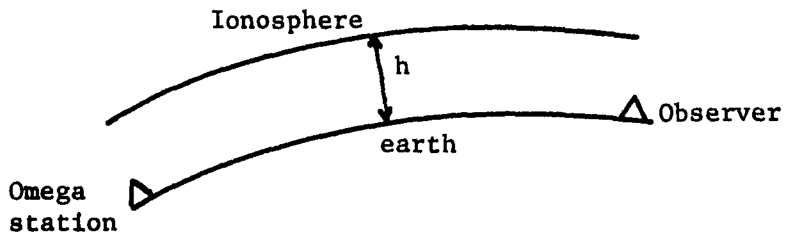

Figure 2. Earth-ionosphere waveguide

The phase velocity of VLF radio waves propagating in this waveguide is a function of many parameters. Among the most important are the effective height of the ionosphere, the orientation of the propagation path with respect to the earth's magnetic field, and the ground conductivity. If any of these parameters vary with time, then the phase velocity of the signal will vary about its nominal value. This will obviously give rise to errors if the phase of the signal is used for timing.

The most troublesome of the time-varying parameters is the effective height of the ionosphere. This parameter is a function of the position of the sun, or time of day, as well as of solar activity. During the day the effective height is approximately 70 km, and during the night it is approximately 90 km. This effect gives rise to relatively large periodic changes in the phase velocity of waves propagating in the earth-ionosphere waveguide. This is known as the diurnal shift in the phase velocity. The period of the diurnal shift is 24 hours.

A typical plot of phase delay, which is inversely proportional to phase velocity, for a typical propagation path is given in Figure 4 (4). The propagation path is from Trinidad to North Dakota. This plot is of 21 days of superimposed data (10-31 March, 1975). It is clear that any kind of filtering operation to reduce this large variation in phase delay will be difficult because of the long period and large amplitude of the variations.

Many on-line methods of mitigating the diurnal shift effect have been devised. Almost all of them involve the calculation of an artificial group delay from the measured phase delays at two or three of the broadcast Omega frequencies (5,6,7,8,9). Therefore, a brief discussion of the group-delay characteristics of Omega signals is in order at this point.

The group velocity v_g is defined as

$$v_g = \frac{d\omega}{d\beta}$$

where phase shift as a function of angular frequency ω is given by

$$\phi(\omega) = \beta(\omega)d$$

and d is the distance of propagation. Then group delay is given by

$$T_g = \frac{d}{v_g} .$$

Physically, group velocity is the velocity with which the signal energy or information propagates, as compared to phase velocity, the velocity of the constant phase fronts (10).

For certain simplifying assumptions the theoretical group velocity characteristics of the earth-ionosphere waveguide have been calculated by Hampton and Watt (11,12). These are displayed in Figure 3 as plots of v_g, the group velocity, versus ω, the angular frequency, and the effective height of the ionosphere.

It is apparent from Figure 3 that at a frequency between 11.5 and 12.5 kHz the group velocity is nearly invariant between day (70 km) and night (90 km). Thus, if one were able to calculate a group velocity referred to a frequency between 11.5 and 12.5 kHz, then the diurnal shift in the group velocity should be small.

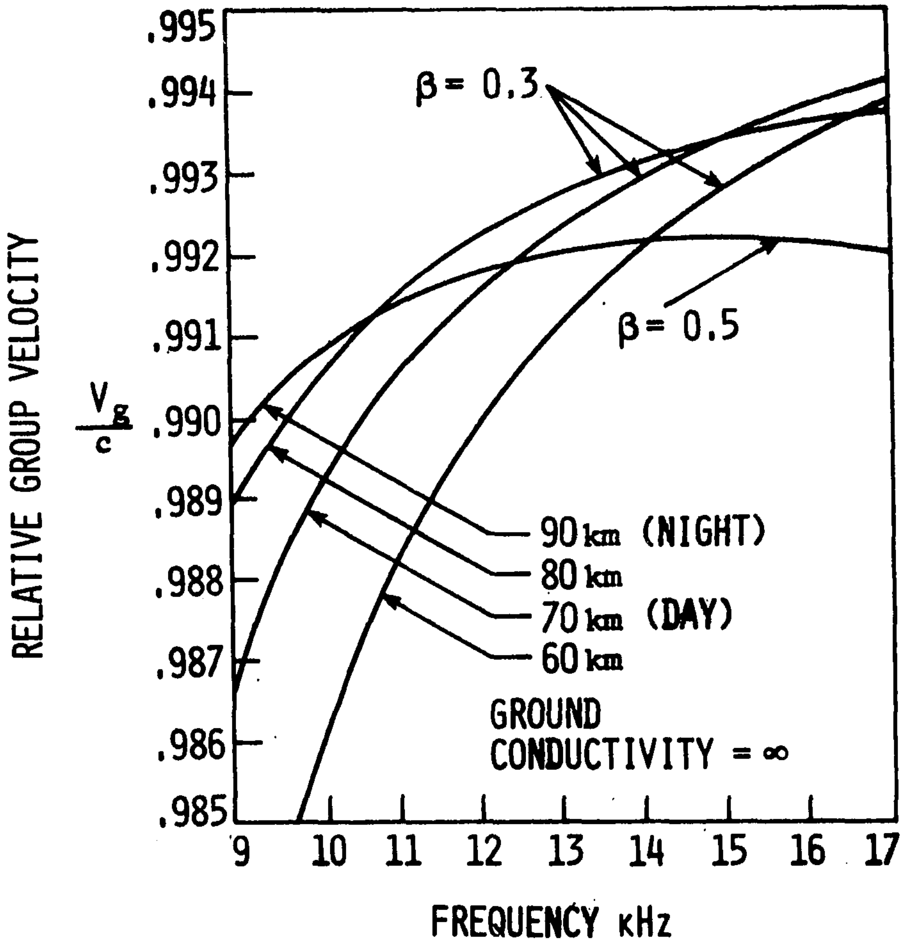

Figure 3. Group velocity versus frequency (11)

A method for calculating an artificial group delay referred to any frequency has been developed by Brown and Van Allen (9). The calculated group delay is a linear combination of the three measured Omega phase delays. This is the composite timing signal referred to previously.

The calculation of this composite signal is described in Appendix A. The composite signals corresponding to the plots in Figure 4 are shown in Figure 5 (4). Note that again 21 days of signals are superimposed. The

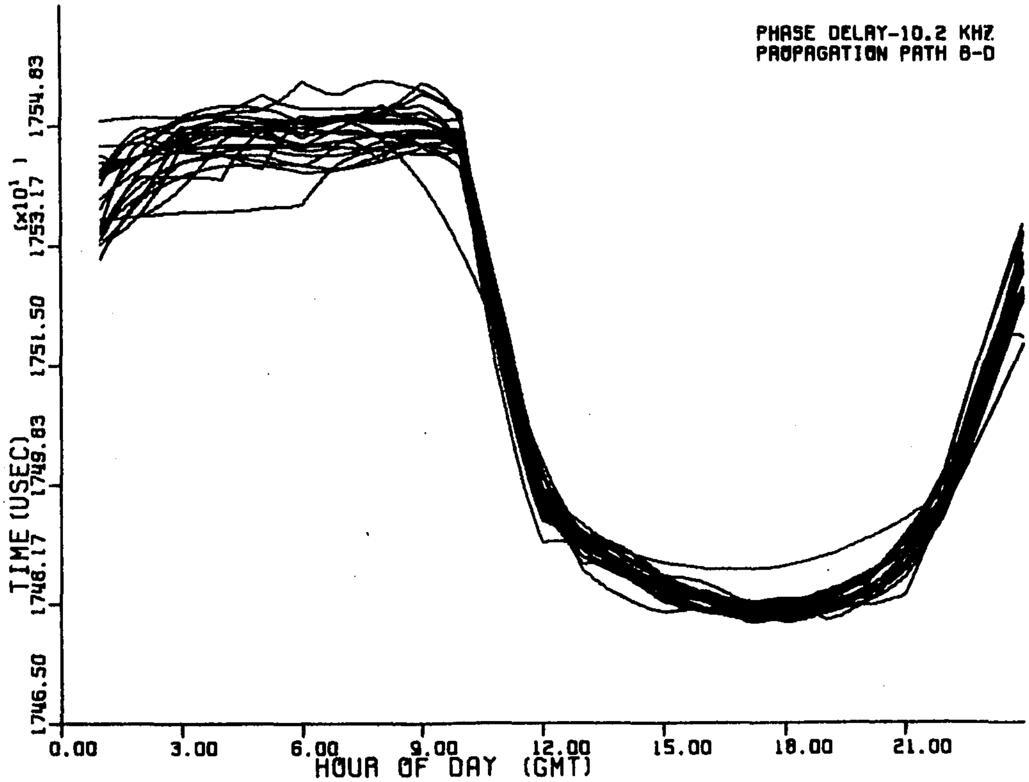

Figure 4. Phase delay at 10.2 kHz for the path Trinidad to N. Dakota (4)

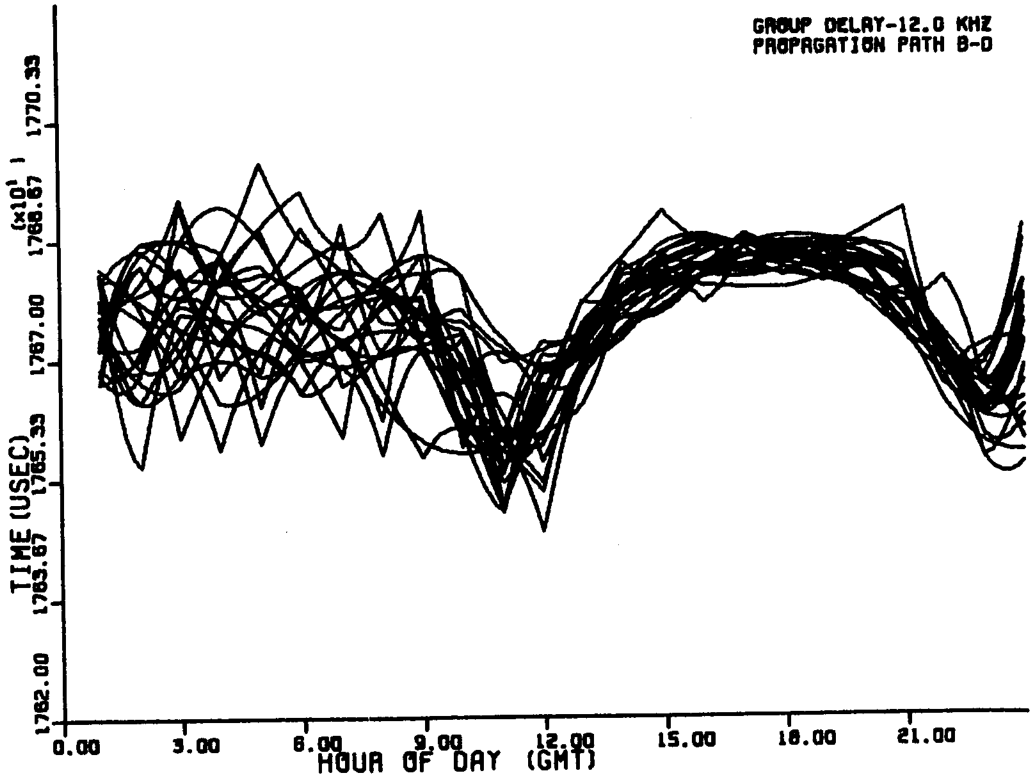

Figure 5. Omega group delay referred to 12.0 kHz corresponding to Figure 4 (4)

reference frequency in this case is 12.0 kHz. Note that the diurnal shift has almost completely been replaced by more "rapid" variations with smaller amplitude. These "high frequency" variations are much easier to filter than the 24 hour errors, so this is the motivation for considering the composite signal. Next, the local timing signal is discussed.

The local signal

The local timing signal is assumed to be the output of a high quality quartz oscillator. Let this signal be

$$w(t) = A(t)\sin(\omega_o t + \phi_n(t))$$

where ω_o is the nominal angular frequency and $\phi_n(t)$ is a perturbing phase noise term due to frequency drift and so forth. If no nonlinearities are present, $A(t)$ is of no consequence for timing purposes, and the time error of this signal is represented by

$$\frac{\phi_n(t)}{\omega_o} .$$

Let this time error be given by

$$y(t) = \frac{\phi_n(t)}{\omega_o} .$$

The characteristics of $y(t)$ have been well-documented in the literature on the stability of frequency standards (13-23).

Essentially, $y(t)$ varies quite slowly in comparison to the variations in the Omega composite timing signal. The characteristics of $y(t)$ will be discussed in more detail in a later section on the modeling of this process. Figures 6, 7, 8, 9, 10 are sample plots of y(t) for the high quality quartz oscillator which supplied the data for this investigation. The wide lines will be discussed in the section on modeling the local timing signal. The thin lines represent y(t). These figures can be compared with Figure 5. If this is done, it is quite clear that y(t) does indeed vary much more slowly than do the variations in the Omega composite timing signal.

Now that the timing signals have been discussed, it is appropriate to discuss how they may be combined to form an improved timing signal.

Integration of the timing signals

First some notation is given. Let the Omega navigation signals be given by

$$w_1(t) = a_1(t)\sin(\omega_1 t - \beta_1 d + \phi_1(t)),$$
$$w_2(t) = a_2(t)\sin(\omega_2 t - \beta_2 d + \phi_2(t)),$$
$$w_3(t) = a_3(t)\sin(\omega_3 t - \beta_3 d + \phi_3(t)),$$

where

$$\omega_1 = 2\pi(10.2) \text{ krad/sec},$$
$$\omega_2 = 2\pi(11\ 1/3) \text{ krad/sec},$$
$$\omega_3 = 2\pi(13.6) \text{ krad/sec}$$

are the known nominal Omega broadcast frequencies, and $\beta_1 d$, $\beta_2 d$, and $\beta_3 d$ are the known nominal phase delays for a particular path, and ϕ_1, ϕ_2, and ϕ_3 are the phase delay variations for each respective signal.

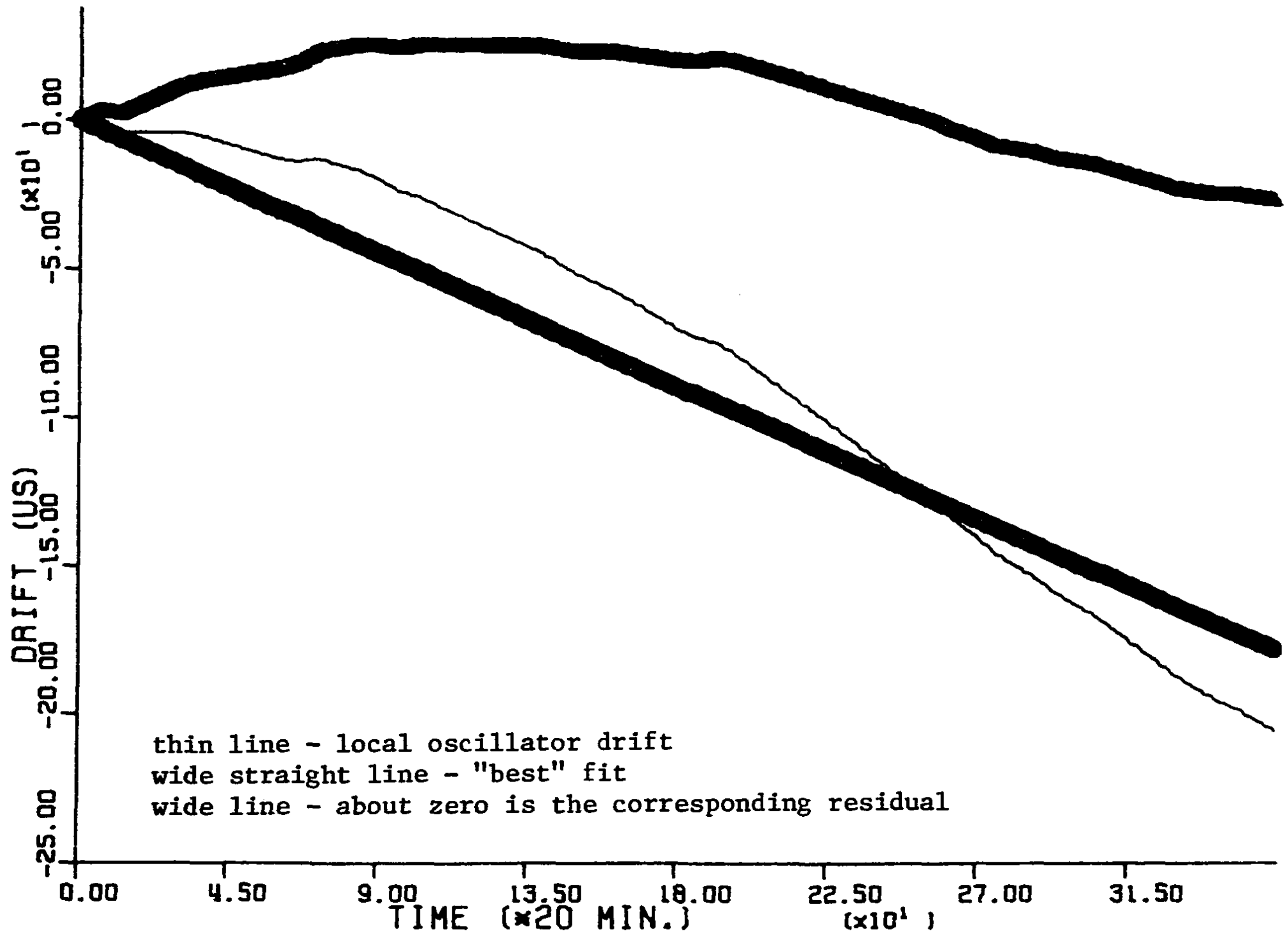

Figure 6. Local oscillator drift

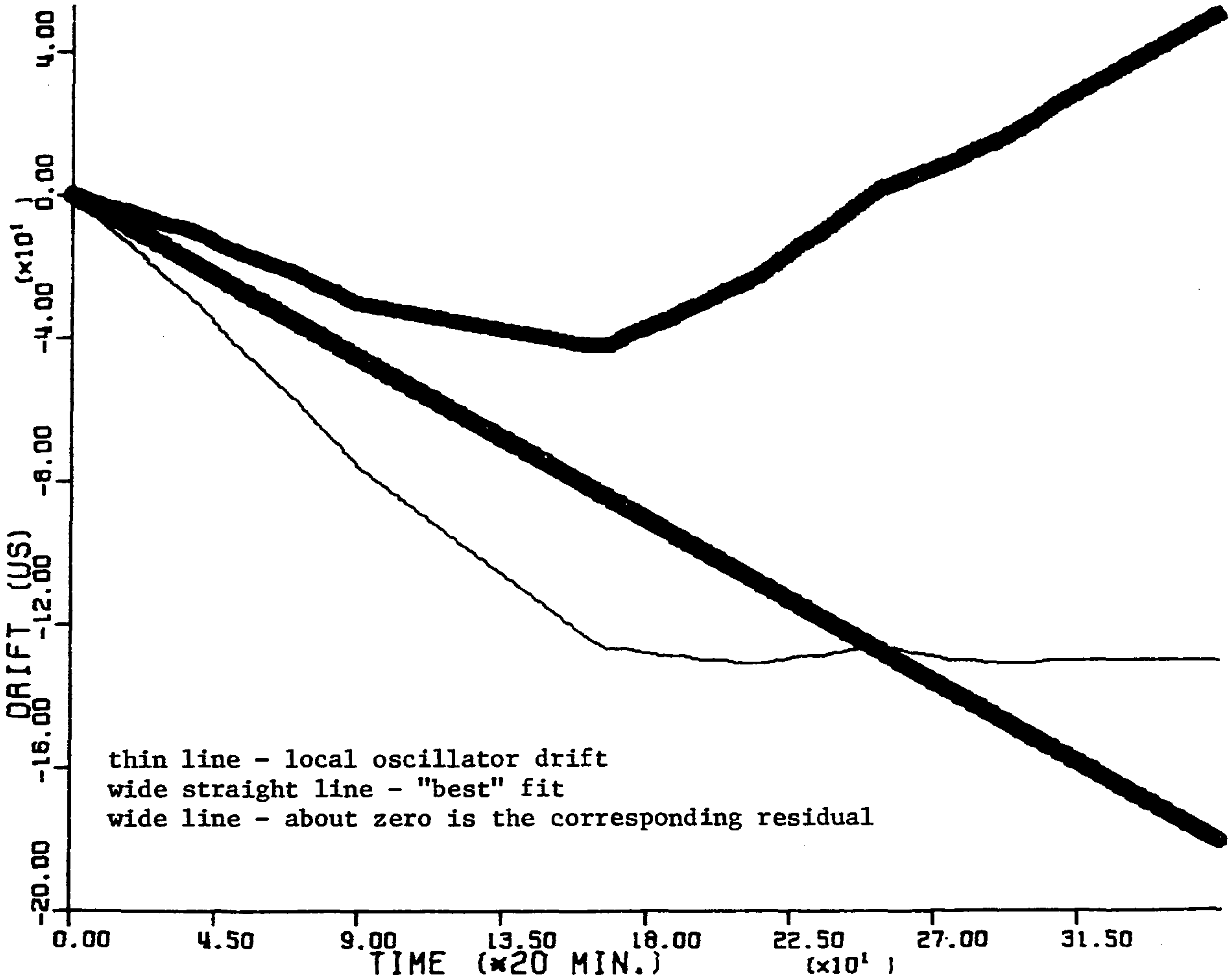

Figure 7. Local oscillator drift

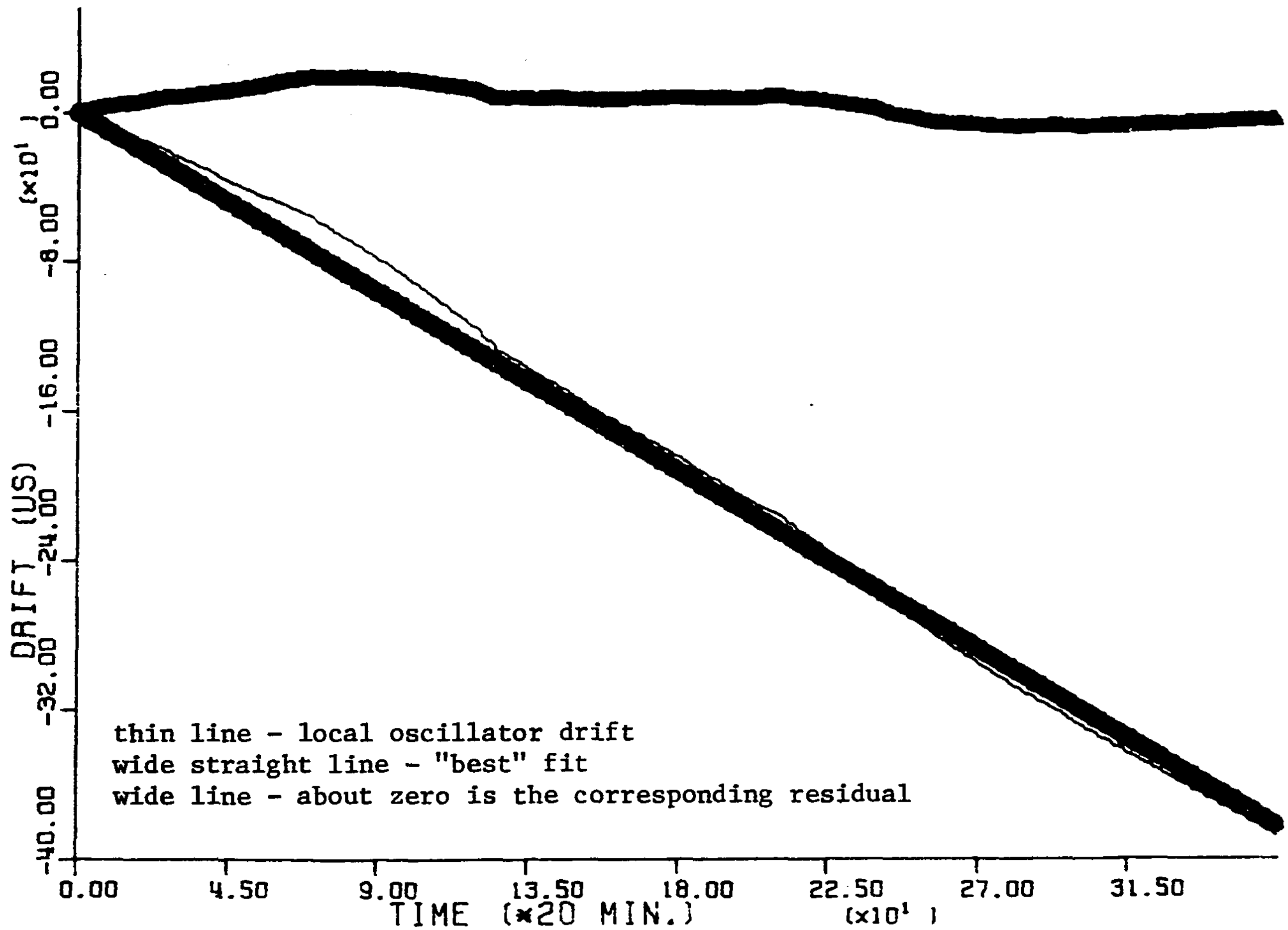

Figure 8. Local oscillator drift

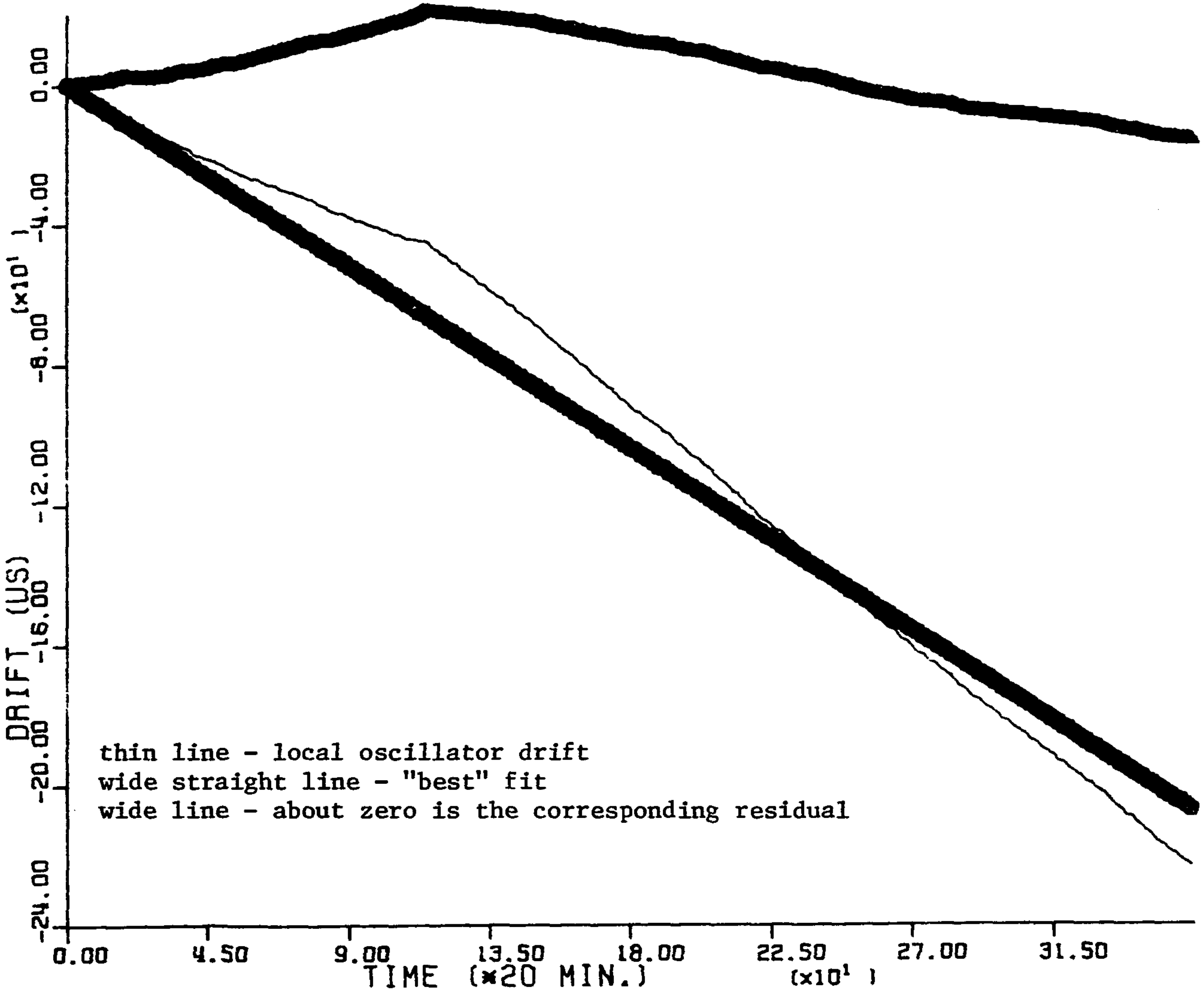

Figure 9. Local oscillator drift

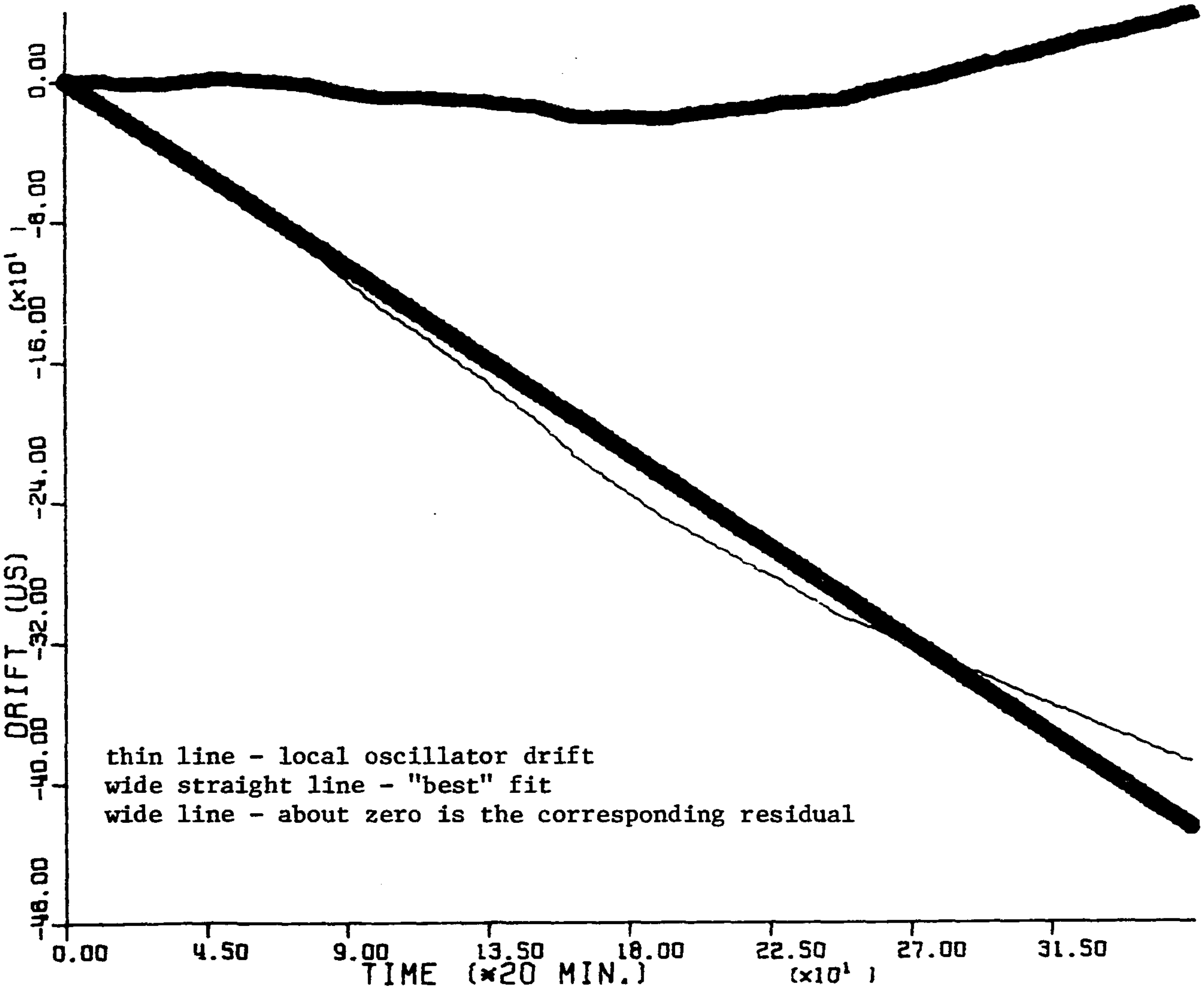

Figure 10. Local oscillator drift

As before, let the local oscillator output be

$$w(t) = A(t)\sin(\omega_o t + \phi_n(t)).$$

Signals of the appropriate frequencies can be derived from this signal. The phases of the derived signals can be compared with the phases of the corresponding Omega signals to yield the phase delays m_1, m_2, and m_3 which are given by (letting $\omega_0 = \omega_1$)

$$m_1 = \phi_1 - \phi_n,$$
$$m_2 = \phi_2 - (\omega_2/\omega_1)\phi_n,$$
$$m_3 = \phi_3 - (\omega_3/\omega_1)\phi_n.$$

From Appendix A the calculated group delay variation is

$$\delta T_g = c_1(\phi_1/\omega_1) + c_2(\phi_2/\omega_2) + c_3(\phi_3/\omega_3)$$

where c_1, c_2, and c_3 are given in Appendix A, and

$$c_1 + c_2 + c_3 = 1.$$

Form m_1/ω_1, m_2/ω_2, and m_3/ω_3 and obtain

$$m_1/\omega_1 = (\phi_1/\omega_1) - (\phi_n/\omega_1),$$
$$m_2/\omega_2 = (\phi_2/\omega_2) - (\phi_n/\omega_1),$$
$$m_3/\omega_3 = (\phi_3/\omega_3) - (\phi_n/\omega_1),$$

so that

$$c_1(m_1/\omega_1) + c_2(m_2/\omega_2) + c_3(m_3/\omega_3) = \delta T_g - y(t).$$

Hence, at the receiver the difference $\delta T_g - y(t)$ (or $y(t) - \delta T_g$) is available.

Now recall that the absolute phase of a signal divided by its angular frequency has dimensions of time. Call the true time s. The composite timing signal is then

$$s + \delta T_g,$$

and the local timing signal is

$$s + y(t).$$

Relabel δT_g and $y(t)$ as

$$y(t) = n_1(t),$$

$$\delta T_g(t) = n_2(t).$$

Then the local timing signal is

$$s + n_1,$$

and the Omega composite timing signal is

$$s + n_2.$$

It has been shown by Brown, Van Allen and Strohbehn and Brown and Nilsson (4, 24) that the problem of the optimum (in the least mean square error sense) means of integration, or combination, of these two timing signals can be considered as a complementary filter problem. To see this consider Figure 11 which shows three mathematically equivalent implementations of a complementary filter. Consider part (a) of Figure 11. Recall that n_1 varies slowly compared to n_2. Heuristically then, it appears that choosing $1-Y(s)$ as a high pass filter, which implies that $Y(s)$ is low pass, would mitigate the effects of n_1 and n_2. Observe that since the two filters are complementary, the desired signal s is undistorted. This is a desirable property for situations where s is not random in character.

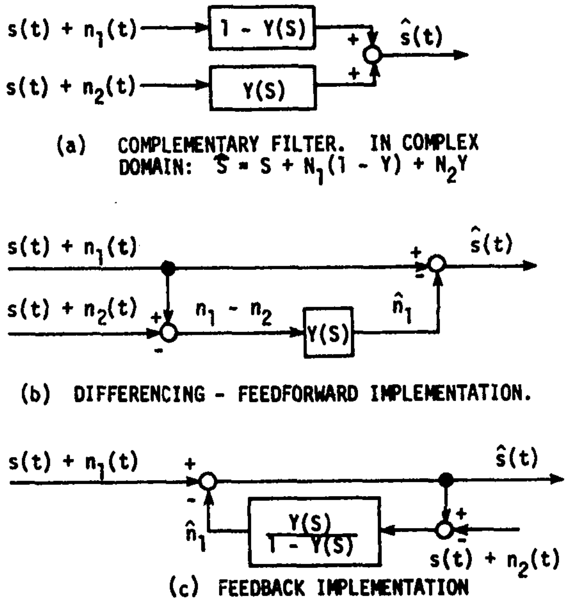

Figure 11. Three equivalent implementations of a complementary filter

Note that $s + n_1$ is not available directly at the receiver, but that n_1-n_2 is available in addition to $s + n_1$. This means that, practically, implementation (b) or (c) of Figure 11 would have to be used. Implementation (b) is convenient for off-line analysis purposes and was used in this work. Implementation (c) would probably be best for an on-line application. This point is discussed by Strohbehn and Brown (25a).

Consider implementation (b) of Figure 11. What is desired is to estimate $n_1(t)$ given the measurement $n_1(t)$-$n_2(t)$. The optimum linear estimator in the minimum-mean-square-error sense is a Kalman filter.

Thus, optimal integration of the timing signals can be accomplished by implementing an appropriate Kalman filter in the complementary filter implementation shown in Figure 11(b). The setting for this investigation has now been described so the objectives of this work will now be stated.

Objectives

In order to implement a Kalman filter the stochastic processes involved, in this case $n_1(t)$ and $n_2(t)$, must be modeled in state-space form. Therefore, one objective of this research was to obtain valid state-space models for both the local timing error process $n_1(t)$ and the Omega composite timing error process $n_2(t)$. An additional objective was to assess the applicability of the precise timing scheme discussed previously, i.e., the complementary Kalman filter using the models developed for $n_1(t)$ and $n_2(t)$.

MODELS FOR THE COMPOSITE OMEGA SIGNAL

Description of data

Stripcharts of Omega data for all three frequencies, 10.2, 11 1/3, and 13.6 kHz for five different propagation paths for the days 1 March, 1975 through 31 March, 1975 were available to the author. They were obtained by Dr. R. L. Van Allen and were used in his work (25b). These data were in the form of phase differences between a cesium reference at the appropriate frequency and the Omega signal. The method of obtaining the absolute phase delay is described in Appendix B.

Five data sets were compiled. Each set consists of phase data for all three frequencies sampled once every 20 minutes. This sampling time is clearly very small compared to the variations of interest. Occasionally, bad data due to equipment malfunction were encountered. In these cases interpolated (not linear) data were substituted. The interpolation was done by observing data on previous or preceding days and essentially "matching endpoints" to produce a short interpolated span of data. The longest stretch of bad data encountered was 3 hours in length.

The first data set consists of 20 days of data, 1 March, 1975 through 20 March, 1975, for the path from Hawaii to North Dakota. The second set consists of 5 days of data, 3 March, 1975, through 7 March, 1975, for the path from Trinidad to North Dakota. The third set consists of 5 days of data, 6 March, 1975, through 10 March, 1975, for the path from Norway to North Dakota. The fourth set consists of 5 days of data, 10 March, 1975, through 14 March 1975, for the path from North Dakota to Hawaii. The fifth and final set consists of 5 days of data, 16 March, 1975, through 20 March, 1975, for the path from Japan to Hawaii.

For each set of data the corresponding group delay signal, i.e., composite timing signal, was calculated for a reference frequency of 12.47 kHz. See Appendix A. The arithmetic mean was then subtracted to simulate $n_2(t)$. Two typical samples of $n_2(t)$ are shown in Figures 12 and 13. Figure 12 shows $n_2(t)$ for the path North Dakota to Hawaii. Figure 13 shows $n_2(t)$ for the path Trinidad to North Dakota.

<u>The form of the models</u>

Estimates of the time autocovariance functions for the 5 sets of data were computed using the estimator (26)

$$\hat{R}(nT) = \frac{1}{N-n} \sum_{i=0}^{N-n-1} x_i x_{i+n}$$

where N is the number of data points, T is the sampling interval, $\{x_i\}_{i=0}^{N-1}$ is the time series for which the estimate of the autocovariance function is desired, in this case $n_2(iT)$, and $\hat{R}(nT)$ is the estimate of the autocovariance function at nT. These estimates are shown in Figures 14, 15, 16, 17, and 18. Figure 14 is for the path Hawaii to North Dakota, Figure 15 is for the path Trinidad to North Dakota, Figure 16 is for the path Norway to North Dakota, Figure 17 is for the path North Dakota to Hawaii, and Figure 18 is for the path Japan to Hawaii.

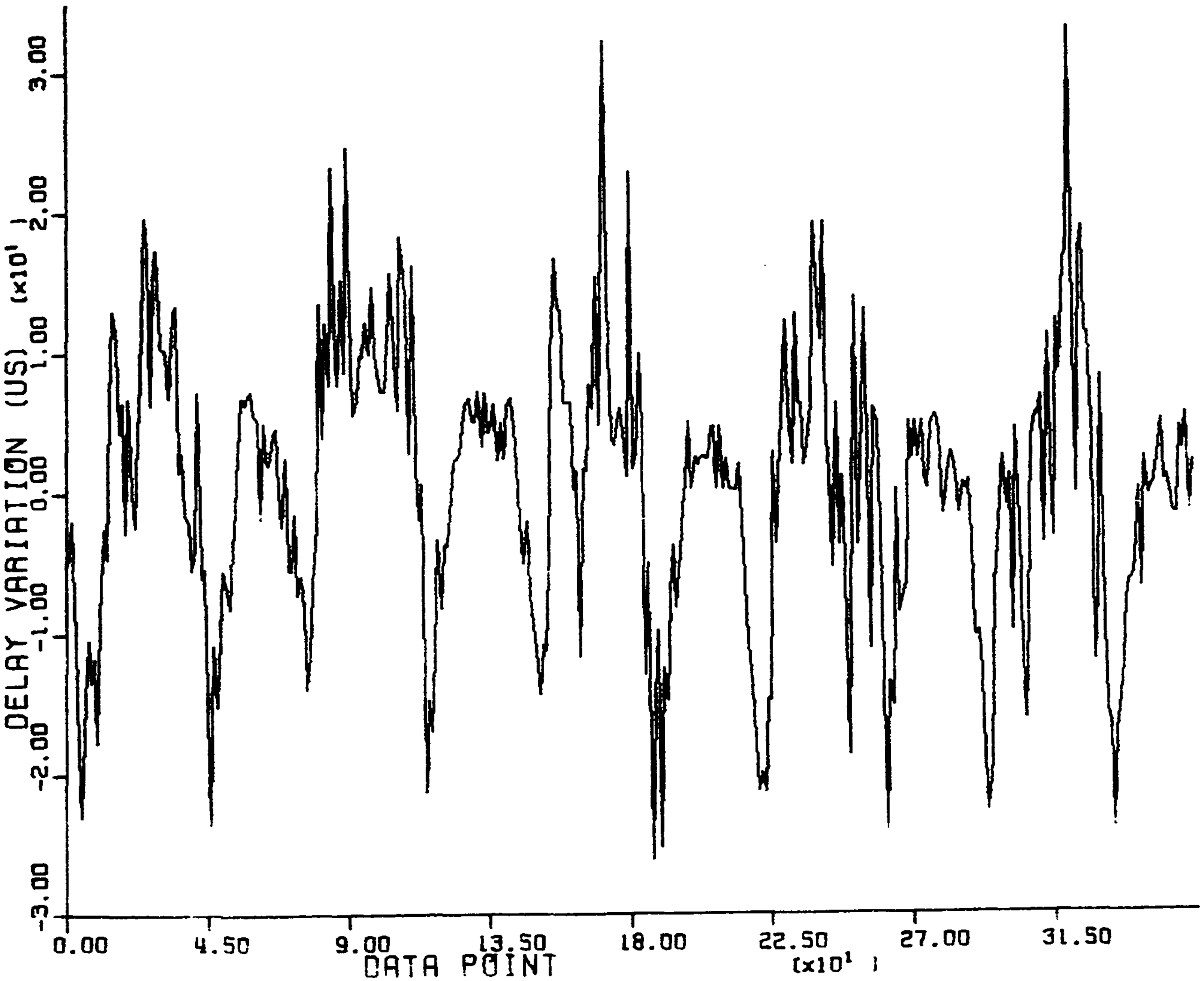

Figure 12. Omega composite timing error for the path N. Dakota to Hawaii

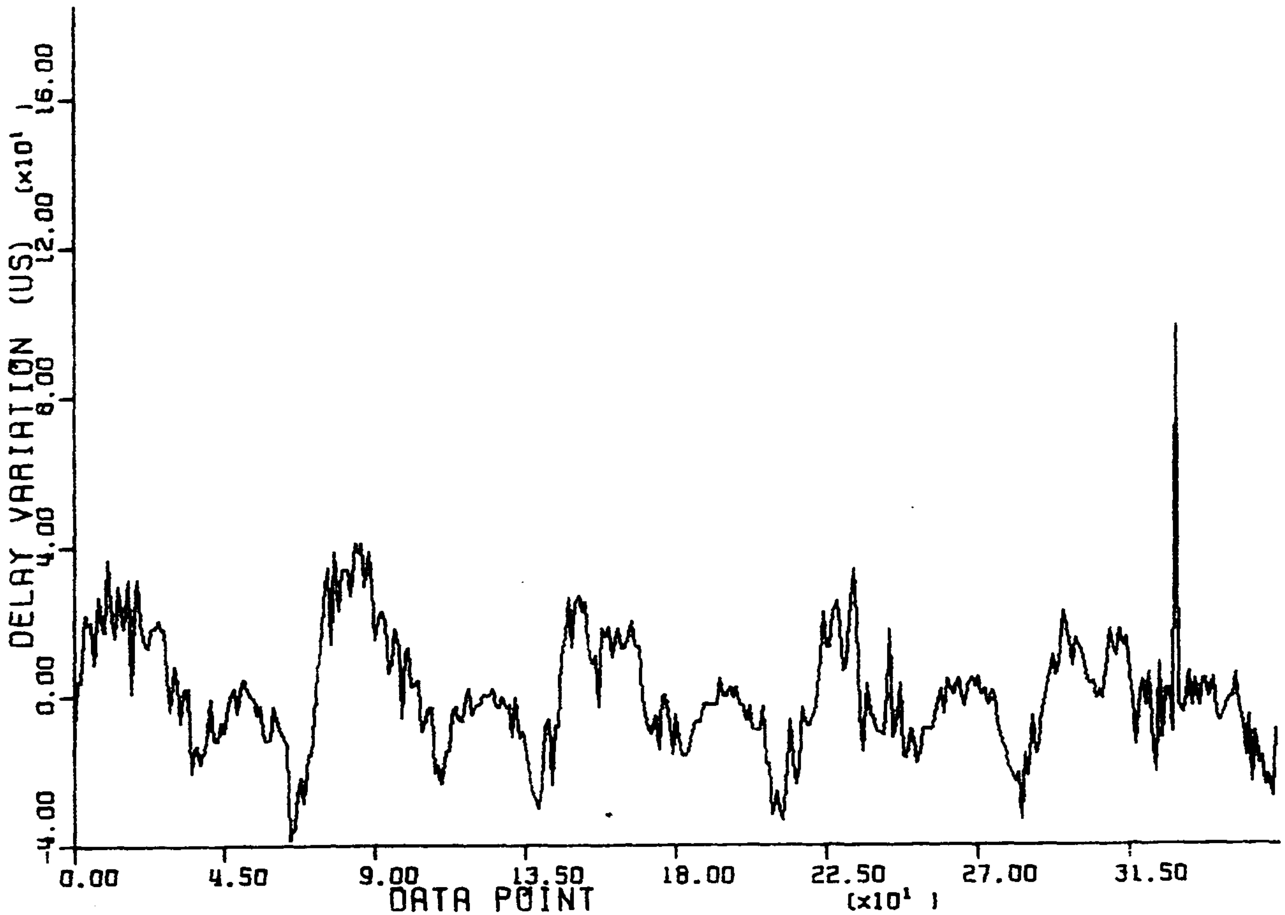

Figure 13. Omega composite timing error for the path Trinidad to N. Dakota

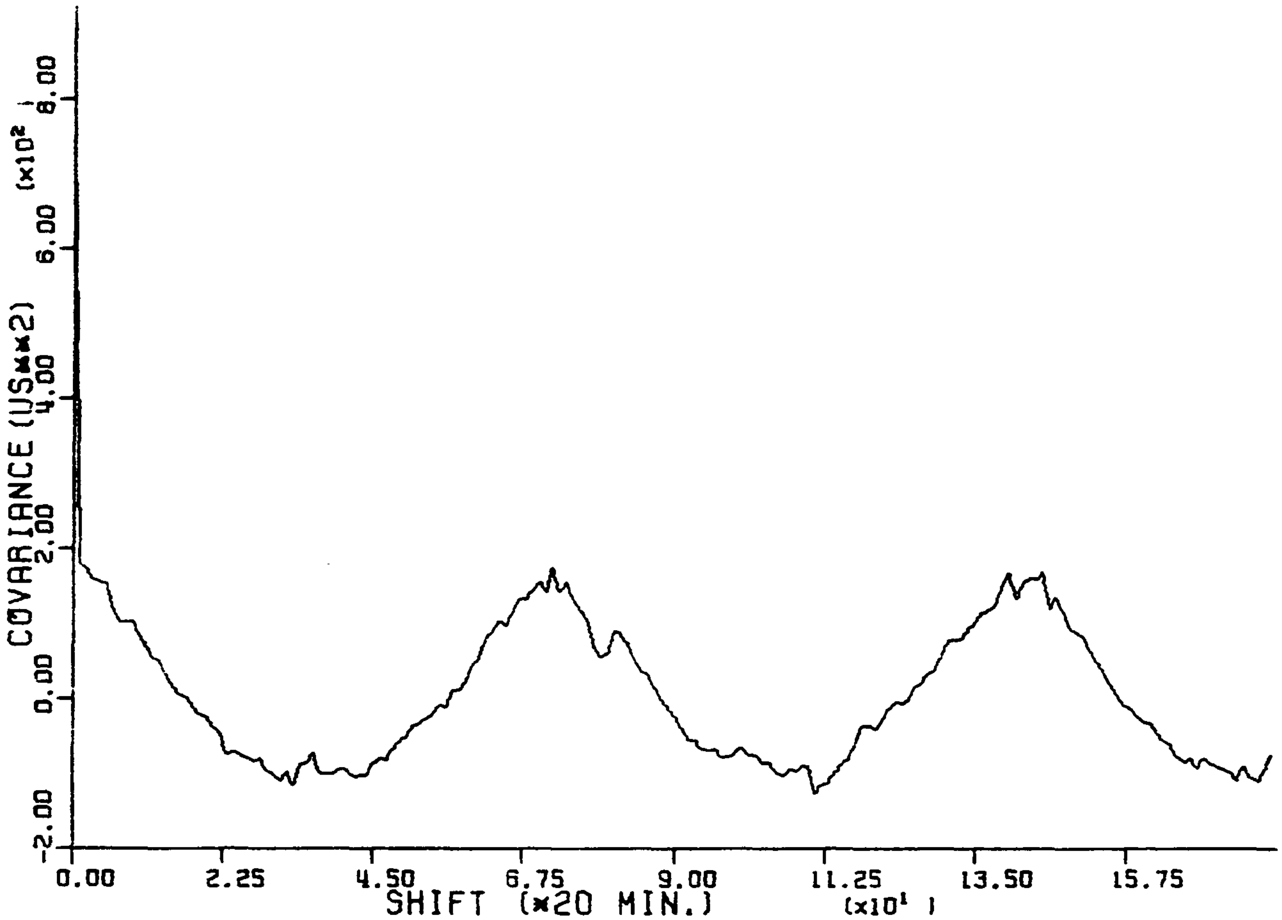

Figure 14. Autocovariance estimate for the path Hawaii to N. Dakota

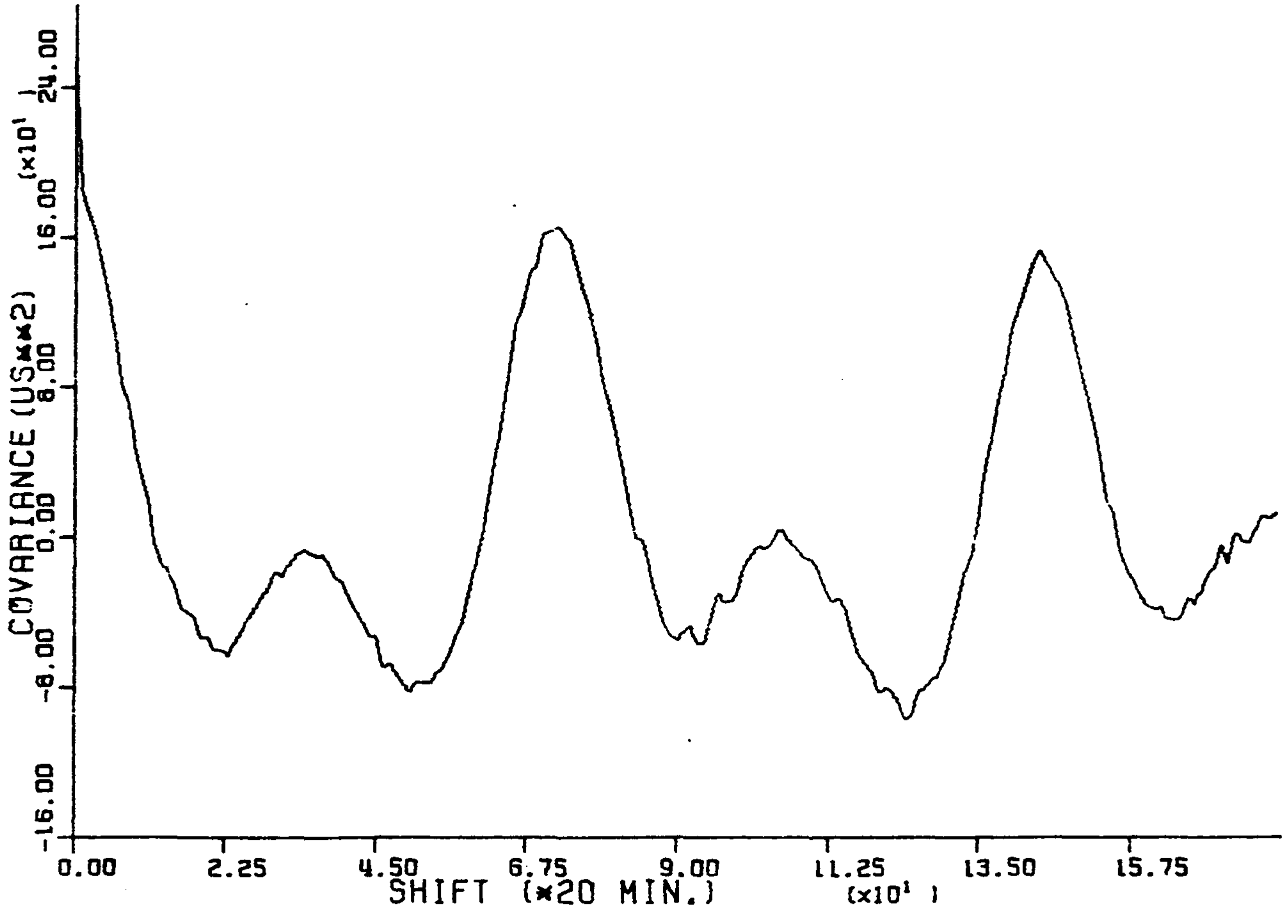

Figure 15. Autocovariance estimate for the path Trinidad to N. Dakota

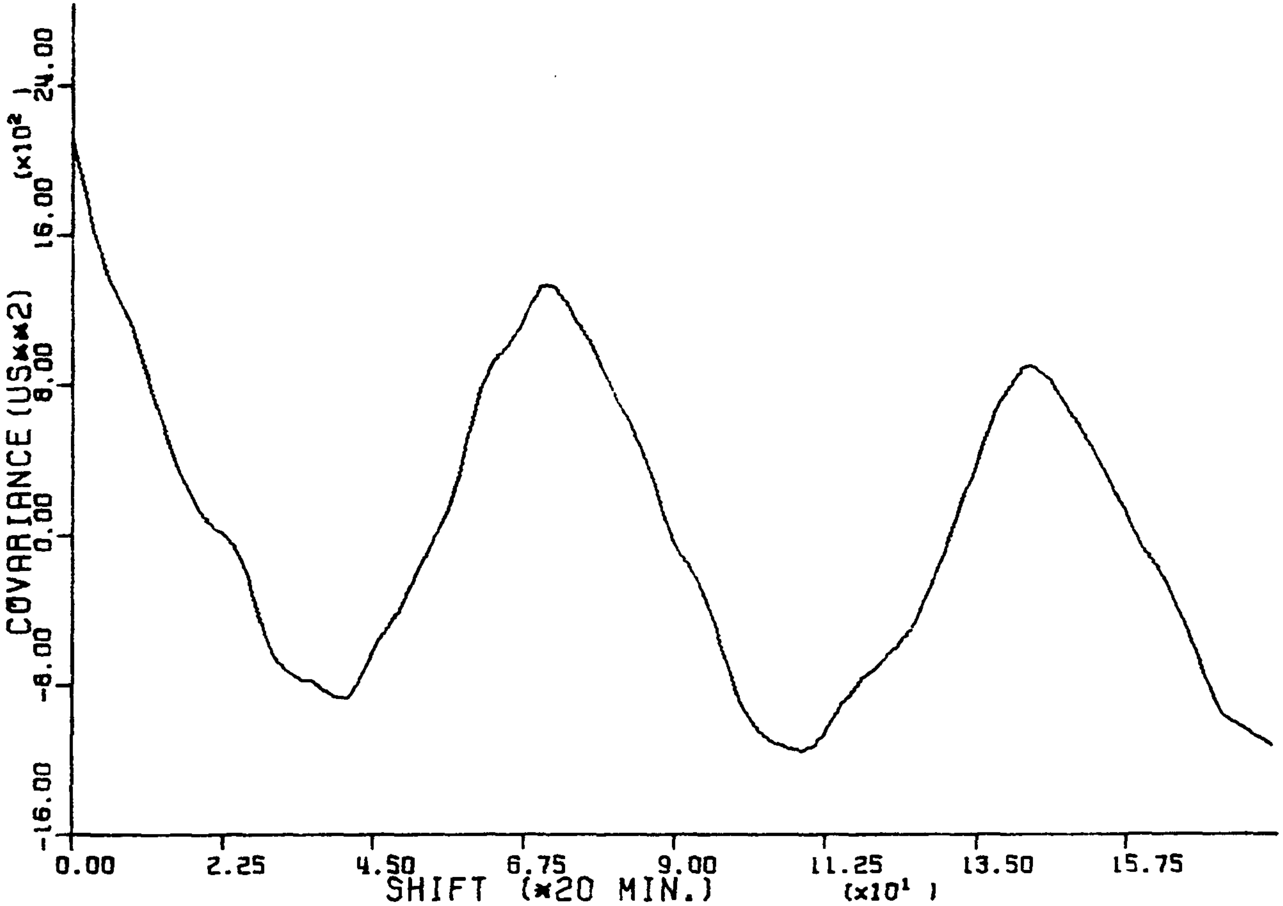

Figure 16. Autocovariance estimate for the path Norway to North Dakota

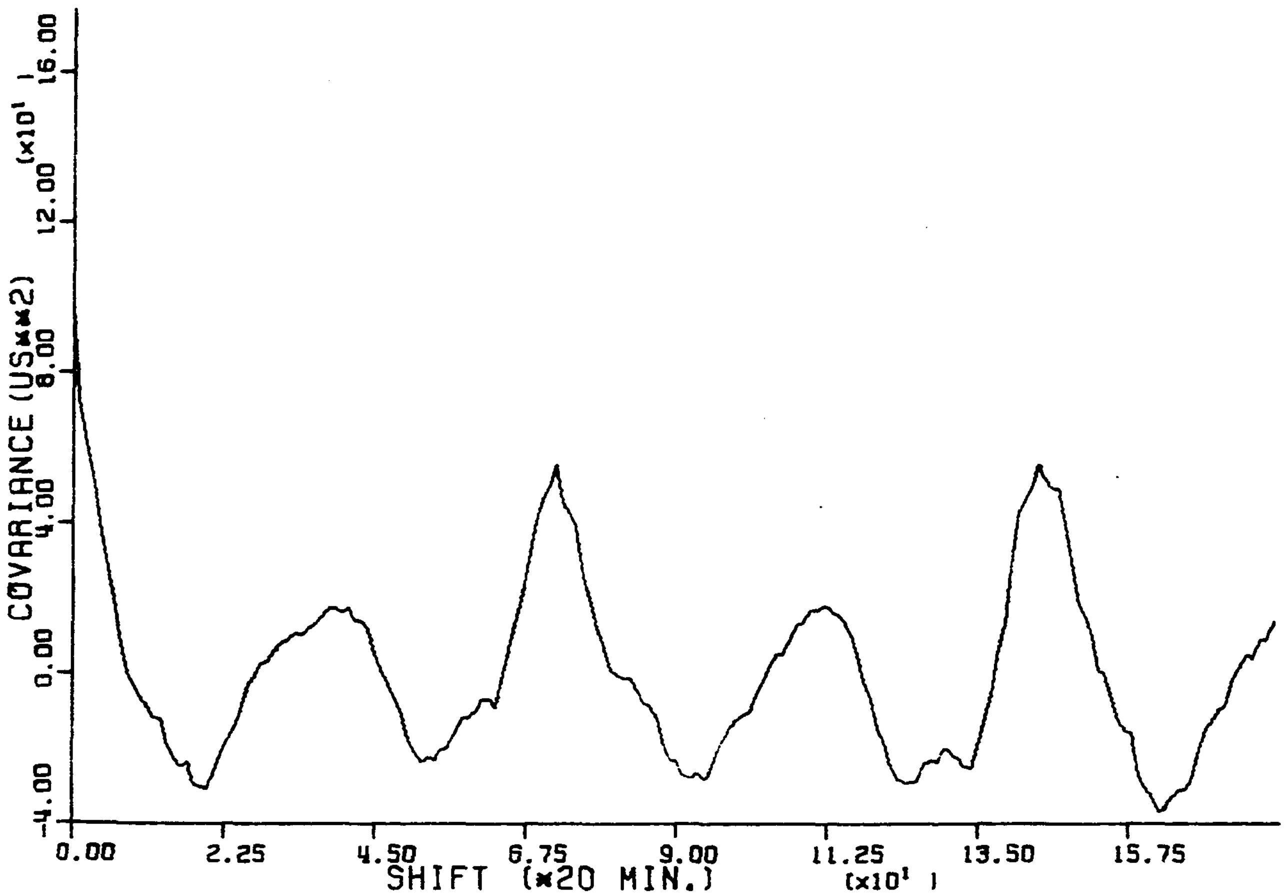

Figure 17. Autocovariance estimate for the path N. Dakota to Hawaii

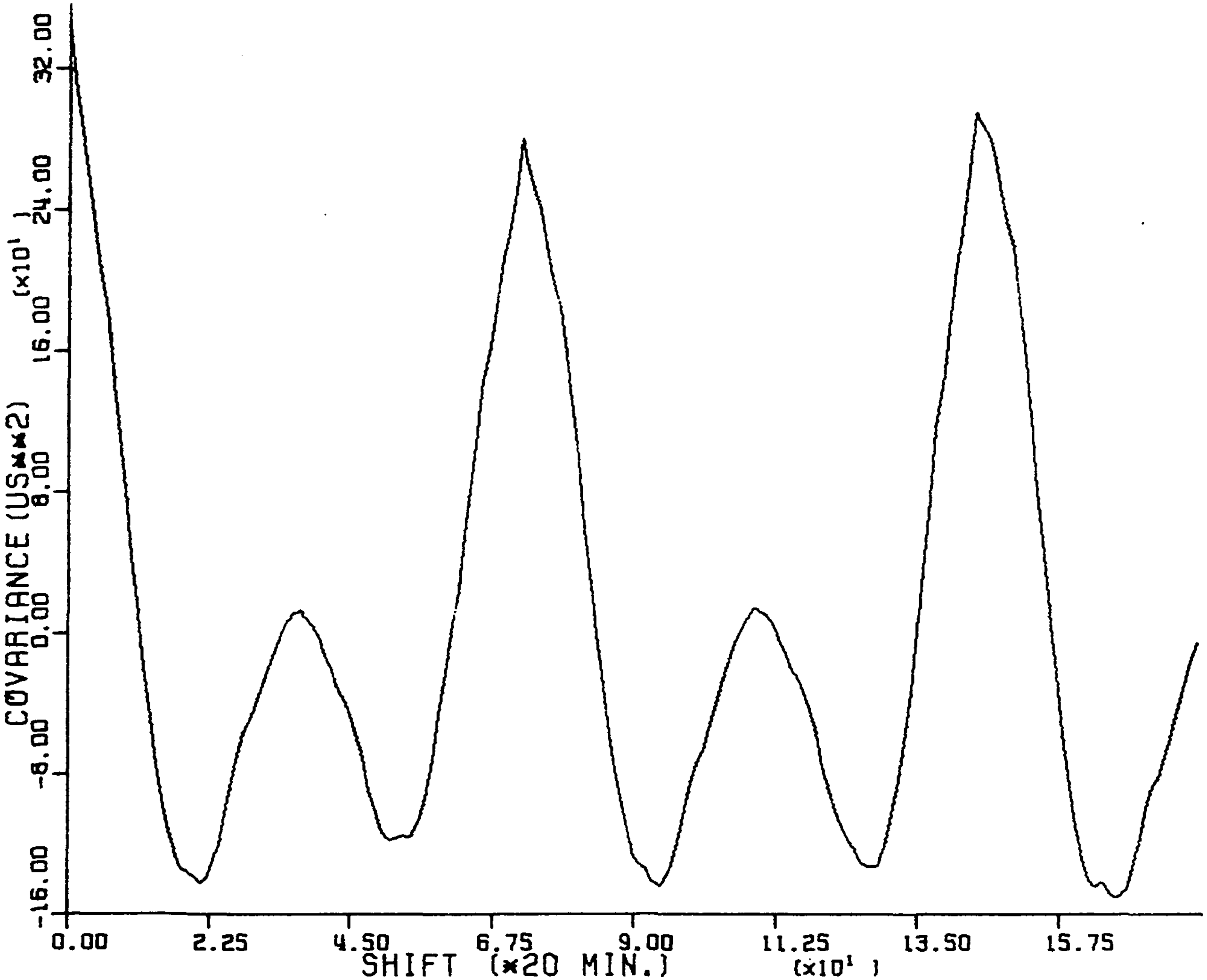

Figure 18. Autocovariance estimate for the path Japan to Hawaii

These estimates of the autocovariance functions have in common the basic features of an exponential decay added to an undamped oscillatory component.

Consider the "deterministic" stochastic process given by

$$z(t) = A\cos(\omega_0 t) + B\sin(\omega_0 t) \tag{1}$$

where A and B are independent normal random variables. It is easily shown that

$$R(\tau) = E[z(t)z(t + \tau)] = \sigma^2\cos(\omega_0\tau)$$

where $E[\cdot]$ is the expectation operator. If the periodic component of the autocovariance function of an $n_2(t)$ process is approximated by its first two Fourier cosine components, then two independent processes such as given by Equation 1 with appropriate parameters would model the periodic component of the $n_2(t)$ process. Note that physically this periodicity arises from the residual diurnal shift remaining in $n_2(t)$. This periodic component should have a period of 24 hours, and indeed, this is what is observed.

An independent Markov process with autocovariance function

$$R(\tau) = ae^{-b|\tau|},$$

where a and b are suitably chosen, added to the independent processes of the form of Equation 1, would then appear to be a reasonable model for an $n_2(t)$ process. This general approach was used by D'Appolito and

Kasper (27) on the residuals of an Omega navigation signal after certain propagation corrections had been made. However, the model considered here contains an additional harmonic component. A block diagram for this type of model is shown in Figure 19. In Figure 19 w(t) is unity white noise,

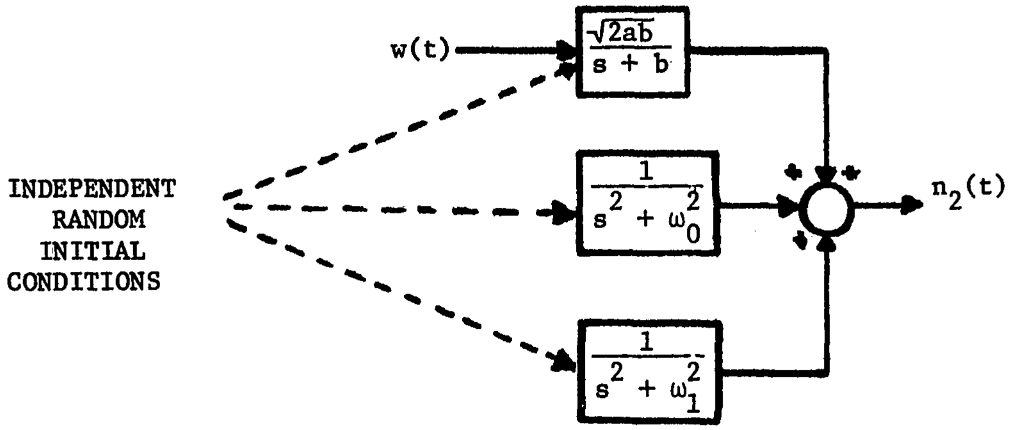

Figure 19. A model for the $n_2(t)$ process

ω_0 corresponds to a period of 24 hours, and ω_1 corresponds to a period of 12 hours. One state representation of this system is clearly

$$\dot{x} = \begin{bmatrix} -b & 0 & 0 & 0 & 0 \\ 0 & 0 & \omega_0 & 0 & 0 \\ 0 & -\omega_0 & 0 & 0 & 0 \\ 0 & 0 & 0 & 0 & \omega_0 \\ 0 & 0 & 0 & -\omega_1 & 0 \end{bmatrix} x + \begin{bmatrix} \sqrt{2ab}\,w(t) \\ 0 \\ 0 \\ 0 \\ 0 \end{bmatrix}, \qquad (2)$$

$$n_2(t) = [1\ 1\ 0\ 1\ 0]\,x$$

where x is the state vector. The initial conditions corresponding to Equation 2 are independent random variables with

$$E[x(0)] = [0\ 0\ 0\ 0\ 0]',$$

$$E[x(0)x^T(0)] = \text{Diag}\left[a\ \sigma_0^2\ \sigma_0^2\ \sigma_1^2\ \sigma_1^2\right],$$

where σ_0^2 is the coefficient of the fundamental periodic component of the autocovariance function, and σ_1^2 is the coefficient of the first harmonic component.

The form of the model to be used for the $n_2(t)$ processes is thus given by Equation 2. This is a state-space dynamical model which, for discrete time, yields the difference equation

$$x_k = \begin{bmatrix} c & 0 & 0 & 0 & 0 \\ 0 & d & e & 0 & 0 \\ 0 & -e & d & 0 & 0 \\ 0 & 0 & 0 & f & g \\ 0 & 0 & 0 & -g & f \end{bmatrix} x_{k-1} + \begin{bmatrix} u_k \\ 0 \\ 0 \\ 0 \\ 0 \end{bmatrix} \tag{3}$$

where

$$x_k \overset{\Delta}{=} x(t_k),$$

$$t_k - t_{k-1} = \Delta T,$$

$$c = e^{-b\Delta T},$$

$$d = \cos(\omega_0 \Delta T),$$

$$e = \sin(\omega_0 \Delta T),$$

$$f = \cos(\omega_1 \Delta T),$$

$$g = \sin(\omega_1 \Delta T),$$

$$u_k \sim \text{normal}(0,\ a(1-e^{-2b\Delta T})).$$

Equation 3 is in the form needed for implementation of a discrete Kalman filter and is derived in Appendix C. Next, the identification of the parameters a, b, σ_0^2, and σ_1^2 will be discussed. Note that ω_0 and ω_1 are known.

<u>The model parameters</u>

The form of the composite timing signal error model has been developed in the previous section. The parameters for this model now must be determined. First, the variances σ_0^2 and σ_1^2 are considered.

Since the exponentially decaying component of the estimated time autocovariance functions dies out rapidly, a numerical Fourier cosine analysis of the periodic component of the autocovariance can be done using the expression (28, 29)

$$a_n = \frac{2}{M} \sum_{k=1}^{M} R_k \cos\left(\left(k-\frac{1}{2}\right)\frac{2nN}{M}\right)$$

where a_n is the coefficient of the n^{th} Fourier cosine component, R_k is the k^{th} value of the autocovariance estimate R such that τ_k, k = 1, ... , M includes exactly one period of the periodic component of R in such a way that the even extension of R_k, k = 1, ... , M, is consistent with the estimate of R and the exponentially damped component has died out.

This was done for each of the 5 estimates of the autocovariance function for each data set. The results are tabulated in Table 1.

Table 1. Parameter estimates for the oscillatory component of $n_2(t)$

Propagation Path	a_1 μsec^2	a_2 μsec^2
Hawaii to North Dakota	120.45	14.22
Trinidad to North Dakota	64.92	66.87
Norway to North Dakota	1046.48	84.68
North Dakota to Hawaii	8.19	25.10
Japan to Hawaii	100.77	122.09
Average Value of a_1:	268.16 μsec^2	
Average Value of a_2:	62.59 μsec^2	

Observe that

$$a_1 = \sigma_0^2,$$

$$a_2 = \sigma_1^2.$$

Thus, Table 1 gives the estimates of the parameters σ_0^2 and σ_1^2. Next, the parameters a and b are considered.

After estimating σ_0^2 and σ_1^2 it was possible to estimate a residual autocovariance function for each case by subtracting $\sigma_0^2\cos(\omega_o\tau) + \sigma_1^2\cos(\omega_1\tau)$ from the previously estimated autocovariance function. A typical result is shown in Figure 20 for the propagation path Hawaii to North Dakota. An exponential decay of the form

$$ae^{-b|\tau|}$$

was fit to each of these residual autocovariance functions. The results are tabulated in Table 2. This completes the determination of the model parameters.

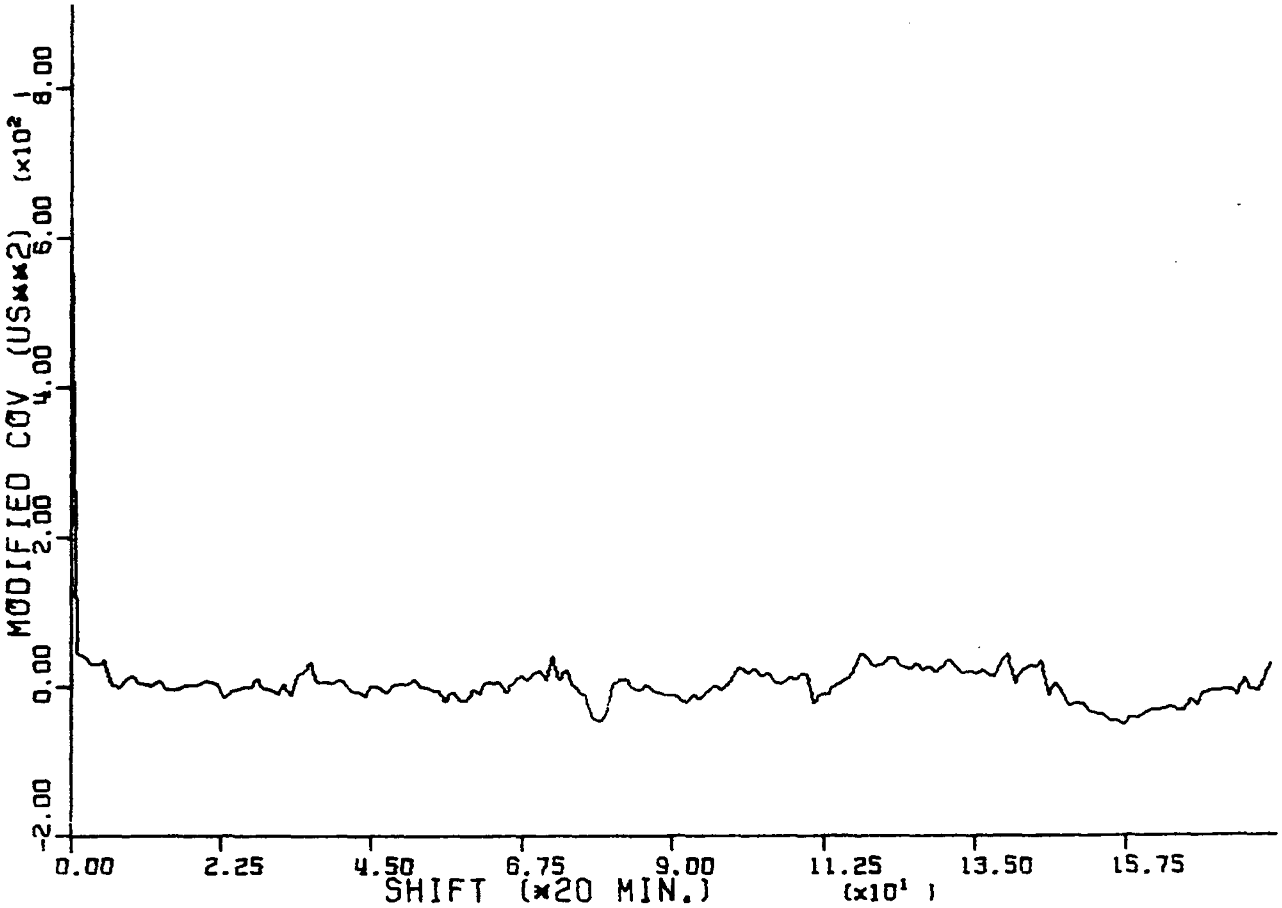

Figure 20. Residual autocovariance for the path Hawaii to N. Dakota

Table 2. Parameter estimates for the Markov component of $n_2(t)$

Propagation Path	a μsec^2	b 10^{-9} μsec^{-1}
Hawaii to North Dakota	625.84	2.170
Trinidad to North Dakota	124.02	0.416
Norway to North Dakota	969.83	0.135
North Dakota to Hawaii	65.21	0.864
Japan to Hawaii	123.70	0.240
Average Value of a:	381.72 μsec^2	
Average Value of b:	7.65×10^{-10} μsec^{-1}	

Two types of models were considered in this work. Both types were of the same form as described in the previous section, but the two types differed in parameter values. One type, called an all-purpose model, was postulated as a possible model for any propagation path. The other type, called a special-purpose model, was to model only a particular propagation path. The special-purpose model for a particular path used the parameter estimates based on the data for that propagation path. The all-purpose model originally used the average values of the parameter estimates; however, one set of parameter estimates (Japan to Hawaii) used in the average was based on data with some spans of spurious data. When these spurious data were later replaced with interpolated data, as described previously, the parameter estimates changed somewhat so that the parameters of the all-purpose model no longer corresponded exactly with the average values of the parameter estimates. However, there was no reason to change the all-purpose model since the values used in this model only need to be roughly representative of all propagation paths. These model parameters are summarized in Table 3.

Table 3. Model parameter estimates

Model	σ_0^2	σ_1^2	a μsec^2	b 10^{-9} μsec^{-1}
Special-Purpose Models:				
Hawaii to North Dakota	120.45	14.22	625.84	2.170
Trinidad to North Dakota	64.92	66.87	124.02	0.416
Norway to North Dakota	1046.48	84.68	969.83	0.135
North Dakota to Hawaii	8.19	25.10	65.21	0.864
Japan to Hawaii	100.77	122.09	123.70	0.240
All-Purpose Model	316.66	38.17	1201.81	0.840

Composite signal model summary

The models to be used for the Omega composite timing signal error have been determined. The models are of the form given by Equation 2 with the parameters summarized in Table 3. In the next section, the state-space models for the local timing signal error will be developed.

MODELS FOR THE LOCAL SIGNAL

Description of data

Stripcharts of local oscillator drift data were available to the author. They were obtained from a high quality quartz oscillator (Hewlett-Packard Model 104AR) maintained by the Dept. of Electrical Engineering, Iowa State University. These data were in the form of μsec of time error as compared with the WWVB timing signal at 60 kHz. This signal contained a diurnal shift which was compensated visually by the author while sampling the stripcharts. This compensation was in the form of linear interpolation. Since the data had obvious linear trends, this procedure appeared to be satisfactory. Linear interpolation was also used in the presence of obvious sudden ionospheric disturbances (SIDs) as well as between sampled data points. The stripcharts were sampled once every two hours. Therefore, when the resulting data were used in later simulations, it was necessary to interpolate between samples.

Five sets of local oscillator drift data were compiled from a single time record by the author as described. These data were all from the same oscillator; however, for each set the initial drift was taken to be zero for the first data point. As mentioned previously, the thin lines on Figure 6 through 10 are plots of these data.

The original model

The precise timing scheme under study in this work has been investigated previously by the author (4, 25a, 30). In one of the referenced papers (25a) the local timing signal error was modeled as a random ramp added to a random walk. This can be seen heuristically as follows. Upon observing the plots in Figures 6 through 10, it is apparent that the data look like a ramp for a period of time, but occasionally, the slope of the ramp changes in some unpredictable fashion. The random ramp component would model the ramp-like periods and the random walk would allow a Kalman filter to adjust to changes in the slope. Also, it is well known that for short-term periods, say 100 seconds, the phase drift of quartz oscillators is well-modeled by a random ramp added to a random walk (16,21). This type of model is similar to the model used by Santamore (31).

In the simulations performed by Strohbehn and Brown (25a) this model performed quite well. Therefore, as a beginning the local timing signal error $n_1(t)$ will be modeled by a random ramp added to a random walk. A block diagram for this model is shown in Figure 21.

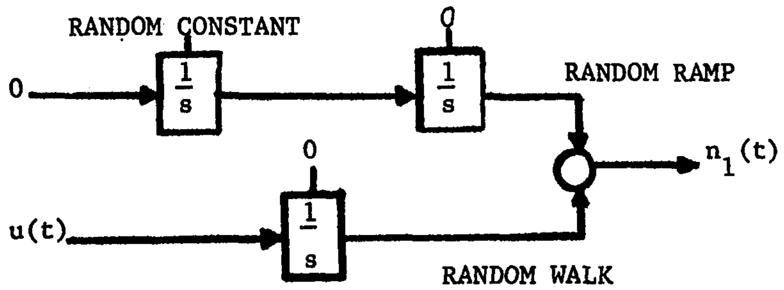

Figure 21. Random ramp plus random walk model for the $n_1(t)$ process

It is apparent from Figure 21 that one state-space representation of this model for $n_1(t)$ is given by

$$\dot{x} = \begin{bmatrix} 0 & 0 & 0 \\ 0 & 0 & 1 \\ 0 & 0 & 0 \end{bmatrix} x + \begin{bmatrix} u(t) \\ 0 \\ 0 \end{bmatrix}, \tag{4}$$

$$n_1(t) = [1\ 1\ 0]x$$

where x is the state vector and u(t) is a white noise. Equation 4 yields the difference equation necessary for implementation of a Kalman filter

$$x_k = \begin{bmatrix} 1 & 0 & 0 \\ 0 & 1 & \Delta T \\ 0 & 0 & 0 \end{bmatrix} x_{k-1} + \begin{bmatrix} a \\ 0 \\ 0 \end{bmatrix} \tag{5}$$

where

$$x_k \overset{\Delta}{=} x(t_k),$$

$$t_k - t_{k-1} = \Delta T,$$

$$a \sim \text{normal}(0,\ S_0 \Delta T),$$

and S_0 is the variance parameter of the random walk. This is derived analogously with Equation 3. Note that the slope k of the random ramp is assumed to be normal (m, σ_k^2) where m and σ_k^2 must be determined.

The original state-space model for the local timing signal error $n_1(t)$ is now given by Equation 5. Only the parameters S_0, m, and σ_k^2 need be determined. This is discussed next.

The parameters m and σ_k^2 were estimated as follows. A straight line of the form

$$n(t) = kt$$

was fitted using "least squares" to each set of drift data. The resulting slopes k were averaged to yield m. The corresponding variance was the estimate of σ_k^2. These "best" straight lines are the straight wide lines in Figures 6 through 10. The results are given by

$$m = -6.37 \times 10^{-10},$$
$$\sigma_k = \sqrt{\sigma_k^2} = 2.77 \times 10^{-10}. \tag{6}$$

Finally, the parameter S_0 was estimated as follows. The corresponding "best" straight line for each data set was subtracted from the data to yield a residual drift. This is the wide line about zero drift in Figures 6 through 10. The ensemble variance for each point of this residual series was estimated. This is the wide line in Figure 22. A "best" straight line was fitted to this ensemble variance to yield

$$\text{variance}(t) = S_0 t.$$

This line is the thin line in Figure 22. This S_0, the desired parameter, is

$$S_0 = 1.16 \times 10^{-9}\ \mu\text{sec}^2/\mu\text{sec}. \tag{7}$$

The original state-space model for the local timing signal error $n_1(t)$ is now entirely specified by Equations 5,6, and 7. The Kalman filter simulation results, discussed later, will show that this model is apparently not a valid description of $n_1(t)$. The next model which is discussed turns out to be a better description of the local timing signal error process $n_1(t)$.

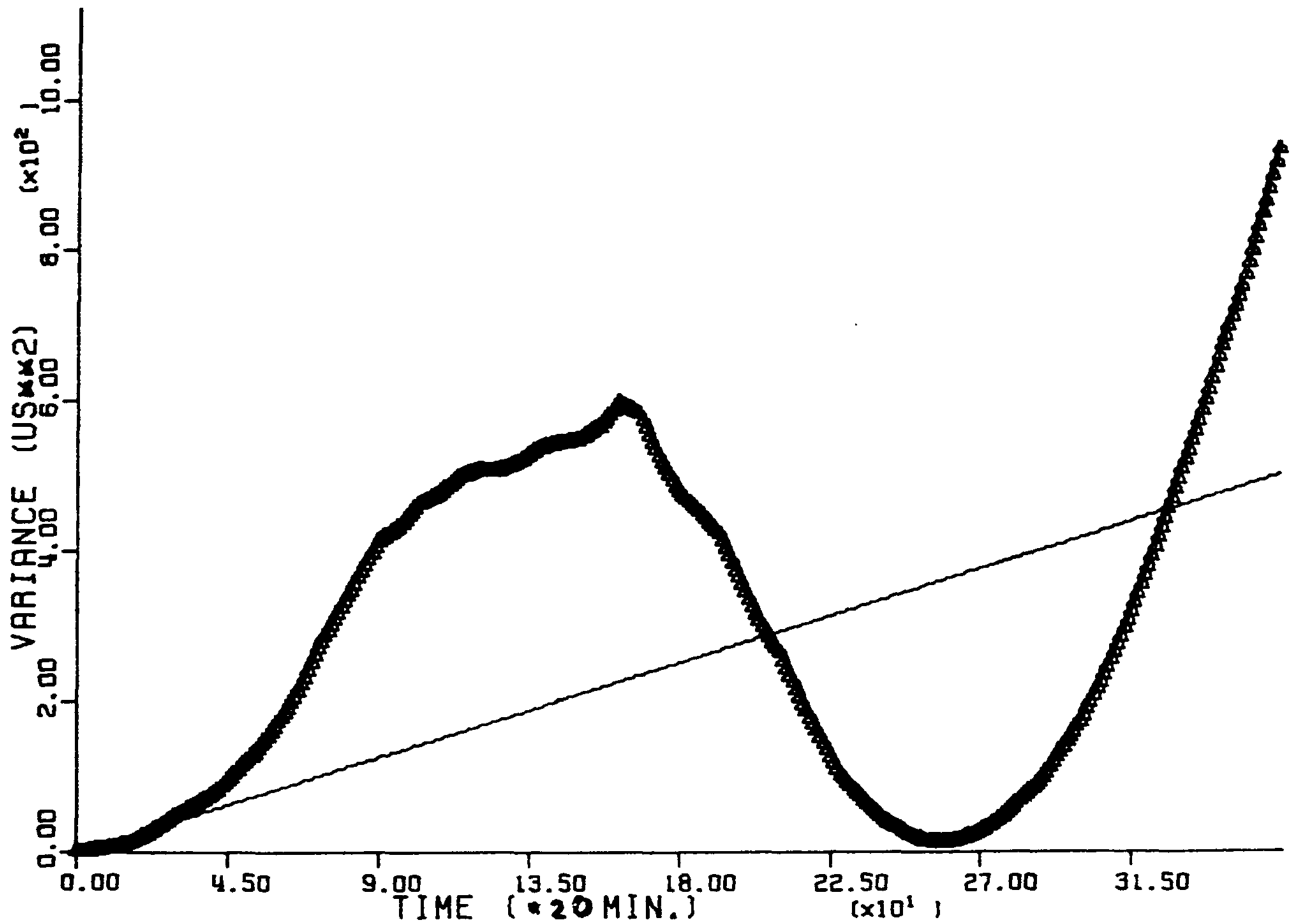

Figure 22. Ensemble variance of the residual drifts

<u>The final model</u>

It is well-known that in quartz oscillators the long term phase drift is dominated by the integral of what is known as "flicker noise" (19, 20, 21, 22). It will be seen that deriving a state-space model for flicker noise is not completely straightforward, but first, a description of flicker noise is in order.

The stochastic process referred to as flicker noise is not stationary so that the concept of a spectral density is not well-defined; however, measurements of the power spectrum of certain physical processes yield a power spectrum of the form

$$S(\omega) = \frac{1}{|\omega|} \tag{8}$$

for all values of ω investigated. Such processes are referred to as flicker noise processes. Note that Equation 8 must break down near zero frequency and above some finite frequency since infinite-energy processes cannot exist physically.

Proceeding formally, consider a linear system with transfer function H(s) given by

$$H(s) = \frac{1}{\sqrt{s}} . \tag{9}$$

Now consider driving this system with a white noise with spectral density S_0. Then if the resulting process had a spectrum, it would be of the form

$$S(\omega) = \frac{S_0}{|\omega|} , \tag{10}$$

i.e., a flicker noise. Hence, one can model the physical processes with power spectrum measurements following Equation 8 by white noise driving a linear system with transfer function given by Equation 9. The problem with this approach is that since the H(s) given by Equation 9 is not a rational function of polynomials, there is no finite state representation of this linear system.

Consider the plot of Equation 10 in Figure 23. The straight line with slope 10 dB/decade can be approximated arbitrarily closely by step-like functions which are the frequency response of a finite number of cascaded lag networks (32). One such approximation is shown in Figure 23. Therefore, the system with transfer function given by Equation 9 can be modeled aribtrarily closely over a frequency range of interest by a cascade of lag networks. Barnes, and Barnes and Jarvis have used this approach for modeling flicker noise processes (18, 32). Although state-space models for these processes have not been considered previously, the method of Barnes, and Barnes and Jarvis (18, 32) readily yields finite state representations for the approximating process.

This approach will be taken for the final model of the $n_1(t)$ process. For simplicity only one low pass filter will be used to model the flicker noise process. Its parameters will be derived after a brief discussion of a heuristic reason for modeling $n_1(t)$ in this manner.

Recall from Figures 6 through 10 that the sample functions of $n_1(t)$ look like random ramps which occasionally change slope. A first-order Markov process with a long time constant would approximate a constant over a certain time interval, but would drift off. This is easily seen by noting that

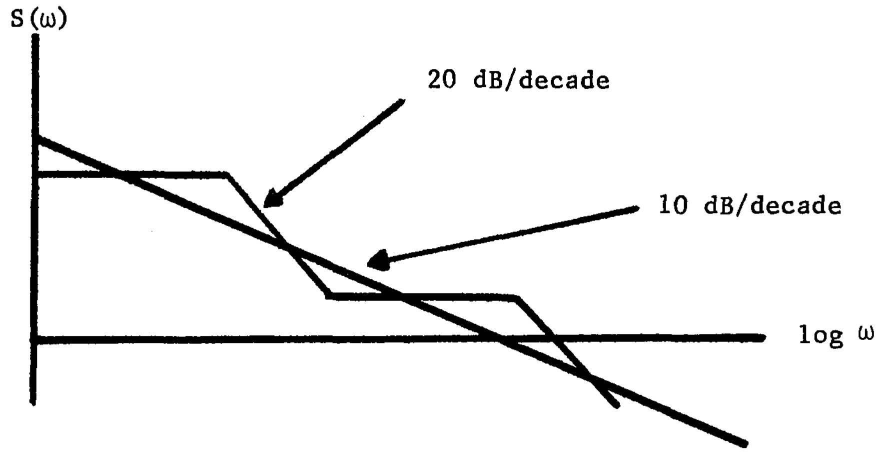

Figure 23. Spectral approximation of a flicker noise process

$$\lim_{b' \to 0} a' e^{-b'|\tau|} = a' \quad \forall \tau,$$

where b approaching zero implies that the time constant approaches infinity. This would be the autocovariance function of a constant process. Thus, integrating the output of a first-order Markov process with the long time constant should produce sample functions of the form shown in Figures 6 through 10. This heuristic reasoning, which would also follow for higher-order Markov processes, agrees with the approach of Barnes, and Barnes and Jarvis (18, 32).

Therefore, the final model for the $n_1(t)$ process is an integrated first-order Markov process. A block diagram is shown in Figure 24. Clearly, a state-space representation for this model of $n_1(t)$ is given by

$$\dot{x} = \begin{bmatrix} -b & 0 \\ 1 & 0 \end{bmatrix} x + \begin{bmatrix} \sqrt{2ab} & u(t) \\ 0 & \end{bmatrix}, \tag{11}$$

$$n_1(t) = [1 \ 0]x$$

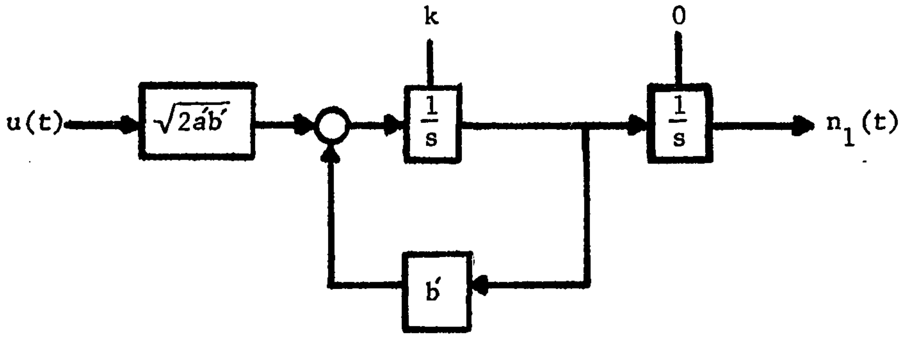

Figure 24. Integrated Markov model for the $n_1(t)$ process

where x is the state vector, u(t) is a unity white noise, and the parameters a' and b' must be determined. Observe that the initial conditions are also random variables. The parameters a' and b' and the initial condition statistics will be determined next.

First, the variance of the Markov process a will be chosen as σ_k^2 which was determined in the last section. The slopes of the sample functions of $n_1(t)$ appear nearly constant for periods of roughly 100 data points. Thus, let b' be given by

$$b' = \frac{1}{100 \text{ points}} = 8.33 \times 10^{-12} \ \mu\text{sec}^{-1}.$$

The $n_1(t)$ process is assumed zeroed at time equal to zero, and the slopes k of the "best" straight line fits to the $n_1(t)$ sample functions have the statistics m and σ_k^2. Thus, let the initial condition on the Markov process be a random variable which is normal (m, σ_k^2). This determines the $n_1(t)$ final model parameters. Note that determining these parameters is equivalent to determining the frequency range of interest and the accuracy of approximation of the flicker noise process.

Equation 11 yields the difference equation

$$x_k = \begin{bmatrix} c & 0 \\ d & 1 \end{bmatrix} x_{k-1} + \begin{bmatrix} q \\ 0 \end{bmatrix} \tag{12}$$

where

$$x_k \overset{\Delta}{=} x(t_k),$$
$$q \sim \text{normal } (0,\ a(1-e^{-2b\Delta T})),$$
$$c = e^{-b\Delta T},$$
$$d = \frac{1}{b}\,(1-e^{-b\Delta T}),$$
$$\Delta T = t_k - t_{k-1}.$$

Equation 12 is derived analogously with Equation 3 and 5.

Local signal model summary

The original state-space model for the local timing signal error process $n_1(t)$ is given by Equation 5. This model will be shown inadequate. The final state-space model for $n_1(t)$ is given by Equation 12. This model will be shown to be better than the random-ramp plus random-walk model previously discussed. Also, this model requires only two states rather than three.

THE KALMAN FILTER SIMULATIONS

Simulation description

Recall that the precise timing scheme under study optimally integrates a local timing signal with an Omega composite timing signal by estimating $n_1(t)$, given $n_1(t)-n_2(t)$. The estimator is a Kalman filter that is based on state-space models of the processes $n_1(t)$ and $n_2(t)$. Models for these processes were developed in the previous sections. Several simulations were done using real data in order to test the validity of these models, and, in addition, assess the precise timing scheme under consideration for the assumed models. The simulations were done off-line by using the data sets described previously to calculate $n_1(t)-n_2(t)$ and then iterating the well-known Kalman filter equations given by Gelb (26). They are

$$\begin{aligned}
K_k &= P_k^- H_k^T [H_k P_k^- H_k^T + R_k]^{-1}, \\
\hat{x}_k^+ &= x_k^- + K_k[z_k - H_k \hat{x}_k^-], \\
P_k^+ &= [I - K_k H_k] P_k^-, \\
\hat{x}_{k+1}^- &= \phi_k \hat{x}_k^+, \\
P_{k+1}^- &= \phi_k P_k^+ \phi_k^T + Q_k,
\end{aligned} \tag{13}$$

where the state vector x to be estimated satisfies

$$\begin{aligned}
x_{k+1} &= \phi_k x_k + w_k, \\
w_k &\sim \text{normal}(0, Q_k), \\
E[w_k w_j^T] &= 0, \ j \neq k,
\end{aligned} \tag{14}$$

and the measurements satisfy

$$n_1(t_k)-n_2(t_k) \overset{\Delta}{=} z_k = H_k x_k + v_k,$$

$$v_k \sim \text{normal } (0,R_k), \tag{15}$$

$$E[v_k v_j^T] = 0, \; j \neq k;$$

and K_k is the Kalman gain vector, $\hat{x}_k^-$ is the a priori estimate of $x(t_k)$, P_k^- is the a priori error covariance matrix, $\hat{x}_k^+$ is the a posteriori estimate of $x(t_k)$, and P_k is the a posteriori error covariance matrix.

Expressions for ϕ_k, Q_k, H_k, and R_k are derived in a straight forward manner in Appendix D. Also derived in Appendix D are the initial conditions P_0^- and $\hat{x}_0^-$. The results will now be given for each model considered.

First, for the original $n_1(t)$ model $x \in R^8$ and

$$\phi_k = \begin{bmatrix} A & 0 & 0 & 0 & 0 & 0 & 0 & 0 \\ 0 & B & C & 0 & 0 & 0 & 0 & 0 \\ 0 & -C & B & 0 & 0 & 0 & 0 & 0 \\ 0 & 0 & 0 & D & E & 0 & 0 & 0 \\ 0 & 0 & 0 & -E & D & 0 & 0 & 0 \\ 0 & 0 & 0 & 0 & 0 & 1 & 0 & 0 \\ 0 & 0 & 0 & 0 & 0 & 0 & 1 & \Delta T \\ 0 & 0 & 0 & 0 & 0 & 0 & 0 & 1 \end{bmatrix} \forall k, \tag{16}$$

$$Q_k = \begin{bmatrix} F & 0 & 0 & 0 & 0 & 0 & 0 & 0 \\ 0 & 0 & 0 & 0 & 0 & 0 & 0 & 0 \\ 0 & 0 & 0 & 0 & 0 & 0 & 0 & 0 \\ 0 & 0 & 0 & 0 & 0 & 0 & 0 & 0 \\ 0 & 0 & 0 & 0 & 0 & 0 & 0 & 0 \\ 0 & 0 & 0 & 0 & 0 & G & 0 & 0 \\ 0 & 0 & 0 & 0 & 0 & 0 & 0 & 0 \\ 0 & 0 & 0 & 0 & 0 & 0 & 0 & 0 \end{bmatrix} \forall k, \tag{17}$$

$$R_k = 0, \; \forall k, \tag{18}$$

$$H_k = [-1 \quad -1 \quad 0 \quad -1 \quad 0 \quad 1 \quad 1 \quad 0] \ \forall k, \tag{19}$$

$$\hat{x}_0^{-T} = [\ 0 \quad 0 \quad 0 \quad 0 \quad 0 \quad 0 \quad 0 \quad -6.37\text{x}10^{-10}], \tag{20}$$

$$P_0^- = \begin{bmatrix} H & 0 & 0 & 0 & 0 & 0 & 0 & 0 \\ 0 & I & 0 & 0 & 0 & 0 & 0 & 0 \\ 0 & 0 & I & 0 & 0 & 0 & 0 & 0 \\ 0 & 0 & 0 & J & 0 & 0 & 0 & 0 \\ 0 & 0 & 0 & 0 & J & 0 & 0 & 0 \\ 0 & 0 & 0 & 0 & 0 & 0 & 0 & 0 \\ 0 & 0 & 0 & 0 & 0 & 0 & 0 & 0 \\ 0 & 0 & 0 & 0 & 0 & 0 & 0 & M \end{bmatrix}, \tag{21}$$

where

$$\Delta T = t_k - t_{k-1} = 1.2 \times 10^9 \ \mu\text{sec},$$
$$A = e^{-b\Delta T},$$
$$B = \cos(\omega_0 \Delta T) = 0.996197,$$
$$C = \sin(\omega_0 \Delta T) = 0.087129,$$
$$D = \cos(\omega_1 \Delta T) = 0.984900,$$
$$E = \sin(\omega_1 \Delta T) = 0.173123,$$
$$F = a(1-3^{-2b\Delta T)},$$
$$G = S_0 \Delta T = 1.397688 \ \mu\text{sec}^2,$$
$$H = a,$$
$$I = \sigma_0^2,$$
$$J = \sigma_1^2,$$
$$M = \sigma_k^2 = 7.678408 \times 10^{-20},$$

and a, b, σ_0^2, and σ_1^2 are given for the all purpose model and each special purpose model in Table 3.

For the final $n_1(t)$ model $x \in R^7$ and

$$\phi_k = \begin{bmatrix} A & 0 & 0 & 0 & 0 & 0 & 0 \\ 0 & B & C & 0 & 0 & 0 & 0 \\ 0 & -C & B & 0 & 0 & 0 & 0 \\ 0 & 0 & 0 & D & E & 0 & 0 \\ 0 & 0 & 0 & -E & D & 0 & 0 \\ 0 & 0 & 0 & 0 & 0 & N & 0 \\ 0 & 0 & 0 & 0 & 0 & T & 1 \end{bmatrix} \quad \forall k, \tag{22}$$

$$Q_k = \begin{bmatrix} F & 0 & 0 & 0 & 0 & 0 & 0 \\ 0 & U & 0 & 0 & 0 & 0 & 0 \\ 0 & 0 & U & 0 & 0 & 0 & 0 \\ 0 & 0 & 0 & V & 0 & 0 & 0 \\ 0 & 0 & 0 & 0 & V & 0 & 0 \\ 0 & 0 & 0 & 0 & 0 & Y & 0 \\ 0 & 0 & 0 & 0 & 0 & 0 & Z \end{bmatrix} \quad \forall k, \tag{23}$$

$$R_k = 0 \quad \forall k,$$

$$H_k = [-1 \quad -1 \quad 0 \quad -1 \quad 0 \quad 0 \quad 1] \quad \forall k, \tag{24}$$

$$\hat{x}_0^{-T} = [0 \quad 0 \quad 0 \quad 0 \quad 0 \quad m \quad 0], \tag{25}$$

$$P_0^- = \begin{bmatrix} H & 0 & 0 & 0 & 0 & 0 & 0 \\ 0 & I & 0 & 0 & 0 & 0 & 0 \\ 0 & 0 & I & 0 & 0 & 0 & 0 \\ 0 & 0 & 0 & J & 0 & 0 & 0 \\ 0 & 0 & 0 & 0 & J & 0 & 0 \\ 0 & 0 & 0 & 0 & 0 & M & 0 \\ 0 & 0 & 0 & 0 & 0 & 0 & 0 \end{bmatrix}, \tag{26}$$

where

$$m = -6.374784 \times 10^{-10},$$

$$Z = 0.158 \ \mu\text{sec}^2,$$

$$Y = 1.519825 \times 10^{-21},$$

$$U = I/1000 \ \mu\text{sec}^2,$$

$$V = J/1000 \ \mu\text{sec}^2,$$

$$N = 0.9900054,$$

$$T = 1.19 \times 10^9,$$

and A, B, C, D, E, F, H, I, J are as in Equations 16 through 21.

Observe that since data for $n_1(t)$ are available, the actual error sequence $\{e_i\}_{i=1}^{N_0}$ and an estimate of its root mean square value (RMS)

$$e_{rms} = \left[\frac{1}{N_0} \sum_{i=1}^{N_0} (e_i - \bar{e})^2 \right]^{1/2}$$

are available for a given simulation where N_0 is the total number of data points used in the simulation.

The simulation results for the Kalman filter based on the original $n_1(t)$ model are reported next.

Results for the original local signal model

Simulations as described previously were carried out using Equations 13 through 21 (See Appendix E for a sample program). First, a simulation was done using an all purpose model and 5 days of data for the path Hawaii to North Dakota. A plot of the resulting timing error is shown in Figure 25. The RMS error predicted by the filter was 32.2 μsec, but the observed RMS error was 8.4 μsec. Also, the filter did not appear to reach a steady-state since the terms of the P-matrix (the a posteriori error covariance matrix) did not appear to have converged, but were steadily increasing. Since this was the case, the last values of the P-matrix were used to predict the RMS error above. For this simulation the filter certainly did not perform well.

To see if perhaps a special purpose model could improve the filter's performance, another simulation was done using the same data, but with

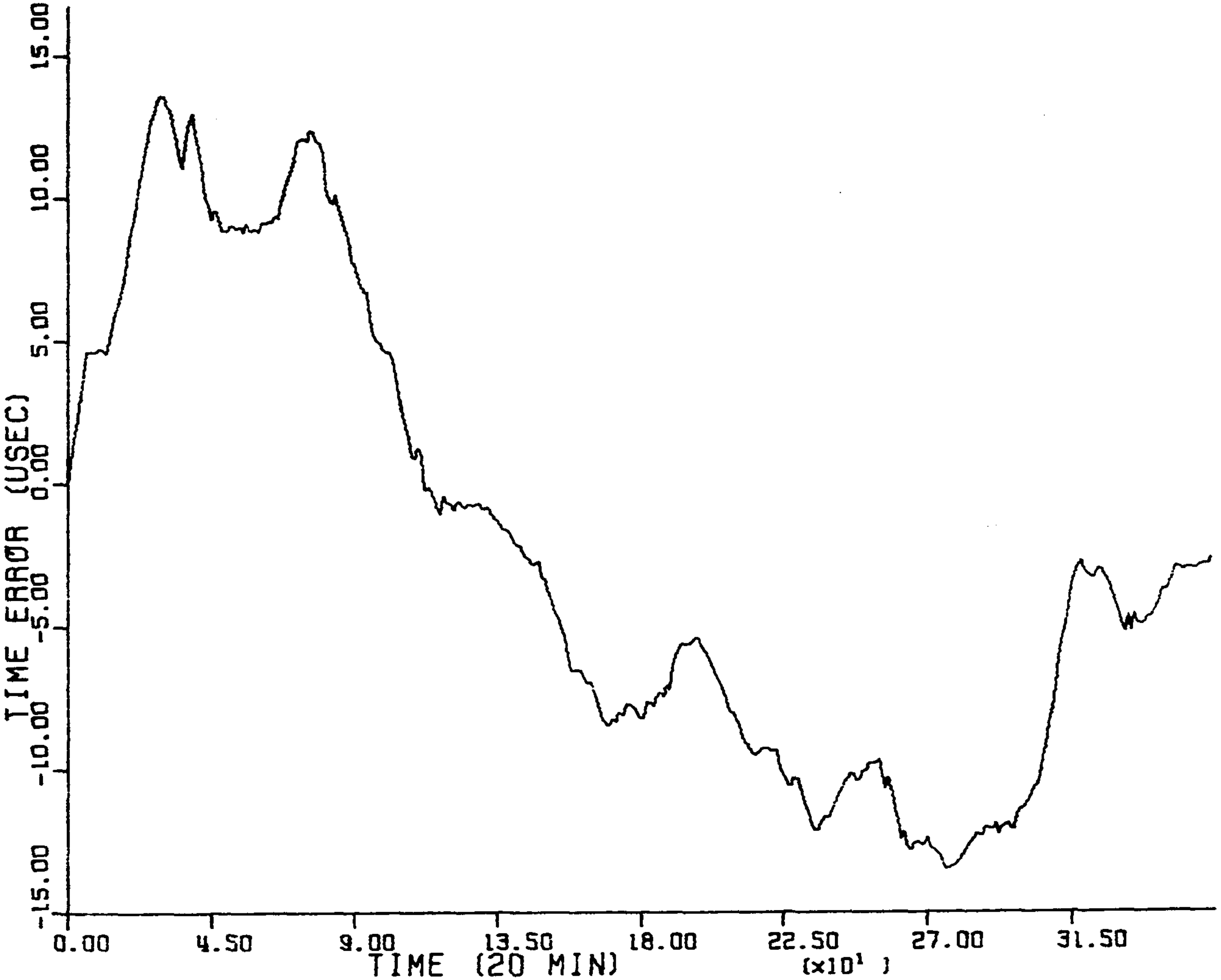

Figure 25. Simulated time error for the path Hawaii to N. Dakota and the all-purpose model

the appropriate special purpose model instead of the all purpose model. A plot of the resulting timing error is shown in Figure 26. Again, the filter did not appear to converge to a steady-state condition. The last values of the P-matrix were used to predict the RMS error to be 31.6 μsec, but the observed RMS error was 5.1 μsec. Again, the filter's performance was poor.

Next, similar simulations were done for the data from the propagation path Trinidad to North Dakota. For both the special purpose and the all purpose models the filter estimates again appeared to diverge. A plot of the timing error for the all purpose model simulation is given in Figure 27, and a plot of the timing error for the special purpose model is shown in Figure 28. The predicted RMS error was 32.2 μsec for the all purpose model, but the observed RMS error was 13.3 μsec. The predicted error for the special purpose model was 31.5 μsec, but the observed error was 6.5 μsec.

As for the path Hawaii to North Dakota the performance of the filter was poor for both simulations; indeed, the filter appeared to diverge for the special purpose and the all purpose models. To remedy this, the standard technique (26) of adding "small" white noises to the "deterministic" and perfectly correlated states of the filter was used. This merely changes Equation 17 to

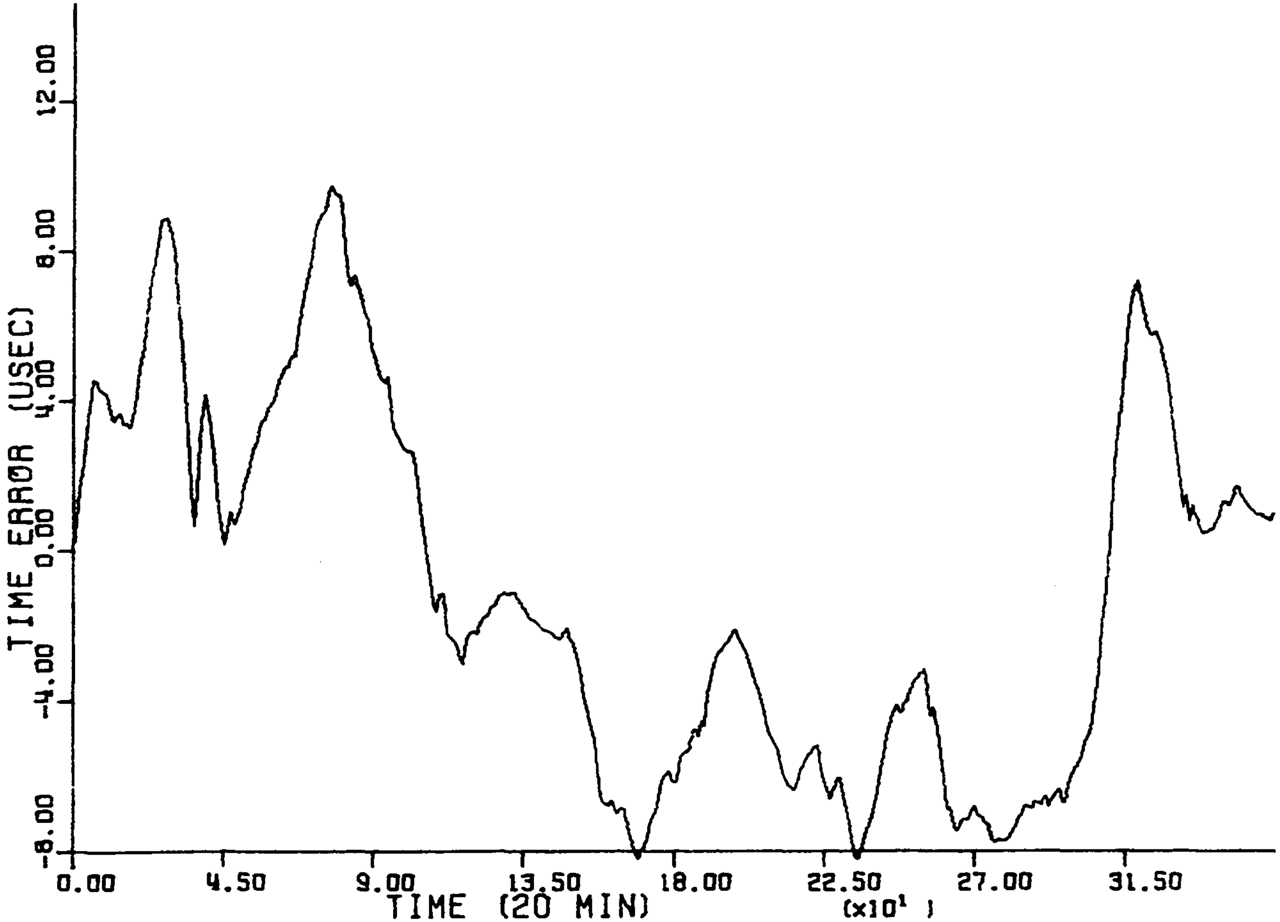

Figure 26. Simulated time error for the path Hawaii to N. Dakota and the special purpose model

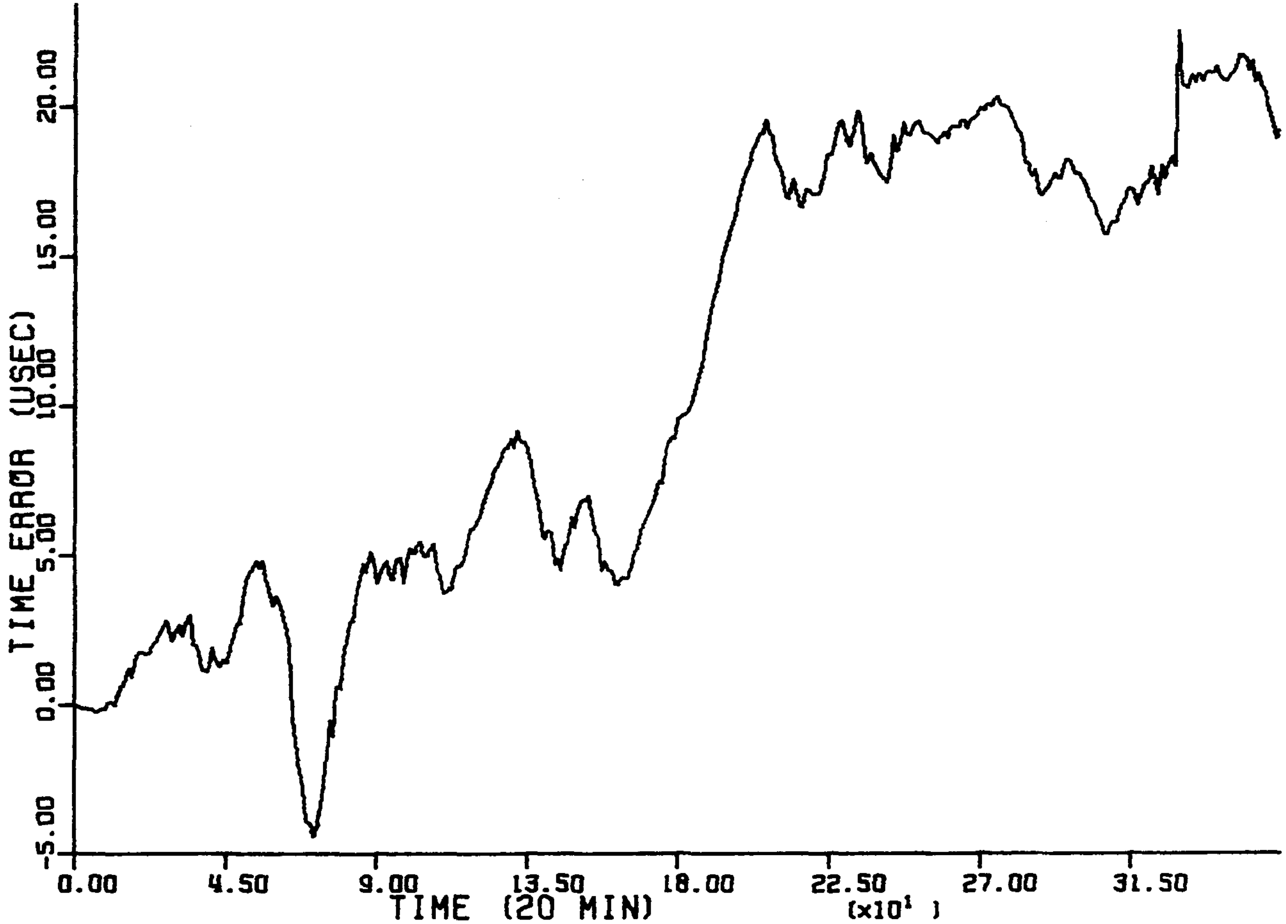

Figure 27. Simulated time error for the path Trinidad to N. Dakota and the all-purpose model

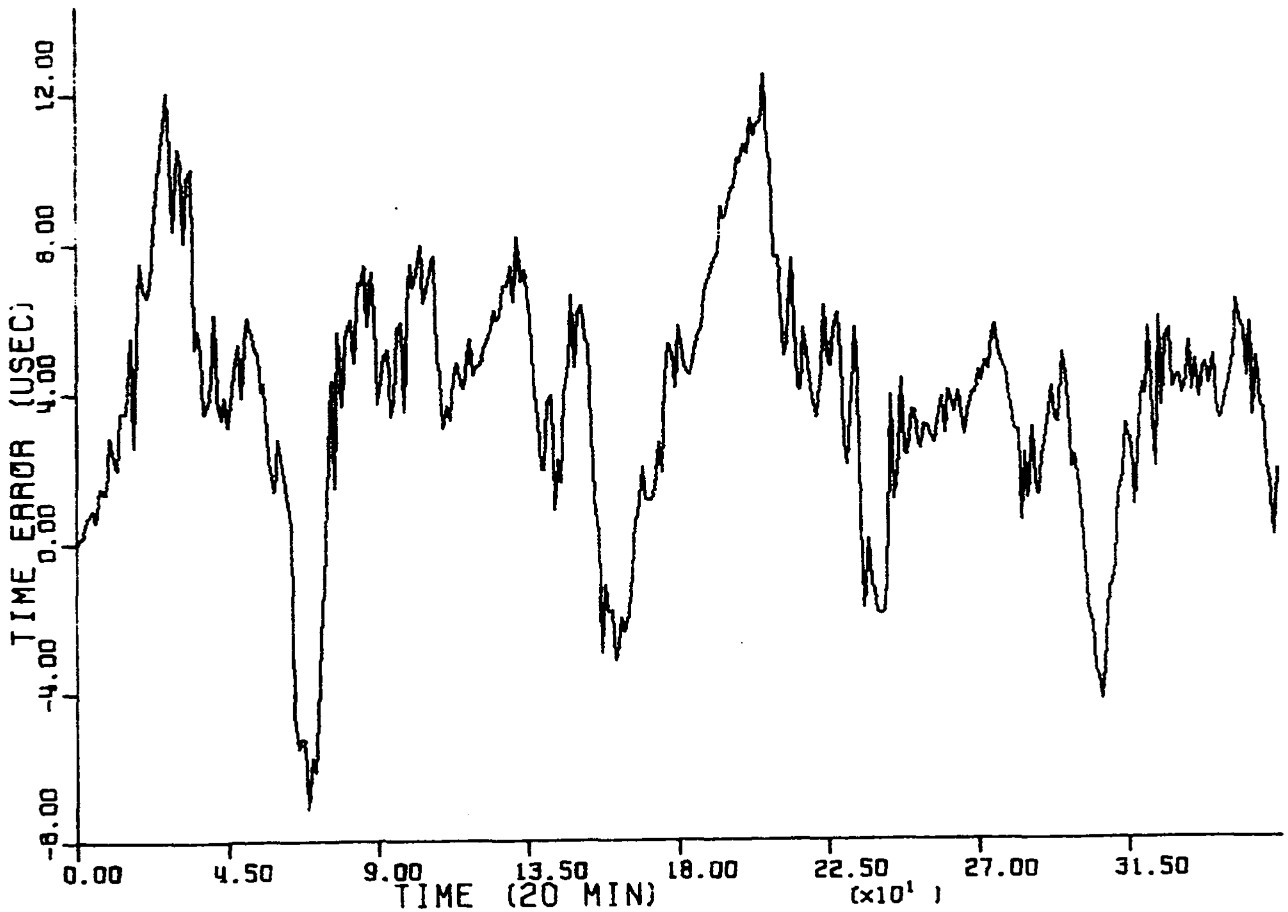

Figure 28. Simulated time error for the path Trinidad to N. Dakota and the special purpose model

$$Q_k = \begin{bmatrix} F & 0 & 0 & 0 & 0 & 0 & 0 & 0 \\ 0 & U & 0 & 0 & 0 & 0 & 0 & 0 \\ 0 & 0 & U & 0 & 0 & 0 & 0 & 0 \\ 0 & 0 & 0 & V & 0 & 0 & 0 & 0 \\ 0 & 0 & 0 & 0 & V & 0 & 0 & 0 \\ 0 & 0 & 0 & 0 & 0 & G & 0 & 0 \\ 0 & 0 & 0 & 0 & 0 & 0 & Z & 0 \\ 0 & 0 & 0 & 0 & 0 & 0 & 0 & r \end{bmatrix} \qquad (27)$$

where the additive noises were picked somewhat arbitrarily as discussed in Appendix D, and

$$r = 1.10 \times 10^{-22}.$$

The simulations for the Trinidad to North Dakota data were repeated using Equation 27 instead of Equation 17. A plot of the timing error for the all purpose model is shown in Figure 29. The predicted RMS error was 32.7 μsec, but the observed RMS error was 9.1 μsec. A plot of the timing error for the special purpose model is shown in Figure 30. The predicted RMS error was 31.7 μsec, but the observed RMS error was 5.1 μsec. Again, as in the previous simulations the filter appeared to diverge, giving poor performance.

The divergence of the filter in these simulations seemed to indicate a basic failure of the models to describe the data. Changing from an all-purpose $n_2(t)$ model to a special purpose $n_2(t)$ model generally lowered the observed RMS error as would be expected, but did not cure the divergence problems. At this point the author decided, based on the heuristic argument given previously, to try the final $n_1(t)$ model with the additional white noise terms. These additional terms make the models for $n_2(t)$ consistent with the techniques for modeling "seasonal" time series given by Box and

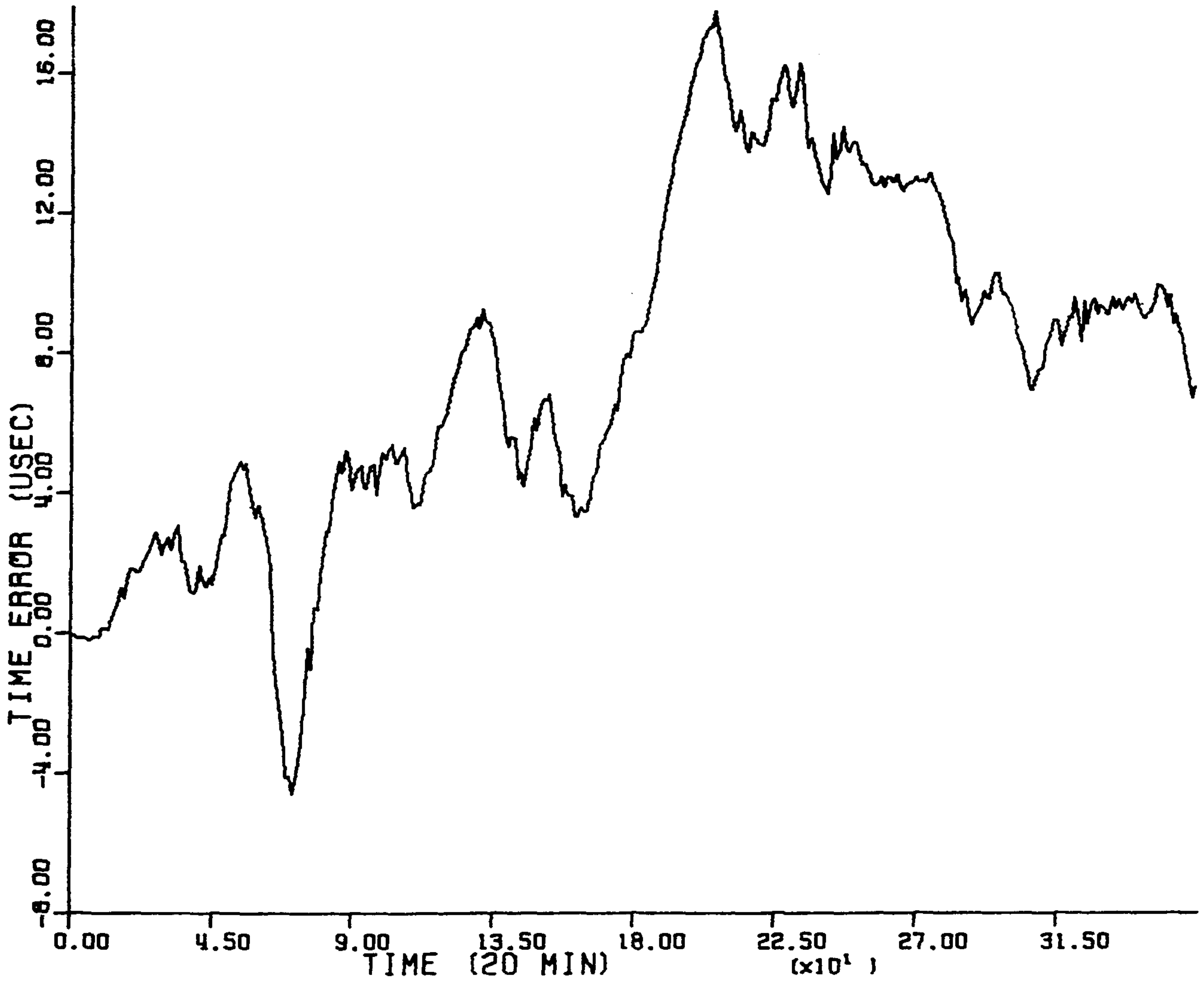

Figure 29. Simulated time error for the path Trinidad to N. Dakota and the all-purpose model with positive definite Q-matrix

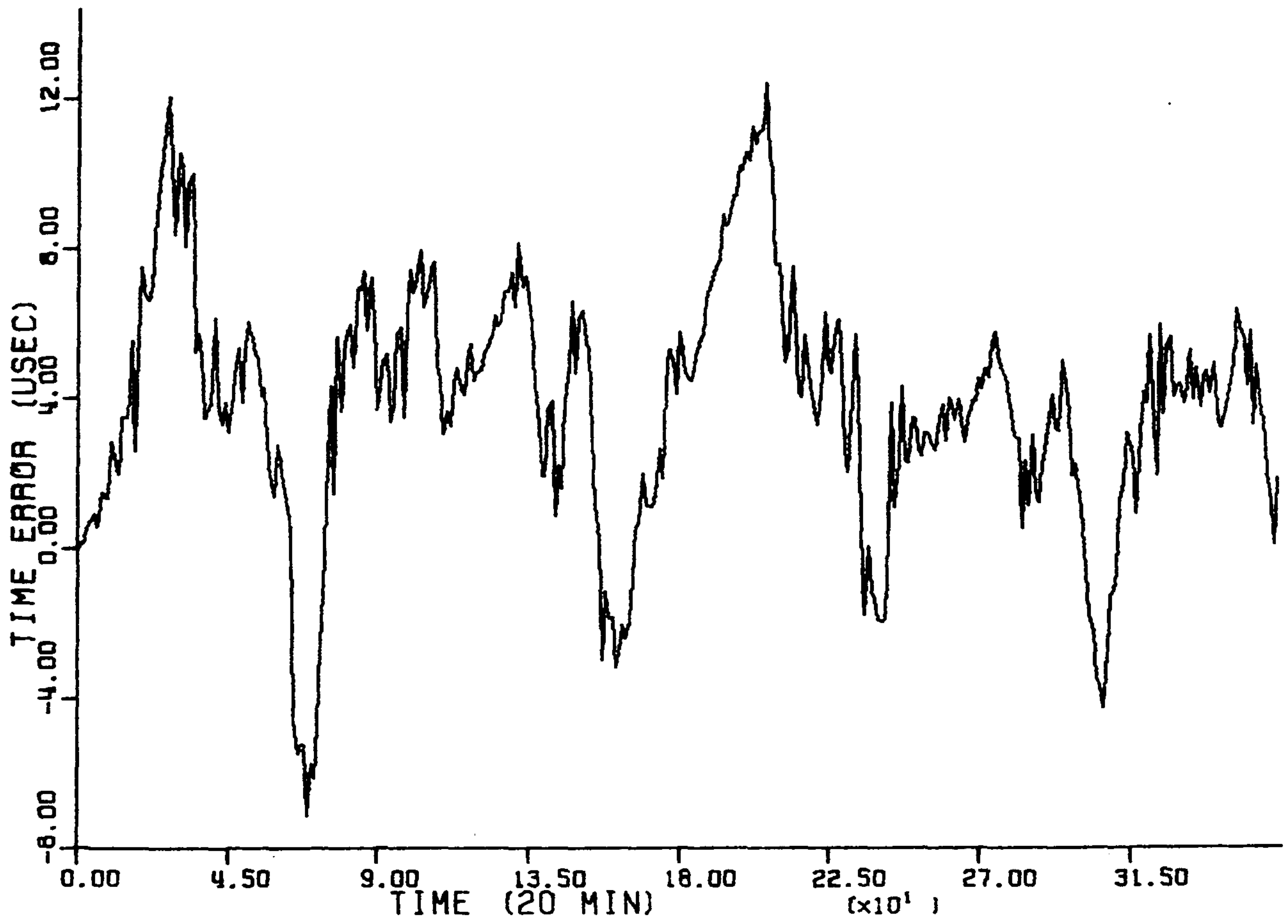

Figure 30. Simulated time error for the path Trinidad to N. Dakota and the special purpose model with positive definite Q-matrix

Jenkins (33) and help stabilize the filter (26). The simulation results for the Kalman filter based on the final model for $n_1(t)$ are given next.

Results for the final local signal model

Simulations as described previously were done using Equations 13, 14, 15, and 22 through 26. In addition, the fractional frequency error for two-hour averaging times was estimated using the equation (recall ΔT is 20 minutes)

$$\frac{e_i - e_{i-6}}{6\Delta T} = \text{fractional frequency error}_i$$

for i such that the timing errors e_i for the last 2 days of the 5-day simulations, or the last 5 days of the 20-day simulations, were used in the computations. The fractional frequency error is important in applications requiring the improved timing system to calibrate less accurate oscillators in a reasonable period of time, for instance two hours.

Two simulations using 20 days of data for the propagation path Hawaii to North Dakota were done. For these simulations the $n_1(t)$ data were concatenated since the data were consecutive, but each point in a set was shifted by an amount equal to the last point of the previous set to correct for the zeroing of the first point of each set as a reference. A plot of the timing error for the simulation based on the all-purpose model is given in Figure 31. The corresponding plot of the fractional frequency error is shown in Figure 32. The filter did not appear to diverge in this case, and the RMS error of 10.0 μsec as predicted by the Kalman filter compares well with the 9.5 μsec error observed. The RMS

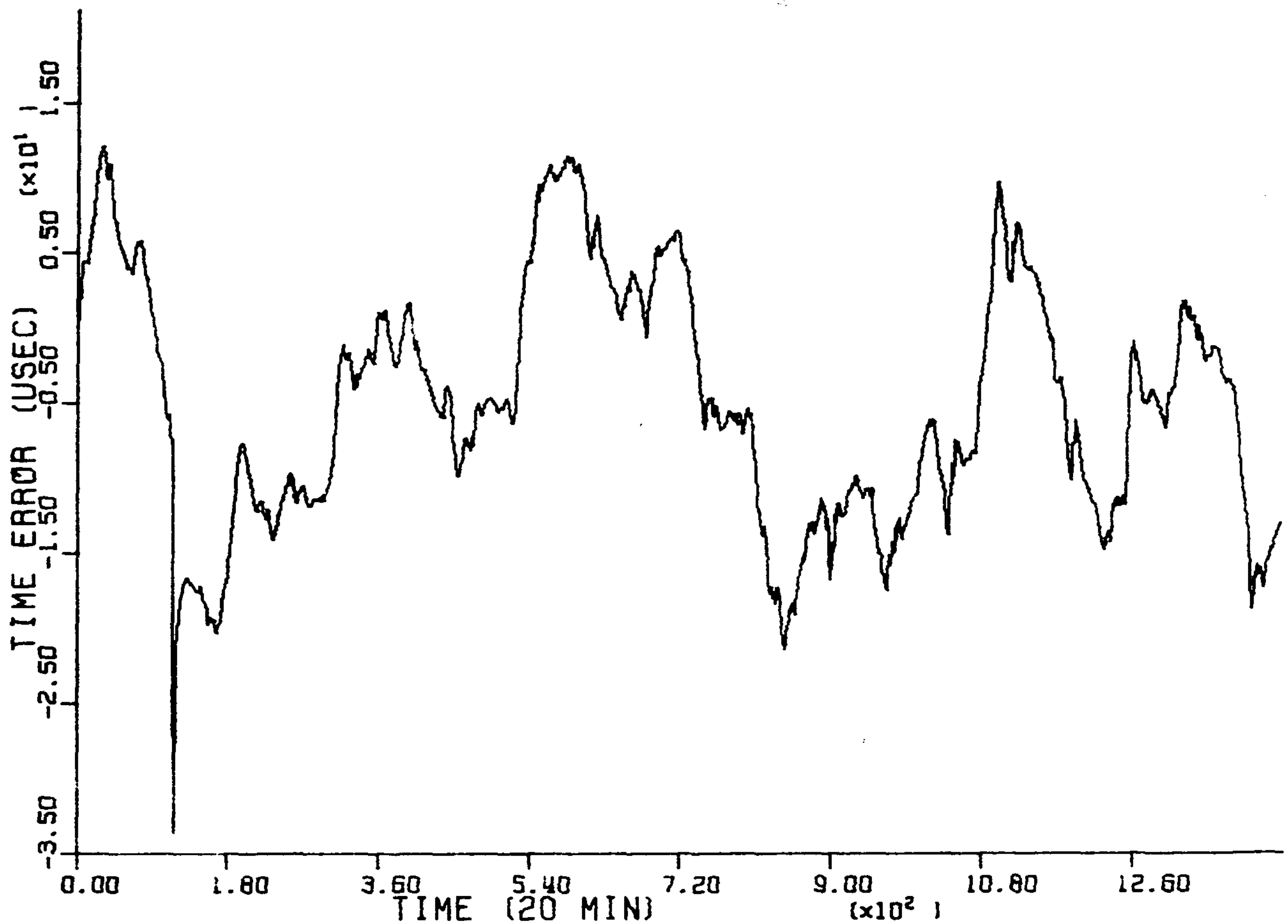

Figure 31. Simulated time error for the path Hawaii to N. Dakota and the all-purpose $n_2(t)$ model with the final $n_1(t)$ model

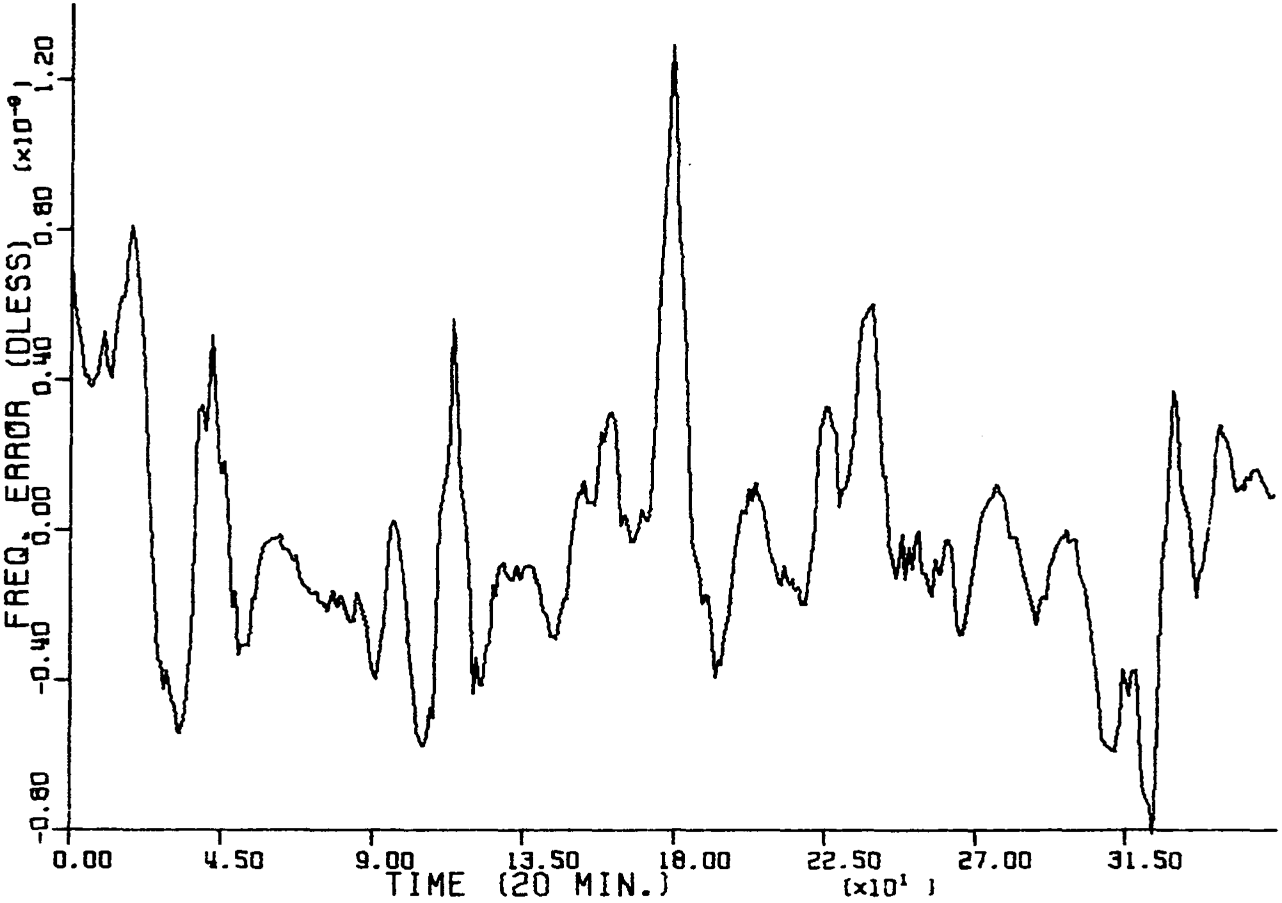

Figure 32. Simulated fractional frequency error corresponding to Figure 31

fractional frequency error was observed to be 3.16×10^{-10}. Plots of the timing error and the fractional frequency error for the simulation based on the special purpose model are shown in Figures 33 and 34, respectively. Again, the filter did not appear to diverge, and the predicted RMS error of 6.5 μsec compares well with the observed RMS error of 6.7 μsec. The observed RMS fractional frequency error was 4.26×10^{-10}.

These two simulations indicated that the final model for $n_1(t)$ and the special purpose and all purpose models for $n_2(t)$ were much better than the models originally used early in the investigation. In addition, the special-purpose filter performed better than the all-purpose filter as would be expected, but the RMS error of 6.5 μsec seemed to be the best one could do. Now that reasonably accurate models of the processes $n_1(t)$ and $n_2(t)$ were ascertained, simulations for both all purpose and special purpose models were done using the data for three other propagation paths.

Plots of the timing error for the simulations based on the all purpose model for the paths Trinidad to North Dakota, North Dakota to Hawaii, and Japan to Hawaii are given in Figures 35, 39 and 43, respectively. Corresponding fractional frequency error plots for these simulations are shown in Figures 36, 40, and 44, respectively. Plots of the timing error for the simulations based on the special purpose models for the same three paths are shown in Figures 37, 41, and 45, respectively, and the corresponding fractional frequency error plots are given in Figures 38, 42, and 46, respectively. None of these filter simulations appeared to

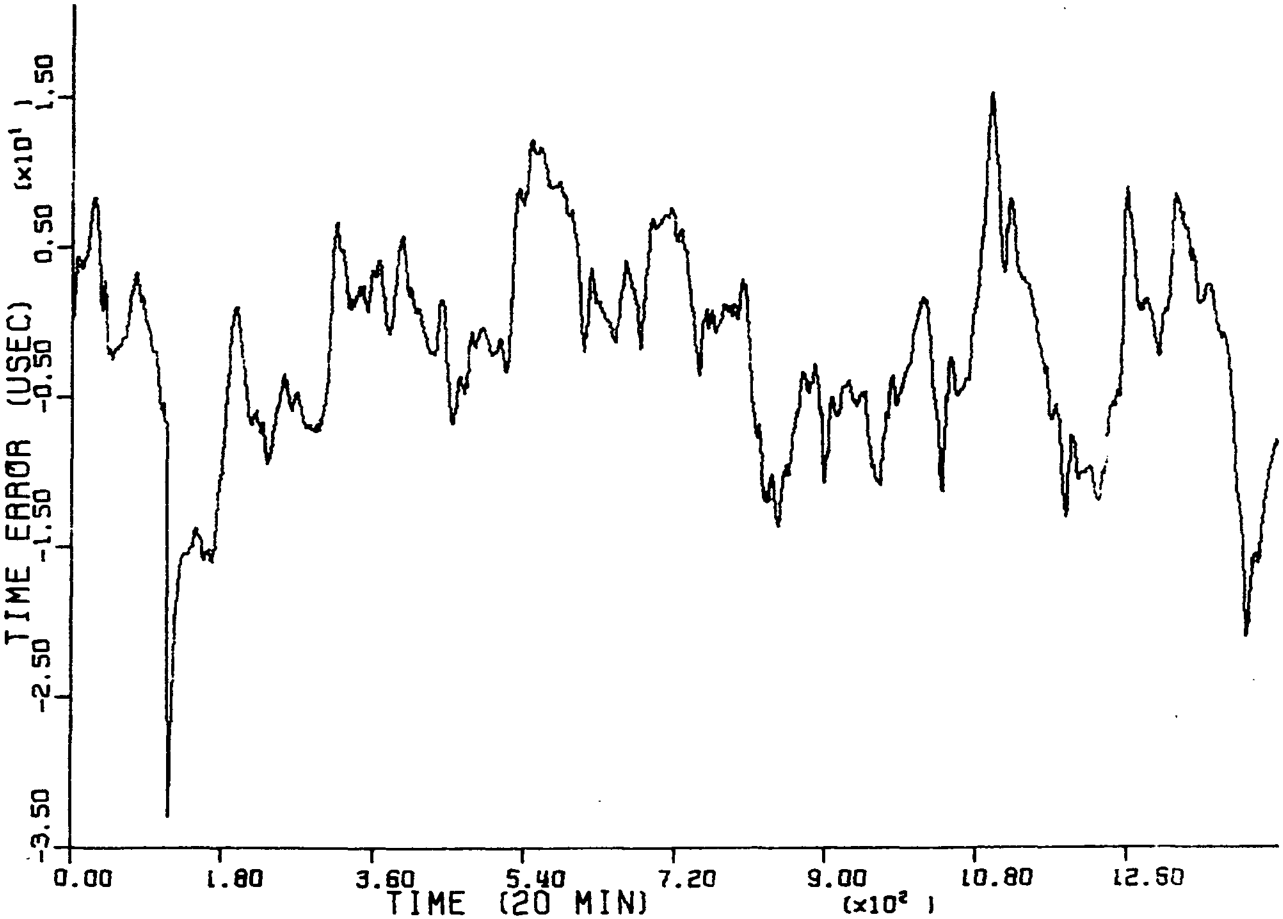

Figure 33. Simulated time error for the path Hawaii to N. Dakota and the special purpose $n_2(t)$ model with the final $n_1(t)$ model

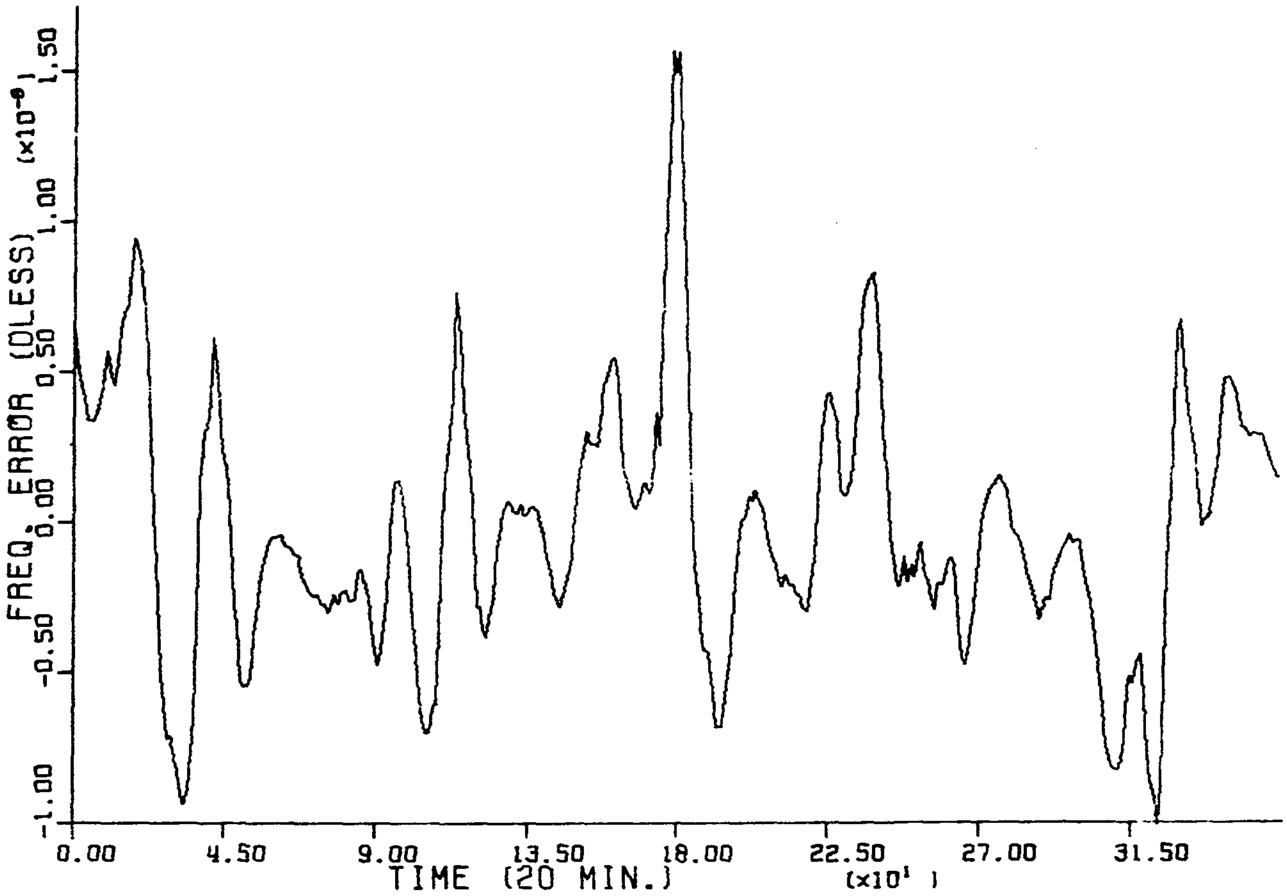

Figure 34. Simulated fractional frequency error corresponding to Figure 33

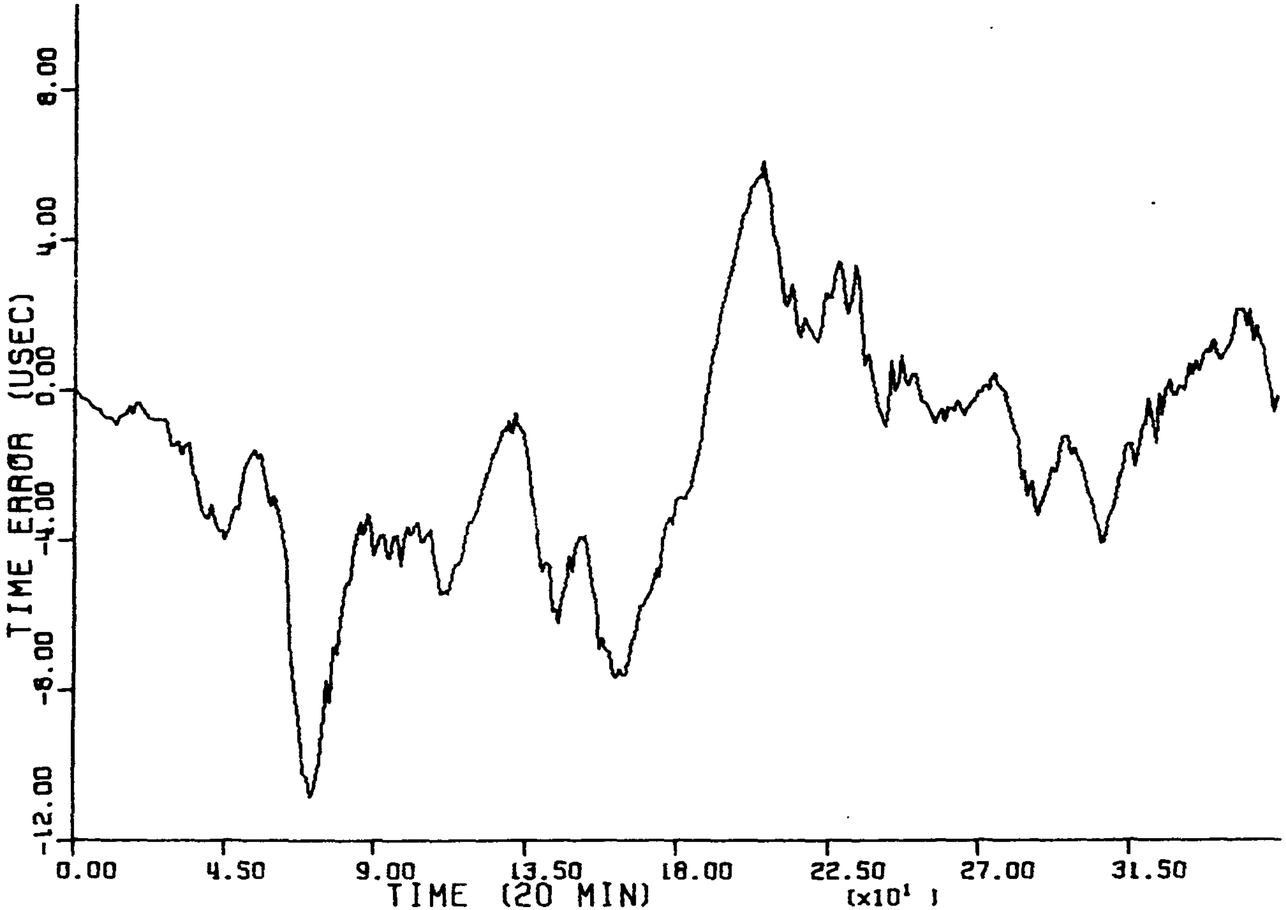

Figure 35. Simulated time error for the path Trinidad to N. Dakota and the all-purpose $n_2(t)$ model with the final $n_1(t)$ model

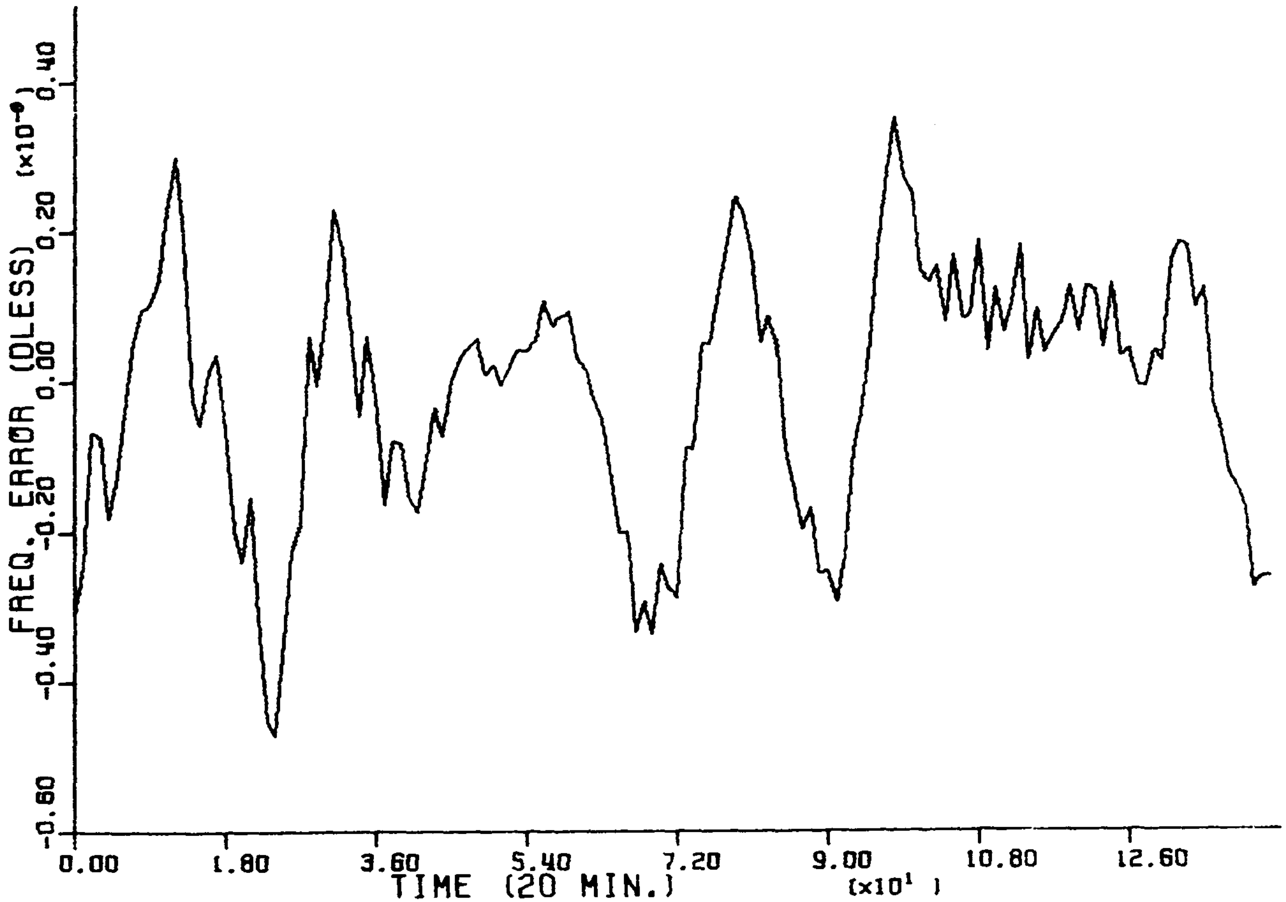

Figure 36. Simulated fractional frequency error corresponding to Figure 35

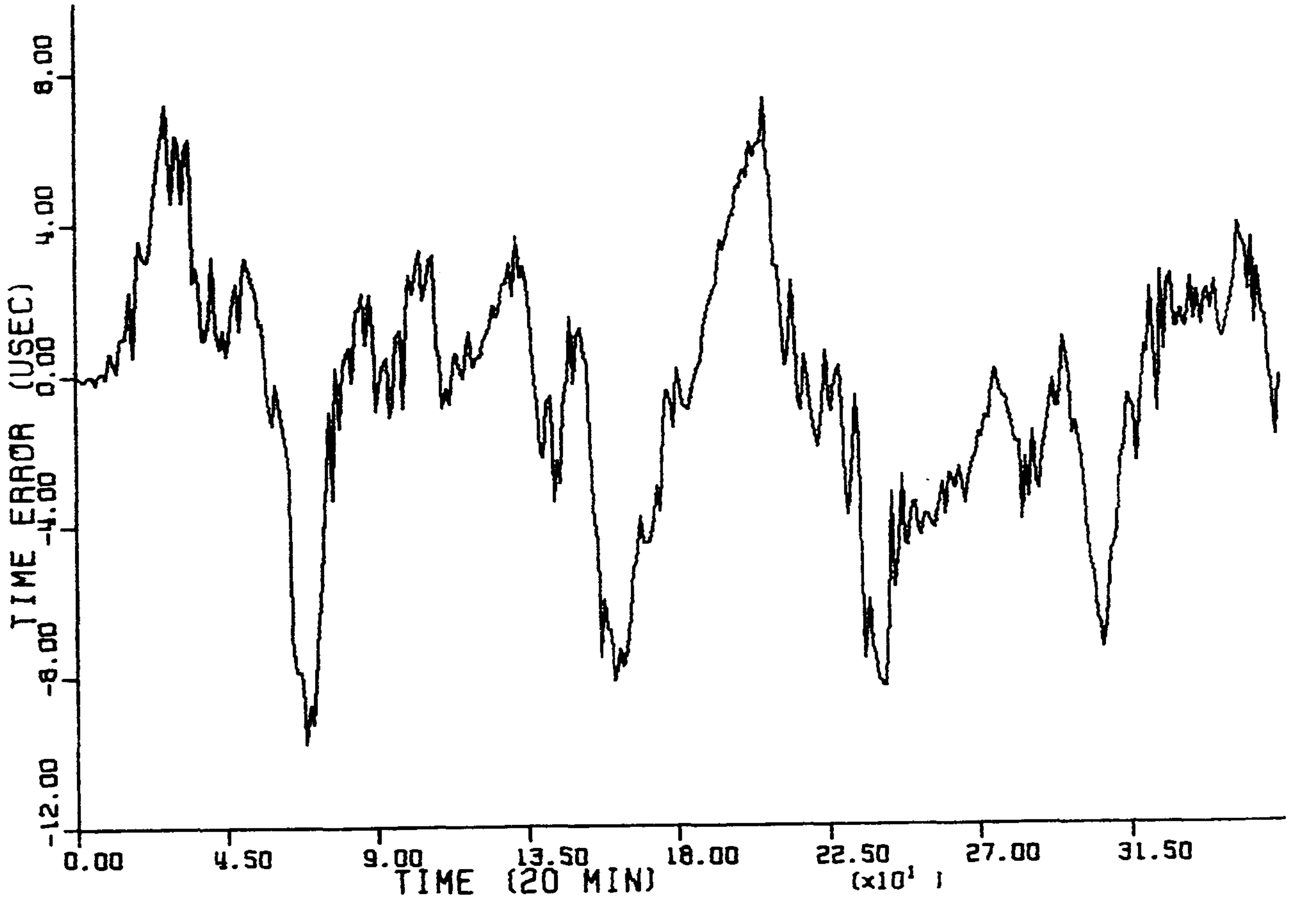

Figure 37. Simulated time error for the path Trinidad to N. Dakota and the special purpose $n_2(t)$ model with the final $n_1(t)$ model

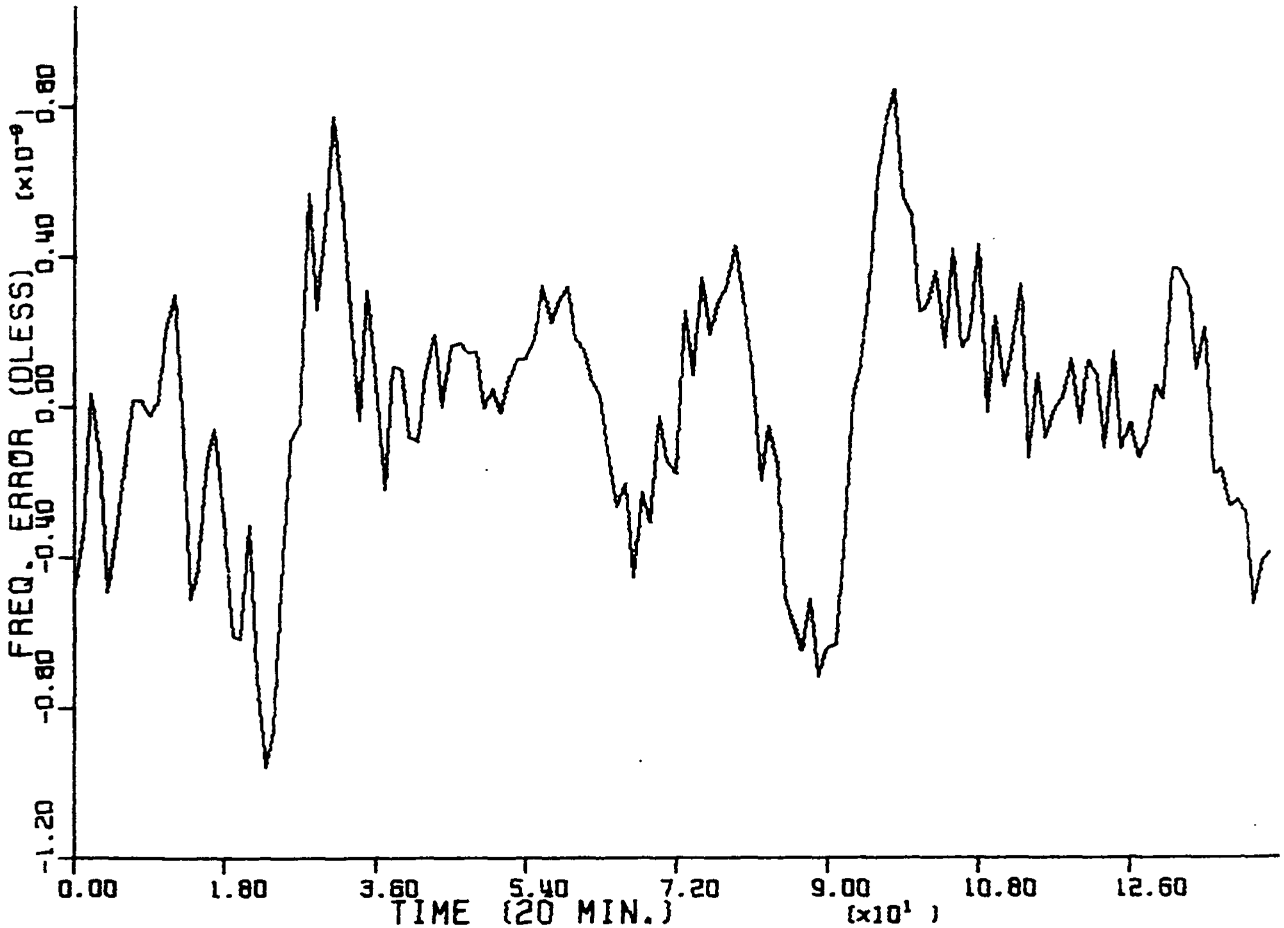

Figure 38. Simulated fractional frequency error corresponding to Figure 37

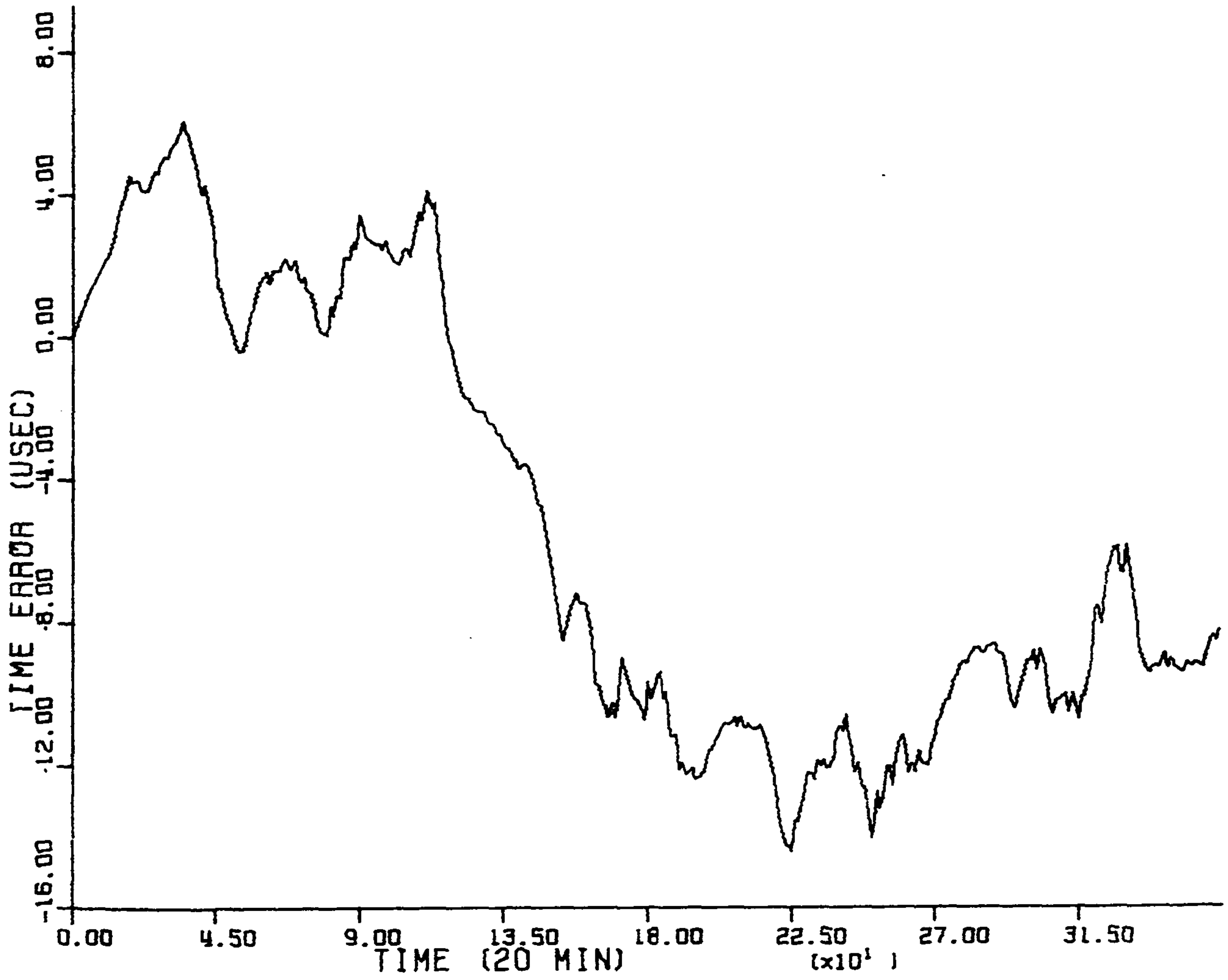

Figure 39. Simulated time error for the path N. Dakota to Hawaii and the all-purpose $n_2(t)$ model with the final $n_1(t)$ model

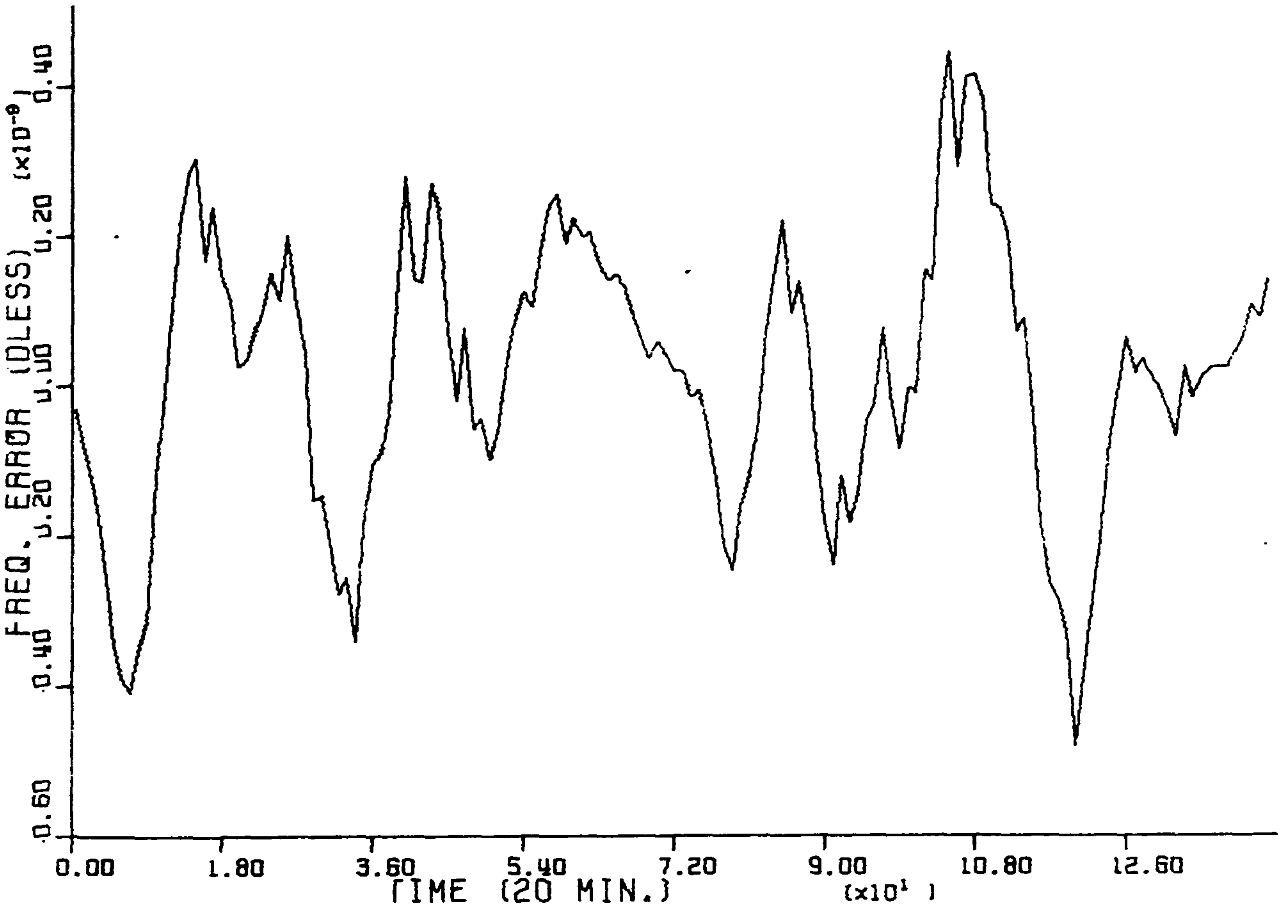

Figure 40. Simulated fractional frequency error corresponding to Figure 39

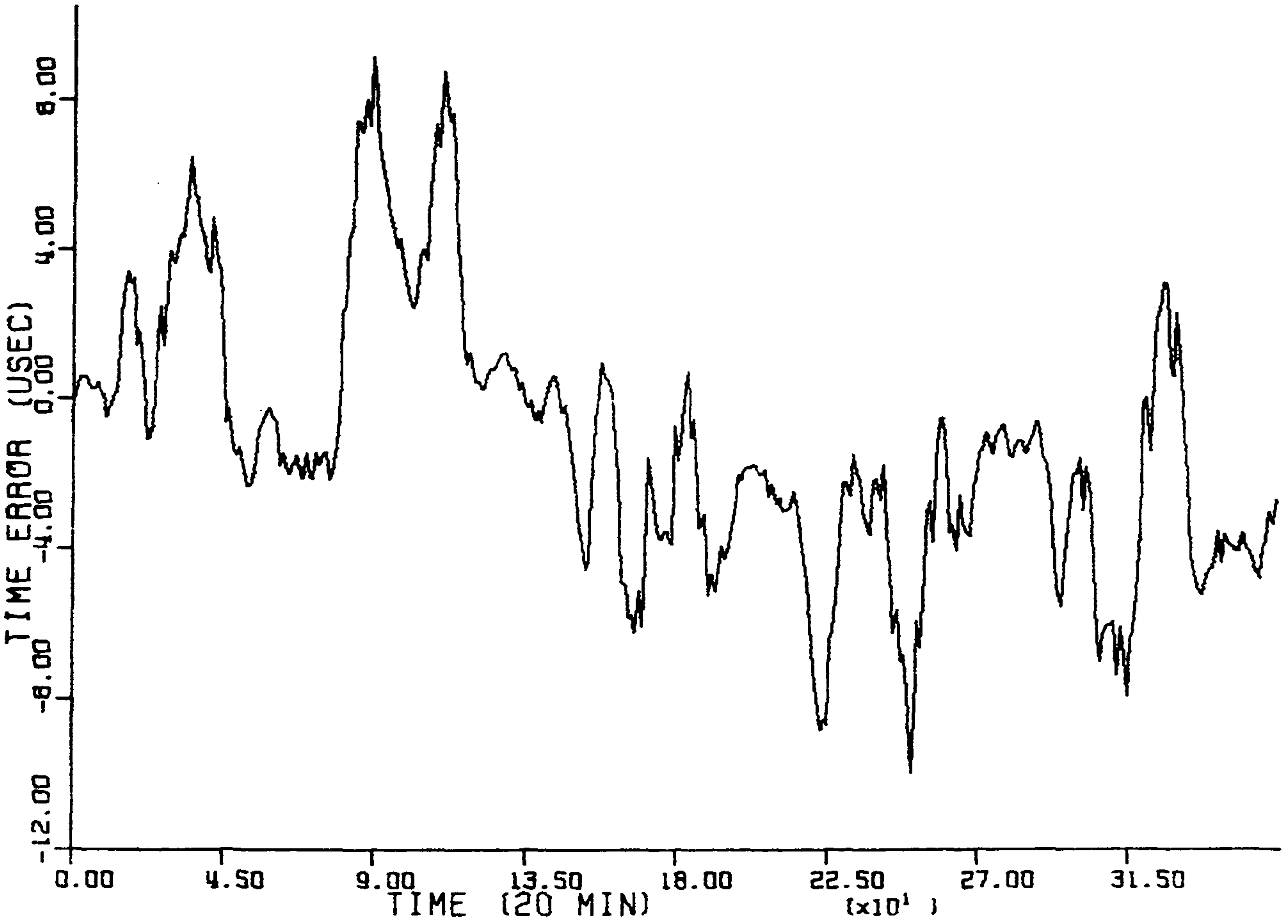

Figure 41. Simulated time error for the path N. Dakota to Hawaii and the special purpose $n_2(t)$ model with the final $n_1(t)$ model

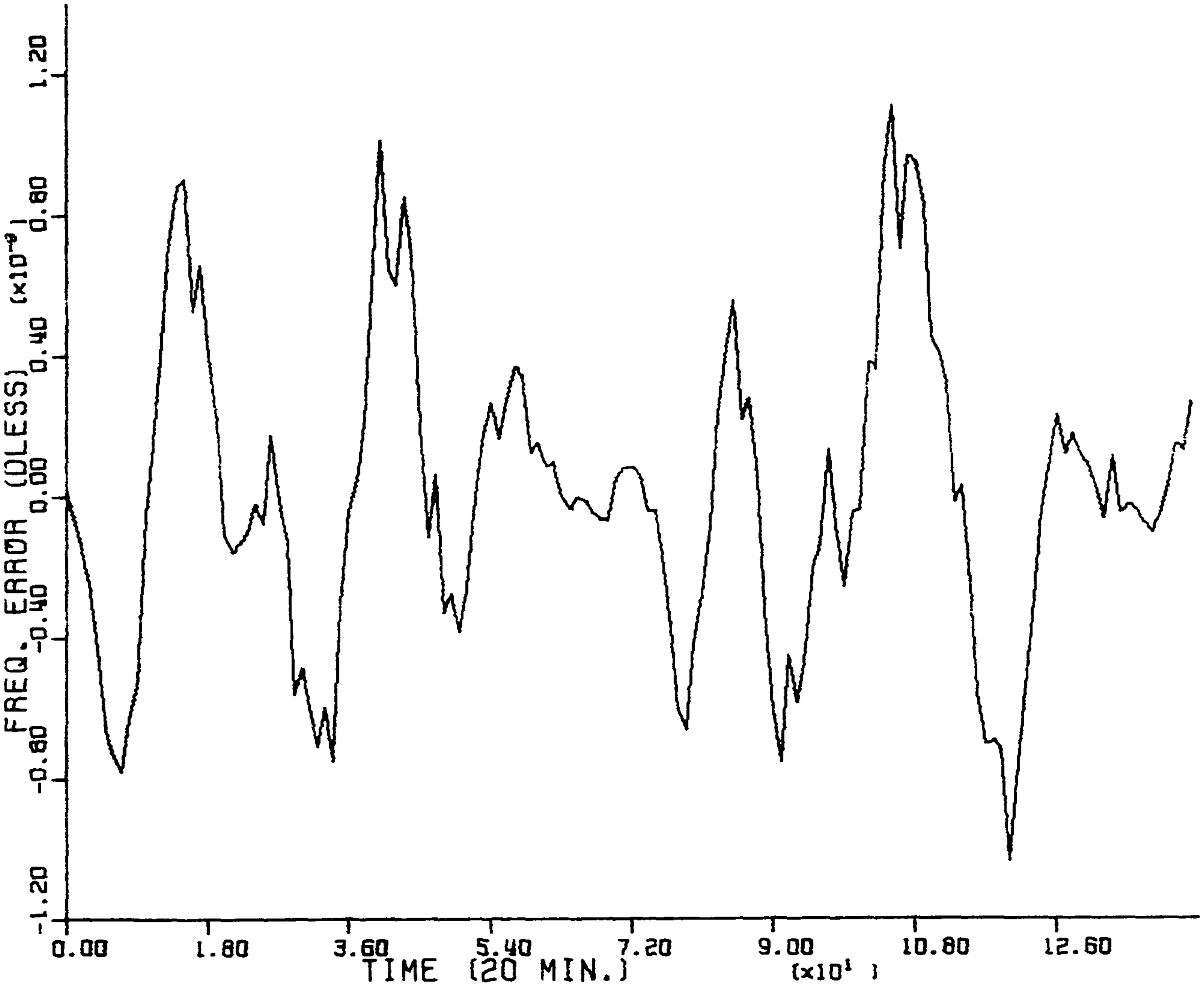

Figure 42. Simulated fractional frequency error corresponding to Figure 41

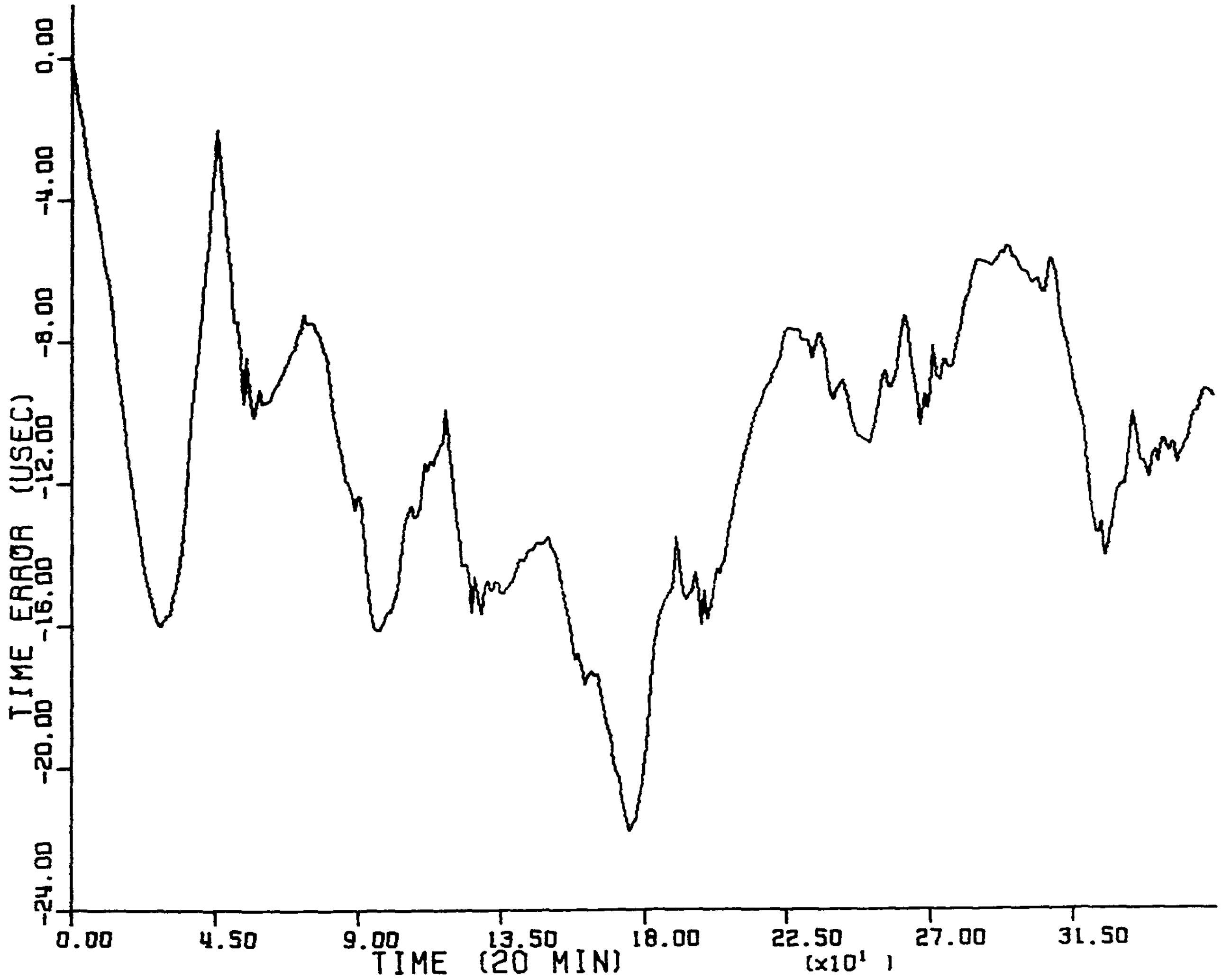

Figure 43. Simulated time error for the path Japan to Hawaii and the all-purpose $n_2(t)$ model with the final $n_1(t)$ model

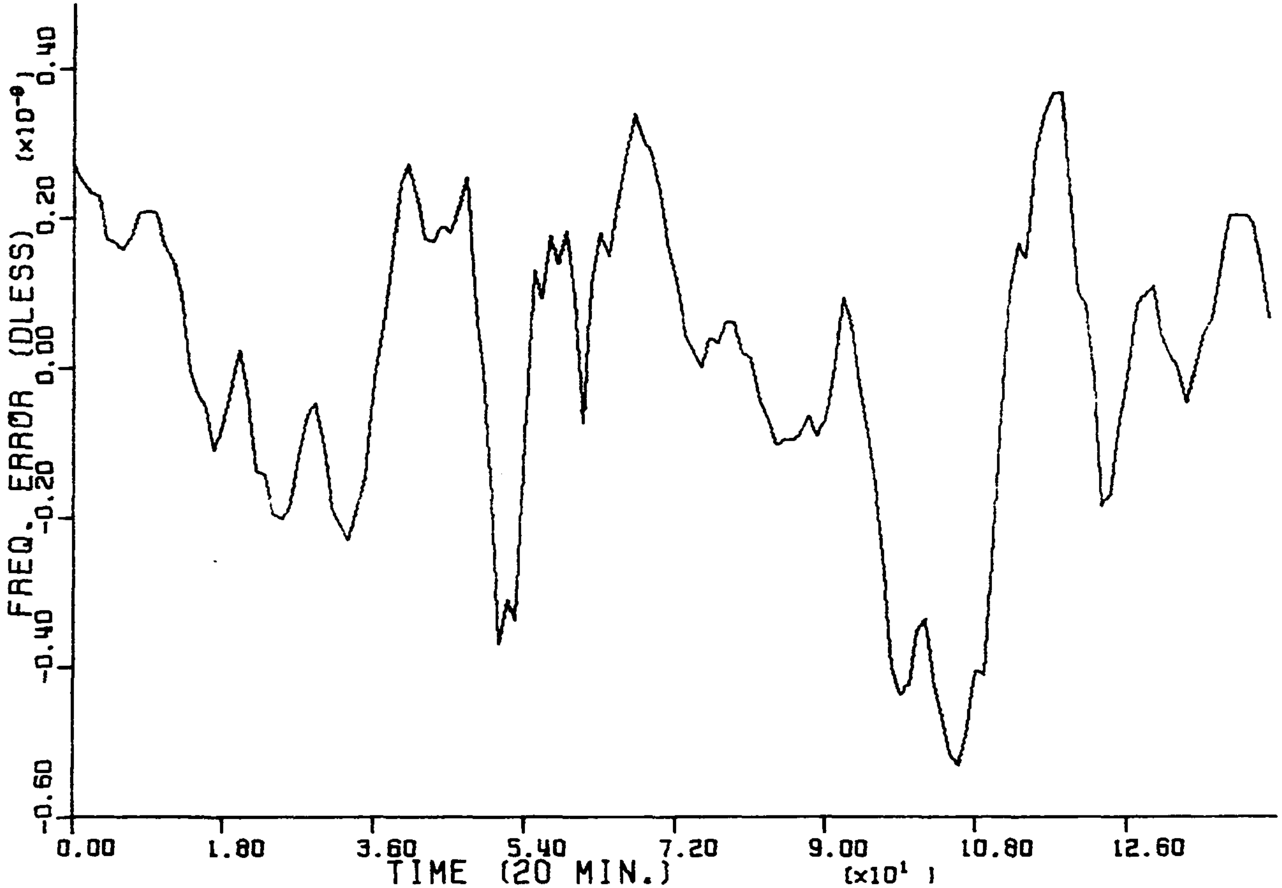

Figure 44. Simulated fractional frequency error corresponding to Figure 43

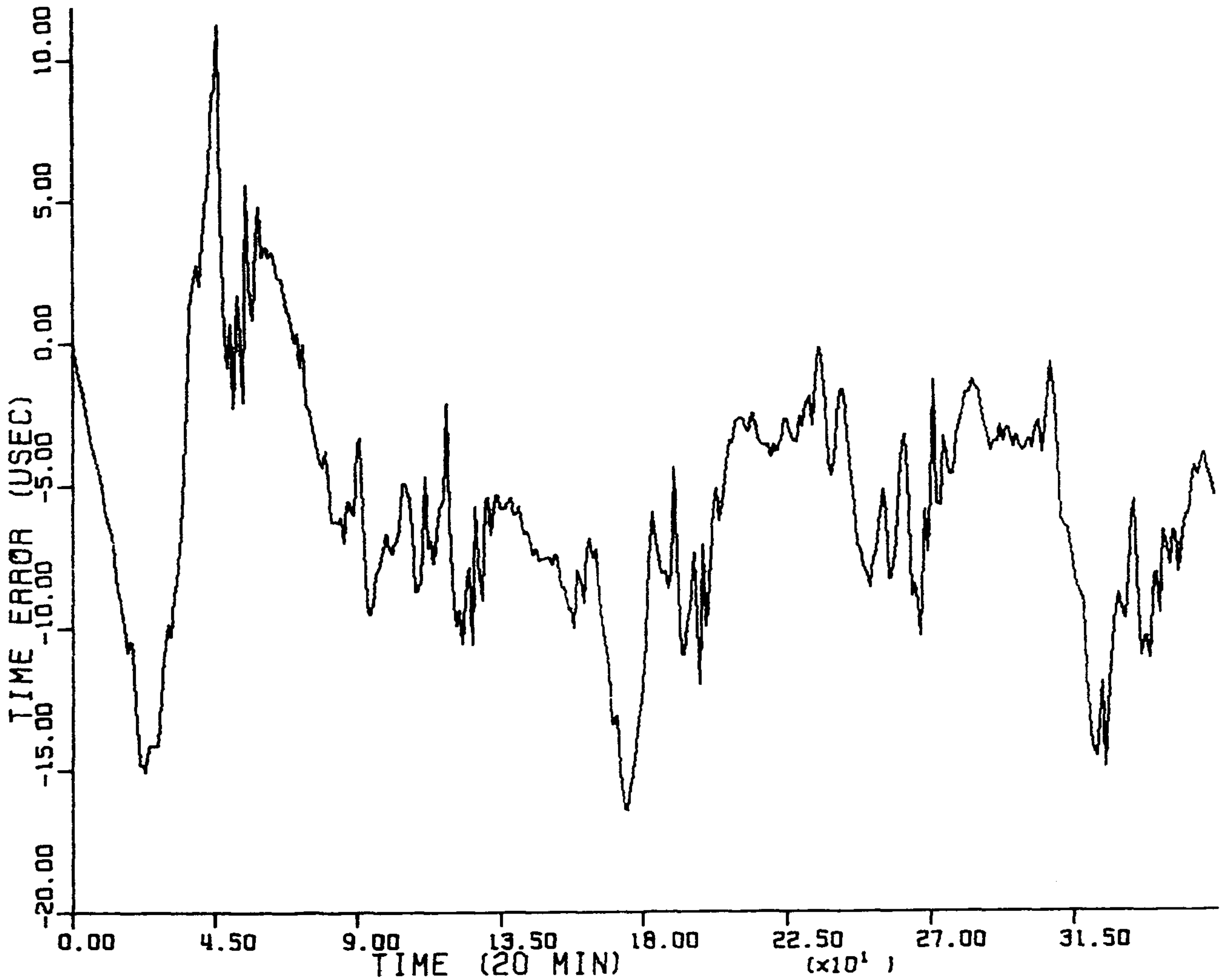

Figure 45. Simulated time error for the path Japan to Hawaii and the special purpose $n_2(t)$ model with the final $n_1(t)$ model

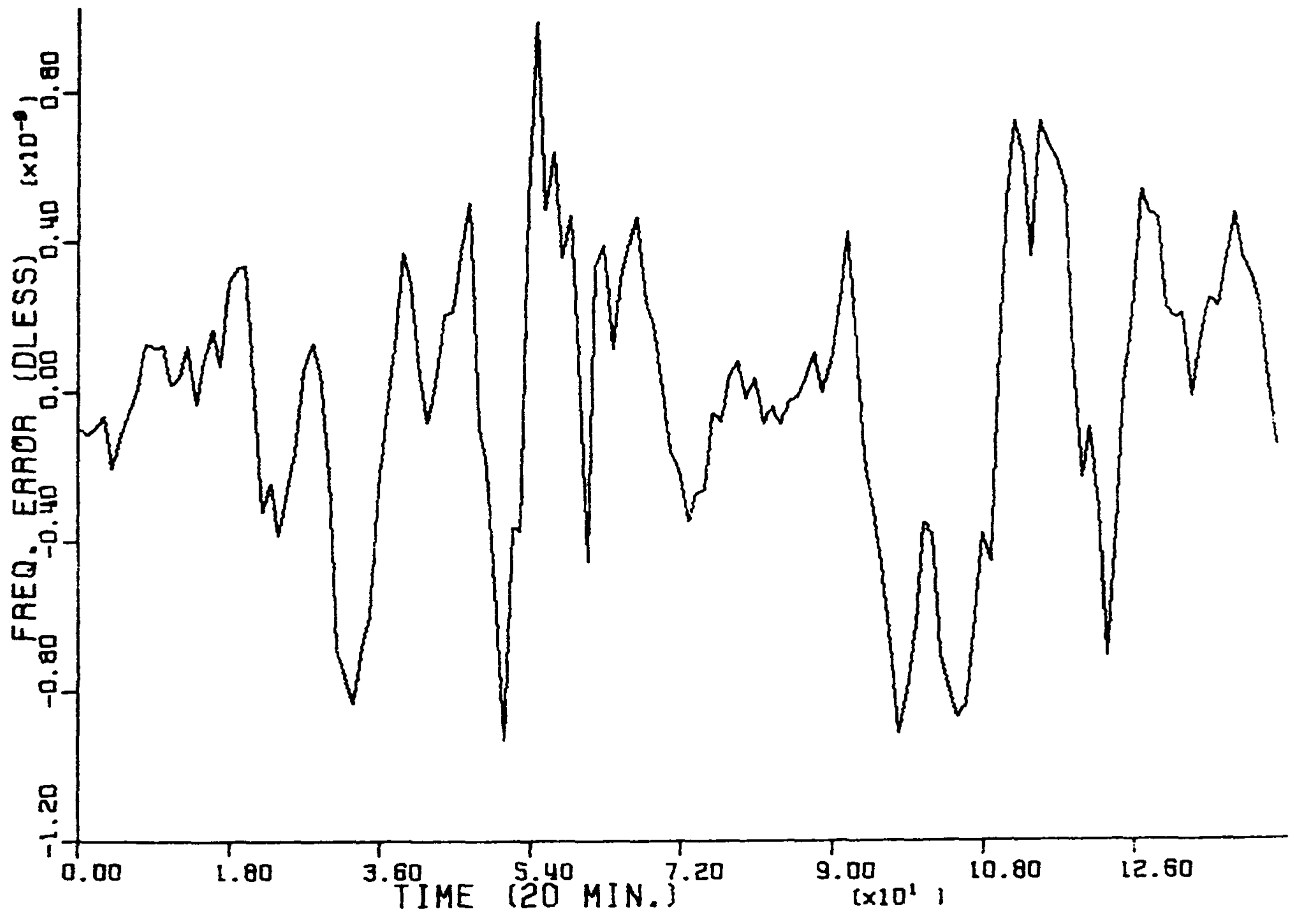

Figure 46. Simulated fractional frequency error corresponding to Figure 45

diverge, and the RMS timing error and fractional frequency error are summarized in Table 4.

Table 4. Summary of Kalman filter simulations

Simulation	RMS Timing Error Predicted	RMS Timing Error Observed	RMS Fractional Frequency Error x 10^{-10}
Hawaii to N. Dakota			
All Purpose	10.0	9.5	3.16
Special Purpose	6.5	6.7	4.26
Trinidad to N. Dakota			
All Purpose	10.0	3.1	1.64
Special Purpose	5.6	3.4	3.31
N. Dakota to Hawaii			
All Purpose	10.0	8.2	1.83
Special Purpose	4.0	3.7	4.31
Japan to Hawaii			
All Purpose	10.0	11.8	2.03
Special Purpose	6.5	7.2	3.86

As can be seen from Table 4 the predicted RMS values agree reasonably well with the observed RMS values. The only exception is the result for the path Trinidad to North Dakota and the all purpose model. The author regards this as a freak result. The RMS fractional frequency errors were all of the order of magnitude of 10^{-10}. The results in Table 4 strengthen the conclusions drawn on the basis of the 20-day simulations.

In light of these results the precise timing application is assessed next along with some concluding discussion of these results.

DISCUSSION OF RESULTS

Validity of the models

The essential results of the Kalman filter simulations described previously are summarized in Table 4. These results indicate that the two-state integrated Markov process model for $n_1(t)$ and the models for $n_2(t)$ are reasonably good since the models performed as expected as indicated by the Kalman filter error covariance matrix. The simulations done prior to the simulations summarized in Table 4 show that the random ramp plus random walk model for $n_1(t)$ is not valid because the Kalman filter simulations based on this model diverge and were not consistent with the errors as predicted by the Kalman filter error covariance matrix. Thus, one of the goals of this work, to obtain valid state-space models for the processes $n_1(t)$ and $n_2(2)$, has been accomplished.

Assessment of the precise timing scheme

From the simulation results summarized in Table 4 it appears that the precise timing scheme under consideration will produce an RMS timing error of 4 to 7 μsec using a special purpose $n_2(t)$ process model, or an RMS timing error of around 10 μsec using an all purpose model. Thus, it appears necessary to implement a Kalman filter based on a special purpose model for the particular propagation path to be used if this timing scheme is to be at all useful.

If a special purpose model is used, then the resulting RMS timing error of 4 to 7 μsec makes this precise timing system marginally useful; however, this RMS error is comparable to that demonstrated by the system considered by Chi and Wardrip (2), and the system considered here has the added advantage of being "closed-loop" in the sense that propagation tables are not necessary as they are in the system considered by Chi and Wardrip. Also, the RMS fractional frequency error of a few parts in 10^{-10} would allow this system to be useful on some occasions.

For example, one could calibrate a second frequency source to within a few parts in 10^{-10} by averaging over short periods of about two hours. Furthermore, this could be done at any time of day. One could not be restricted to the zero-diurnal shift periods, as could be the case if single frequency Omega were used as the remote reference. Also, it should be noted that this sytem, with a stability of roughly 4 parts in 10^{-10} for a two hour averaging time, is an improvement over the experimentally determined stability of about 7.5×10^{-10} for the oscillator used in this work.

Therefore, the optimal integration of composite Omega and local timing signals yields a timing system that is not spectacularly stable, but one that is still useful and probably better than other systems without optimal filtering, e.g. the system considered by Chi and Wardrip (2).

This assessment of the timing system completes the objectives of this work. A few ideas for additional investigation will be given next.

Possible further investigation

There are several possible topics for additional investigation related to this work. One might be an actual on-line implementation of the timing system using a microprocessor to experimentallly evaluate the timing system.

Another topic would be the development of an adaptive filter to determine the special purpose model parameters on-line. Also, the "seasonal" time series modeling techniques of Box and Jenkins (33) could be tried directly on the Omega data with some analytic diagnostic checking. It also would be interesting to try similar analyses using lower "composite" reference frequencies (e.g. 12.0 kHz) where there might be less noise but more diurnal shift.

REFERENCES

1. Wilson, J. J.; Britt, J. E.; and Chi, A. "Omega Timing Receiver, Design and System Test." Proc. of the 4th Annual NASA and Dept. of Defence Precise Time and Time Interval (PTTI) Planning Meeting, November 1972.

2. Chi, A. R., and Wardrip, S. C. "Clock Syncronization Experiments Using Omega Transmissions." Proc. of the 5th Annual NASA and Dept. of Defence Precise Time and Time Interval (PTTI) Planning Meeting, December 1973.

3. Swanson, E. R. "Omega VLF Timing." Proc. of the 25th Annual Symposium on Frequency Control, April 1971.

4. Brown, R. G.; Van Allen, R. L.; and Strohbehn, K. "Calculation of Omega Propagation Group Delay and Application to Local Time Standard Monitoring." Proc. of the 8th Annual Precise Time and Time Interval (PTTI) Planning Meeting, November 1976.

5. Beavers, A. N., Jr.; Gentry, D. E.; and Kasper, J. F., Jr. "Evaluation of Real-Time Algorithms for Omega Propagation Prediction." J. Inst. Navigation 22, No. 3, (Fall 1975), 252-258.

6. Pierce, J. A. "The Use of Composite Signals at Very Low Radio Frequencies." Harvard University Technical Report 552, February 1968.

7. Papousek, W., and Reder, F. H. "A Modified Composite Wave Technique for Omega." J. Inst. Navigation, 20, No. 2, (Summer 1973), 171-177.

8. Mactaggart, D. "An Empirical Computed Evaluation of Composite Omega." Proc. of the Second Omega Symposium (Sponsored by the Inst. of Navigation), November 1974.

9. Brown, R. G., and Van Allen, R. L. "Three Frequency Difference Omega." Proc. of the National Aerospace Symposium (Sponsored by the Inst. of Navigation), April 1976.

10. Brown, R. G.; Sharpe, R. A.; Hughes, W. L; and Post, R. E. <u>Lines, Waves, and Antennas</u>. 2nd ed. New York: Ronald Press, 1973.

11. Hampton, D. E. "Group Velocity Variations of V.L.F. Signals." Royal Aircraft Establishment Report No. 65282, December 1965.

12. Watt, A. D. <u>VLF Radio Engineering</u>. New York: Pergamon Press, 1967.

13. Cutler, L. S. "Stability Characteristics and Application Techniques for Precision Frequency Sources." Proc. of the 3rd Annual Dept. of Defense Precise Time and Time Interval (PTTI) Strategic Planning Meeting, November 1971.

14. Barnes, J. A.; Chi, A. R.; Cutler, L. S.; et al. "Characterization of Frequency Stability." IEEE Trans. Instrum. Meas., 20, No. 2, (1971), 105-120.

15. Winkler, G. M. R. "A Brief Review of Frequency Stability Measures." Proc. of the 8th Annual Precise Time and Time Interval (PTTI) Applications and Planning Meeting, December 1976.

16. Lindsey, W. C.; Chie, C. M.; and Leavitt, W. E. "Interpretation and Application of Oscillator Instability Measures Using Structure Functions." Proc. of the 8th Annual Precise Time and Time Interval (PTTI) Applications and Planning Meeting, December 1976.

17. Fischer, M. C. "Frequency Stability Measurement Procedures." Proc. of the 8th Annual Precise Time and Time Interval (PTTI) Applications and Planning Meeting, December 1976.

18. Barnes, J. A. "Models for the Interpretation of Frequency Stability Measurements." NBS TN 683, August 1976.

19. Allan, D. W. "Statistics of Atomic Frequency Standards." Proc. IEEE, 54, No. 2, (February 1966), 221-230.

20. Barnes, J. A. "Atomic Timekeeping and the Statistics of Precision Signal Generators." Proc. IEEE, 54, No. 2, (February 1966), 207-220.

21. Cutler, L. and Searle, C. "Some Aspects of the Theory and Measurement of Frequency Fluctuations in Frequency Standards." Proc. IEEE, 54, No. 2, (February 1966), 136-154.

22. Leeson, D. B. "A Simple Model of Feedback Oscillator Noise Spectrum." Proc. IEEE, 54, No. 2, (February 1966), 329-330.

23. Atkison, W. R.; Fey, R. L.; and Newman, J. "Spectrum Analysis of Extremely Low Frequency Variations of Quartz Oscillators." Proc. IEEE, 51, (February 1963), 379.

24. Brown, R. G., and Nilsson, J. W. Introduction to Linear Systems Analysis. New York: John Wiley and Sons, 1962.

25a. Strohbehn, K., and Brown, R. G. "Filtering Precise Time Signals." Proc. of the 21st Midwest Symposium on Circuits and Systems, August 1978.

25b. Van Allen, R. L. "Compensation for Propagation Uncertainties in the Omega Navigation System." Unpublished Ph.D. dissertation. Iowa State University, Ames, Iowa, 1976.

26. Gelb, Arthur, ed. Applied Optimal Estimation. Cambridge, Mass.: M.I.T. Press, 1974.

27. D'Appolito, J. A., and Kasper, J. F. "Predicted Performance of an Integrated Omega/Inertial Navigation System." Proc. of the National Aerospace Electronics Conference, May 1971.

28. Kerchner, R. M., and Corcoran, G. F. Alternating-Current Circuits. New York: John Wiley and Sons, 1952.

29. Bendat, J. S., and Piersol, A. G. Measurement and Analysis of Random Data. New York: John Wiley and Sons, 1968.

30. Strohbehn, K. "Filtering of Propagation Group Delay of Omega Navigation Signals." Unpublished M.S. thesis. Iowa State University, Ames, Iowa, 1977.

31. Santamore, H. J. "Omega Synchronization: Current Operations and Future Plans." Proc. of the 8th Annual PTTI Applications and Planning Meeting, December 1976.

32. Barnes, J. A., and Jarvis, S. "Efficient Numerical and Analog Modeling of Flicker Noise Processes." NBS TN 604, June 1971.

33. Box, G. E. P., and Jenkins, G. M. Time Series Analysis: Forecasting and Control. San Francisco: Holden-Day, 1976.

34. Omega Propagation Correction Tables. Washington, D.C.: Defense Mapping Agency Hydrographic Center, October 1972.

ACKNOWLEDGEMENTS

Many thanks are due to the various persons and institutions that made this work possible. In particular, the Department of Electrical Engineering and the Engineering Research Institute, Iowa State University, provided financial support in the form of a graduate assistantship, and Dr. R. Grover Brown provided valuable suggestions and guidance throughout the work. Dr. R. L. Van Allen was responsible for securing the Omega phase data, and Dr. and Mrs. A. M. Strohbehn provided encouragement and financial assistance. To all of the above, the author is indeed grateful.

Finally, this work is dedicated to Rosa Maria and Xochitl Sunshine Strohbehn for their patience and support and to Arthur and Dorothy Strohbehn for always encouraging the author in his studies.

APPENDIX A: CALCULATION OF THE COMPOSITE OMEGA SIGNAL

Consider three Omega phase measurements ϕ_1, ϕ_2, and ϕ_3 at frequencies ω_1, ω_2, and ω_3, respectively. A quadratic function

$$\phi(\omega) = \beta(\omega)d = k_0 + k_1\omega + k_2\omega^2$$

can be fit to these measurements. This yields

$$\phi_1 = k_0 + k_1\omega_1 + k_2\omega_1^2,$$

$$\phi_2 = k_0 + k_1\omega_2 + k_2\omega_2^2,$$

$$\phi_3 = k_0 + k_1\omega_3 + k_2\omega_3^2,$$

which can be solved for k_0, k_1, and k_2.

Recall that group delay T_g is given by

$$T_g = \frac{d}{v_g} = \frac{d}{(d\omega/d\beta)} = \frac{d\phi}{d\omega},$$

or

$$T_g = 2k_2\,\omega + k_1$$

in this case. Substitution of the solutions for k_0, k_1, and k_2 into the expression for T_g and using the proportional relationship

$$\omega_1 : \omega_2 : \omega_3 = 9:10:12$$

yields the desired expression

$$T_g(\omega) = c_1T_1 + c_2T_2 + c_3T_3, \tag{1a}$$

where

$$c_1 = 60\omega/\omega_2 - 66,$$

$$c_2 = -100\omega/\omega_2 + 105,$$

$$c_3 = 40\omega/\omega_2 - 38.$$

$$T_1 = \phi_1/\omega_1,$$

$$T_2 = \phi_2/\omega_2,$$

$$T_3 = \phi_3/\omega_3.$$

The composite time signal is then computed by using the appropriate phase measurements for ϕ_1, ϕ_2, and ϕ_3 in Equation 1a.

For the work described here the reference frequency was selected to be 12.47 kHz which is exactly halfway between the Omega broadcasts of 11 1/3 and 13.6 kHz. This frequency was chosen because it is close to the crossover point where the day and night group velocities are the same (recall Figure 3).

The variation of the group delay T_g is calculated by using the changes from the nominal phase delays as ϕ_1, ϕ_2, and ϕ_3 instead of the absolute phases of the signals.

APPENDIX B: ABSOLUTE PHASE OF OMEGA DATA

The Omega phase data available to the author were described previously, and were obtained by Dr. R. L. Van Allen and used in his dissertation (25b). The data were stripcharts of phase differences between the received Omega signal and a cesium-beam frequency standard at the appropriate frequency. Thus, the absolute phase of the Omega signal was not contained in the stripcharts. The absolute phase was recovered as follows.

A reading of Omega phase was taken for a particular propagation path, time of day, date, and frequency. A nominal LOP (line of position) number N was read from the propagation correction tables published by the United States Dept. of Defense (34) that corresponded to the path, time, date, and frequency. Also, the corresponding propagation correction PC was read. All readings were in cycles. Then the equation

$$P + PC + W = N \tag{1b}$$

where

$W = 900$ for 10.2 kHz,

$W = 1000$ for 11 1/3 kHz,

$W = 1200$ for 13.6 kHz,

and P is the absolute phase, would determine P exactly if the value of PC were exactly correct. Since PC is only a nominal correction, then P was only approximately determined by Equation 1b. However, this approximate value of P determined the correct number of cycles to add to the stripchart reading which then established the correct absolute phase reading for this particular data point. The absolute phase at one data point then established the absolute phase at all surrounding data points. This procedure was repeated a few times for each path and frequency as a check. An example follows.

As an example consider the path Hawaii to North Dakota, at 10.2 kHz, on 1 March 1975, at 0100 hours. The reading from the stripchart was 0.795 cycles. The corresponding correction was -0.170 cycles, and the corresponding LOP number was 1101.533 for the North Dakota receiver location. The Equation 1b yields

$$P + 900 - 0.170 = 1101.533$$

or

$$P = 201.703.$$

The reading of 0.795 corresponds most closely then to 201.795 cycles. This example illustrates the procedure used for recovering the absolute phase of the Omega data.

APPENDIX C: DERIVATION OF EQUATION 3

Recall Equation 2 of the text, which for convenience is repeated here as Equation 1c.

$$\dot{x} = \begin{bmatrix} -b & 0 & 0 & 0 & 0 \\ 0 & 0 & \omega_0 & 0 & 0 \\ 0 & -\omega_0 & 0 & 0 & 0 \\ 0 & 0 & 0 & 0 & \omega_1 \\ 0 & 0 & 0 & -\omega_1 & 0 \end{bmatrix} x + \begin{bmatrix} \sqrt{2ab}w(t) \\ 0 \\ 0 \\ 0 \\ \end{bmatrix}$$

where w(t) is unity white noise. The solution of Equation 1c is clearly given by

$$x(t) = \begin{bmatrix} \tilde{A} & 0 & 0 & 0 & 0 \\ 0 & \tilde{B} & \tilde{C} & 0 & 0 \\ 0 & -\tilde{C} & \tilde{B} & 0 & 0 \\ 0 & 0 & 0 & \tilde{D} & \tilde{E} \\ 0 & 0 & 0 & -\tilde{E} & \tilde{D} \end{bmatrix} x(0) + \begin{bmatrix} \tilde{F} \\ 0 \\ 0 \\ 0 \\ 0 \end{bmatrix}$$

where

$$\tilde{A} = e^{-bt},$$

$$\tilde{B} = \cos(\omega_0 t),$$

$$\tilde{C} = \sin(\omega_0 t),$$

$$\tilde{D} = \cos(\omega_1 t),$$

$$\tilde{E} = \sin(\omega_1 t),$$

$$\tilde{F} = \sqrt{2ab} \int_0^t e^{-b(t-\tau)} w(\tau) d\tau .$$

Then, clearly

$$E[F] = 0,$$

and

$$E[F^2] = 2abE[\int_0^t\int_0^t e^{-2bt}e^{b(\tau+u)}w(\tau)w(u)d\tau du]$$

$$= 2abe^{-2bt}\int_0^t\int_0^t e^{b(\tau+u)}E[w(\tau)w(u)]d\tau du$$

$$= 2abe^{-2bt}\int_0^t\int_0^t e^{b(\tau+u)} \quad \delta(\tau-u)d\tau u$$

$$= 2abe^{-2bt}\int_0^t e^{2bu}du$$

$$= a(1-e^{-2bt}).$$

Since Equation 1c is time invariant and w(t) is a white noise, then the solution of Equation 1 at times t_k where

$$\Delta T = t_k - t_{k-1}$$

is given by Equation 3c as

$$x_k = \begin{bmatrix} A & 0 & 0 & 0 & 0 \\ 0 & B & C & 0 & 0 \\ 0 & -C & B & 0 & 0 \\ 0 & 0 & 0 & D & E \\ 0 & 0 & 0 & -E & D \end{bmatrix} x_{k-1} + \begin{bmatrix} F \\ 0 \\ 0 \\ 0 \\ 0 \end{bmatrix} \tag{3c}$$

where

$$A = e^{-b\Delta T},$$

$$B = \cos(\omega_0\Delta T),$$

$$C = \sin(\omega_0\Delta T),$$

$$D = \cos(\omega_1 \Delta T),$$

$$E = \sin(\omega_1 \Delta T),$$

$$E[F] = 0,$$

$$E[F^2] = a(1-e^{-2b\Delta T}).$$

Equation 3c is the desired result.

APPENDIX D: DERIVATION OF THE SIMULATION EQUATIONS

In this appendix Equations 16 through 27 of the text will be derived. First, consider the general form of the $n_2(t)$ process model given by Equation 2 of the text and the original $n_1(t)$ process model given by Equation 4 of the text. Let y be the state vector of the $n_2(t)$ process and z be the state vector of the $n_1(t)$ process, and then form a new augmented state vector

$$x^T = [y^T \ z^T].$$

It then follows from Equations 2 and 4 that $x \in R^8$, the augmented state vector satisfies

$$\dot{x} = \begin{bmatrix} -b & 0 & 0 & 0 & 0 & 0 & 0 & 0 \\ 0 & 0 & \omega_0 & 0 & 0 & 0 & 0 & 0 \\ 0 & -\omega_0 & 0 & 0 & 0 & 0 & 0 & 0 \\ 0 & 0 & 0 & 0 & \omega_1 & 0 & 0 & 0 \\ 0 & 0 & 0 & -\omega_1 & 0 & 0 & 0 & 0 \\ 0 & 0 & 0 & 0 & 0 & 0 & 0 & 0 \\ 0 & 0 & 0 & 0 & 0 & 0 & 0 & 1 \\ 0 & 0 & 0 & 0 & 0 & 0 & 0 & 0 \end{bmatrix} x + \begin{bmatrix} \sqrt{2a\bar{b}}w(t) \\ 0 \\ 0 \\ 0 \\ 0 \\ u(t) \\ 0 \\ 0 \end{bmatrix} \tag{1d}$$

and

$$n_1(t)-n_2(t) = [-1 \ -1 \ 0 \ -1 \ 0 \ 1 \ 1 \ 0]x \tag{2d}$$

where the parameters are defined for Equations 2 and 4 of the text. Equations 16 through 19 of the text follow from Equations 1d and 2d analogously with Appendix C.

The statistics of the initial state of the $n_2(t)$ process are given with Equation 2 in the text. The original model for $n_1(t)$ would have initial state statistics

$$E[x(0)]^T = [0\ 0\ m],$$

$$E[x(0)x^T(0)] = \mathrm{diag}(0\ 0\ \sigma_k^2) \tag{3d}$$

which follow from the original model statistics for $n_1(t)$ and Figure 21. The initial conditions x_0^- and P_0^- are chosen as

$$\hat{x}_0^- = E[x(0)],$$

$$P_0^- = E[x(0)x^T(0)]$$

which yield Equations 20 and 21 of the text.

Next, consider the final model for the $n_1(t)$ process together with the $n_2(t)$ process model. These are given by Equations 11 and 2 of the text, respectively. Forming an augmented state vector $x \epsilon R^7$ as before results in the equations

$$\dot{x} = \begin{bmatrix} -b & 0 & 0 & 0 & 0 & 0 & 0 \\ 0 & 0 & \omega_0 & 0 & 0 & 0 & 0 \\ 0 & -\omega_0 & 0 & 0 & 0 & 0 & 0 \\ 0 & 0 & 0 & 0 & \omega_1 & 0 & 0 \\ 0 & 0 & 0 & -\omega_1 & 0 & 0 & 0 \\ 0 & 0 & 0 & 0 & 0 & -b & 0 \\ 0 & 0 & 0 & 0 & 0 & 1 & 0 \end{bmatrix} x + \begin{bmatrix} \sqrt{2a\bar{b}}w(t) \\ 0 \\ 0 \\ 0 \\ 0 \\ \sqrt{2\acute{a}\bar{b}}u(t) \\ 0 \end{bmatrix} \tag{4d}$$

and

$$n_1(t)-n_2(t) = [-1\ -1\ 0\ -1\ 0\ 1\ 0]x. \tag{5d}$$

Analogously with Appendix C, Equations 4d and 5d yield Equations 22 and 24 of the text as well as

$$Q_k = \begin{bmatrix} F & 0 & 0 & 0 & 0 & 0 & 0 \\ 0 & 0 & 0 & 0 & 0 & 0 & 0 \\ 0 & 0 & 0 & 0 & 0 & 0 & 0 \\ 0 & 0 & 0 & 0 & 0 & 0 & 0 \\ 0 & 0 & 0 & 0 & 0 & 0 & 0 \\ 0 & 0 & 0 & 0 & 0 & Y & 0 \\ 0 & 0 & 0 & 0 & 0 & 0 & 0 \end{bmatrix} \quad \forall k. \tag{6d}$$

A standard method of mitigating filter divergence problems associated with "deterministic" or perfectly correlated states is to add small white-noise driving terms (26). This changes the Q_k expression and was done as follows.

Assuming the additive noises are independent and affect each state equally with the change in variance arbitrarily set to 10 percent over a time span of 100 data points yields the values of U and V in Equations 23 and 26 of the text.

The change in slope of the $n_1(t)$ data appeared to be roughly 40 percent over a time span of 100 points. The output of the integrator is perfectly correlated with the Markov process input in the final $n_1(t)$ model. Assume then arbitrarily that a noise changes the output 4 percent over 100 data points. This yields the value of Z in Equation 23 of the text. As can be seen, these values U, V, and Z are arbitrary, but reasonable. These values U, V, and Z and Equation 6d yield Equation 23 of the text. Equations 25 and 26 of the text are derived in exactly the same manner as Equations 20 and 21 of the text.

Recall Equation 17 of the text. The same values U, V, and Z just discussed were used to produce Equation 27 of the text. The value of r along with U, V, and Z and Equation 17 yields Equation 27 of the text. These Equations 16 through 27 are the desired results to be used in the Kalman filter simulations.

APPENDIX E: SIMULATION PROGRAM

The simulations described in this work were done at the Iowa State University Computation Center and were programmed in Fortran. The following computer listing is a listing for a Kalman filter simulation using 5 days of data and the special purpose model for Japan to Hawaii. The programs for the other simulations were similar and will be omitted.

```
C
C     KALMAN FILTER SIMULATION PROGRAM USING REAL OMEGA PHASE DATA
C     AND REAL LOCAL OSCILLATOR DRIFT DATA
C
      REAL K(8)
      REAL R1(8)
      DIMENSION P1(360),P2(360),P3(360),D(60),DR(360),TS(360),Z(360)
      DIMENSION X(8),P(8,8),H(8),PHI(8,8),Q(8,8),TE(8),TF(8),ET(8,8)
      DIMENSION EE(8,8),V(8,8),ER(360),XX(360)
      DIMENSION FE(144)
C
C     AQUIRE PHASE MEASUREMENTS
C
      WRITE(6,1)
    1 FORMAT('1',10X,'PHASE DATA (CYCLES)')
      DO 10 I=1,360
      READ(5,2) P1(I),P2(I),P3(I),ID
    2 FORMAT(3F10.3,19X,I1)
      N=I-1
      WRITE(6,3) P1(I),P2(I),P3(I),ID,N
    3 FORMAT(' ',10X,3F10.3,19X,I1,26X,I4)
   10 CONTINUE
C
C     AQUIRE DRIFT MEASUREMENTS
C
      WRITE(6,4)
    4 FORMAT('1',10X,'DRIFT DATA (USEC)')
      DO 20 I=1,60
      READ(5,5) D(I),IDA
    5 FORMAT(F10.2,39X,I1)
      N=I-1
      WRITE(6,6) D(I),IDA,N
    6 FORMAT(' ',10X,F10.2,39X,I1,27X,I3)
   20 CONTINUE
      WRITE(6,7) ID,IDA
```

```
    7 FORMAT('1',10X,'PATH=',I1,10X,'DRIFT SET=',I1)
C
C     INTERPOLATE DRIFT MEASUREMENTS
C
      WRITE(6,8)
    8 FORMAT('-',10X,'INTERPOLATED DRIFT DATA (USEC)')
      DO 30 I=1,59
      J=I+1
      DO 30 L=1,6
      N=L-1
      M=L+(I-1)*6
      DR(M)=D(I)+(D(J)-D(I))/6.*FLOAT(N)
      WRITE(6,9) DR(M),M
    9 FORMAT(' ',10X,F10.2,39X,I4)
   30 CONTINUE
      DO 40 L=1,6
      N=L-1
      M=354+L
      DR(M)=D(60)+(D(60)-D(59))/6.*FLOAT(N)
      WRITE(6,9) DR(M),M
   40 CONTINUE
C
C     READ REFERENCE FREQUENCY F
C
      READ(5,11) F
   11 FORMAT(F10.3)
      WRITE(6,12) F
   12 FORMAT('1',10X,'REFERENCE FREQUENCY=',F10.3,' KHZ')
C
C     DETERMINE COMPOSITE TIME SIGNAL ERROR
C
      WRITE(6,15)
   15 FORMAT('1',10X,'COMPOSITE TIME SIGNAL ERROR (USEC)')
      C1=(60.*F/34.*3.)-66.
      C2=(-100.*F/34.*3.)+105.
```

```
      C3=(40.*F/34.*3.)-38.
      SUM1=0.
      SUM2=0.
      DO 50 I=1,360
      T1=P1(I)/10200.*1000000.
      T2=P2(I)/34000.*3000000.
      T3=P3(I)/13600.*1000000.
      TS(I)=C1*T1+C2*T2+C3*T3
      SUM1=SUM1+TS(I)/360.
   50 CONTINUE
C
C     DETERMINE MEASUREMENTS Z
C
      DO 60 I=1,360
      Z(I)=TS(I)-SUM1
      N=I-1
      WRITE(6,14) Z(I),N
   14 FORMAT(' ',10X,E16.6,40X,I3)
   60 CONTINUE
      WRITE(6,13)
   13 FORMAT('1',10X,'MEASUREMENTS (USEC)')
      DO 70 I=1,360
      Z(I)=DR(I)-Z(I)
      N=I-1
      WRITE(6,14) Z(I),N
   70 CONTINUE
C
C     INPUT MODEL PARAMETERS AND INITIAL CONDITIONS
C
      IFLAG=0
      CALL PARM(X,P,H,PHI,Q,R)
C
C     WRITE PARAMETERS
C
      WRITE(6,75)
```

```
 75 FORMAT('1',60X,'SYSTEM MODEL'/'-',62X,'Q-MATRIX'/'-',8X,'1',
   *15X,'2',15X,'3',15X,'4',15X,'5',15X,'6',15X,'7',15X,'8'/)
    DO 110 I=1,8
    WRITE(6,16) I,(Q(I,J),J=1,8)
 16 FORMAT(' ',I1,1X,8E16.6)
110 CONTINUE
    WRITE(6,17)
 17 FORMAT('-',57X,'TRANSITION MATRIX'/'-',8X,'1',15X,'2',15X,'3',
   *15X,'4',15X,'5',15X,'6',15X,'7',15X,'8'/)
    DO 120 I=1,8
    WRITE(6,16) I,(PHI(I,J),J=1,8)
120 CONTINUE
    WRITE(6,18)
 18 FORMAT('-',45X,'H-VECTOR',10X,'MEASUREMENT COVARIANCE R')
    WRITE(6,19) H(1),R
 19 FORMAT('-',38X,'1',2X,EI6.6,14X,E16.6)
    DO 130 I=2,8
    WRITE(6,21) I,H(I)
 21 FORMAT(' ',38X,I1,2X,E16.6)
130 CONTINUE
    WRITE(6,22)
 22 FORMAT('-',57X,'INITIAL CONDITIONS'/'-',62X,'P-MATRIX'/'-',8X,
   *'1',15X,'2',15X,'3',15X,'4',15X,'5',15X,'6',15X,'7',15X,'8'/)
    DO 140 I=1,8
    WRITE(6,16) I,(P(I,J),J=1,8)
140 CONTINUE
    WRITE(6,23)
 23 FORMAT('-',61X,'ESTIMATE X')
    DO 150 I=1,8
    WRITE(6,24) I,X(I)
 24 FORMAT(' ',50X,I1,7X,E16.6)
150 CONTINUE
    WRITE(6,26)
 26 FORMAT('1',56X,'KALMAN FILTER RESULTS'/' ',59X,'8-STATE FILTER'/
   *' ',38X,'RESULTS IN USEC OR USEC**2 OR DIMLESS WHERE APPROPRIATE')
```

```
C
C     8-STATE KALMAN FILTER
C
C
C     READ MAXIMUM RESIDUAL AGC AND END OF TRANSIENT PERIOD IEND
C
      READ(5,306) AGC,IEND
  306 FORMAT(F10.2,I3)
      DO 80 II=1,360
C
C     COMPUTE GAINS
C
      IT=1
      CALL VECOP(X,H,P,IT,TE,S)
      IT=3
      CALL VECOP(TE,H,P,IT,R1,S)
      B=S+R
      IT=2
      CALL VECOP(X,H,P,IT,K,S)
      DO 100 I=1,8
  100 K(I)=K(I)/B
C
C     UPDATE ESTIMATES
C
      IT=3
      CALL VECOP(H,X,P,IT,TE,S)
      RR=Z(II)-S
C
C     CHECK RESIDUALS
C
      IF(II.LT.IEND) GO TO 305
      RRR=ABS(RR)
      IF(RRR.LT.AGC) GO TO 305
      IFLAG=1
      GO TO 304
```

```
  305 CONTINUE
      DO 90 J=1,8
      K(J)=K(J)*RR
      X(J)=X(J)+K(J)
   90 K(J)=K(J)/RR
      DO 160 I=1,8
      DO 160 J=1,8
  160 ET(I,J)=-K(I)*H(J)
      DO 170 I=1,8
  170 ET(I,I)=ET(I,I)+1.
      CALL MULT(ET,P,V)
      DO 171 I=1,8
      DO 171 J=1,8
  171 P(I,J)=(V(I,J)+V(J,I))/2.
  304 CONTINUE
      ES=X(7)
      ER(II)=DR(II)-ES
      IF(II.LT.217) GO TO 400
      LL=II-216
      JJ=II-6
      FE(LL)=(ER(II)-ER(JJ))/7.2E9
  400 CONTINUE
C
C     PRINT OUT RESULTS
C
C
C     PRINT OUT EVERY SIXTH POINT
C
      ICHK=II/6
      IL=II-6*ICHK
      IF(IL.NE.0) GO TO 401
      WRITE(6,85)
   85 FORMAT('-',23X,'GAIN',10X,'ESTIMATE X',10X,'ESTIMATED DRIFT',
     *10X,'ACTUAL DRIFT',10X,'ERROR'/)
      WRITE(6,86) K(1),X(1),ES,DR(II),ER(II)
```

```
 86 FORMAT('-','1   ',13X,E16.6,5X,E16.6,7X,E16.6,7X,E16.6,8X,E16.6)
    DO 180 I=2,8
    WRITE(6,27) I,K(I),X(I)
 27 FORMAT(' ',I1,15X,E16.6,5X,E16.6)
180 CONTINUE
    WRITE(6,28)
 28 FORMAT('-',62X,'P-MATRIX'/'-',8X,'1',15X,'2',15X,'3',15X,'4',
   *15X,'5',15X,'6',15X,'7',15X,'8'/)
    DO 190 I=1,8
    WRITE(6,16) I,(P(I,J),J=1,8)
190 CONTINUE
    WRITE(6,301) II,Z(II)
301 FORMAT('-',41X,'ITERATION=',I4,10X,'MEASUREMENT=',F10.3,'USEC')
    IF(IFLAG.NE.1) GO TO 302
    WRITE(6,303)
303 FORMAT('-',58X,'TRIVIALLY UPDATED')
302 CONTINUE
    IFLAG=0
    IF(II.LE.1080) GO TO 401
    LL=II-1080
    WRITE(6,402) FE(LL)
402 FORMAT('-',44X,'FRACTIONAL FREQUENCY ERROR=',E16.6)
401 CONTINUE
C
C   PROJECT AHEAD
C
    IT=2
    CALL VECOP(X,X,PHI,IT,TE,S)
    DO 200 I=1,8
200 X(I)=TE(I)
    CALL MULT(PHI,P,V)
    DO 210 I=1,8
    DO 210 J=1,8
210 ET(I,J)=PHI(J,I)
    CALL MULT(V,ET,EE)
```

```
      DO 220 I=1,8
      DO 220 J=1,8
  220 P(I,J)=EE(I,J)+Q(I,J)
   80 CONTINUE
C
C     PLOT ERROR
C
      N=360
      XSIZE=8.
      XSF=45.
      XMIN=0.
      YSIZE=6.5
      YSF=0.
      YMIN=-35.
      MODE=2
      ISYM=0
      DO 230 I=1,360
  230 XX(I)=FLOAT(I-1)
      IF(ID.NE.1) GO TO 240
      CALL GRAPH(N,XX,ER,ISYM,MODE,XSIZE,YSIZE,XSF,XMIN,YSF,YMIN,
     *'TIME (20 MIN);','TIME ERROR (USEC);','EXPERIMENT 1;',' ;')
  240 CONTINUE
      IF(ID.NE.2) GO TO 250
      CALL GRAPH(N,XX,ER,ISYM,MODE,XSIZE,YSIZE,XSF,XMIN,YSF,YMIN,
     *'TIME (20 MIN);','TIME ERROR (USEC);','EXPERIMENT 2;',' ;')
  250 CONTINUE
      IF(ID.NE.3) GO TO 260
      CALL GRAPH(N,XX,ER,ISYM,MODE,XSIZE,YSIZE,XSF,XMIN,YSF,YMIN,
     *'TIME (20 MIN);','TIME ERROR (USEC);','EXPERIMENT 3;',' ;')
  260 CONTINUE
      IF(ID.NE.4) GO TO 270
      CALL GRAPH(N,XX,ER,ISYM,MODE,XSIZE,YSIZE,XSF,XMIN,YSF,YMIN,
     *'TIME (20 MIN);','TIME ERROR (USEC);','EXPERIMENT 4;',' ;')
  270 CONTINUE
      IF(ID.NE.5) GO TO 280
```

```
      CALL GRAPH(N,XX,ER,ISYM,MODE,XSIZE,YSIZE,XSF,XMIN,YSF,YMIN,
     *'TIME (20 MIN);','TIME ERROR (USEC);','EXPERIMENT 5;',' ;')
  280 CONTINUE
      N=144
      XSF=18.
      CALL GRAPH(N,XX,FE,ISYM,MODE,XSIZE,YSIZE,XSF,XMIN,YSF,YMIN,
     *'TIME (20 MIN.);','FREQ. ERROR (DLESS);',' ;',' ;')
C
C     ERROR ANALYSIS
C
      SUM1=0.
      SUM2=0.
      DO 290 I=1,360
      SUM1=SUM1+ER(I)/360.
  290 SUM2=SUM2+ER(I)**2/360.
      STD=SQRT(SUM2-SUM1**2)
      WRITE(6,29) SUM1,STD
   29 FORMAT('1',10X,'OVERALL AVERAGE=',E16.6,' USEC',10X,'RMS=',E16.6,
     *' USEC')
      SUM1=0.
      SUM2=0.
      M=217
      DO 300 I=M,360
      SUM1=SUM1+ER(I)/144.
  300 SUM2=SUM2+ER(I)**2/144.
      STD=SQRT(SUM2-SUM1**2)
      WRITE(6,31) SUM1,STD
   31 FORMAT('-',10X,'STEADY STATE AVERAGE=',E16.6,' USEC',10X,'RMS=',
     *E16.6,' USEC')
      SUM1=0.
      SUM2=0.
      DO 403 I=1,144
      SUM1=SUM1+FE(I)/144.
  403 SUM2=SUM2+FE(I)**2/144.
      STD=SQRT(SUM2-SUM1**2)
```

```
      WRITE(6,404) SUM1,STD
  404 FORMAT('-',45X,'FRACTIONAL FREQUENCY ERROR (DIMENSIONLESS)'/
     *'-',41X,'AVERAGE=',E16.6,10X,'RMS=',E16.6)
      STOP
      END
      SUBROUTINE VECOP(V,H,P,IT,TE,S)
      DIMENSION V(8),H(8),P(8,8),TE(8)
      DO 70 I=1,8
   70 TE(I)=0.
      S=0.
      IF(IT.NE.1) GO TO 20
      DO 10 I=1,8
      DO 10 J=1,8
   10 TE(I)=TE(I)+P(J,I)*H(J)
   20 CONTINUE
      IF(IT.NE.2) GO TO 40
      DO 30 I=1,8
      DO 30 J=1,8
   30 TE(I)=TE(I)+P(I,J)*H(J)
   40 CONTINUE
      IF(IT.NE.3) GO TO 60
      DO 50 I=1,8
   50 S=S+V(I)*H(I)
   60 CONTINUE
      RETURN
      END
      SUBROUTINE MULT(A,B,C)
      DIMENSION A(8,8),B(8,8),C(8,8)
      DO 20 I=1,8
      DO 20 J=1,8
   20 C(I,J)=0.
      DO 10 I=1,8
      DO 10 J=1,8
      DO 10 L=1,8
   10 C(I,J)=C(I,J)+A(I,L)*B(L,J)
```

```
      RETURN
      END
      SUBROUTINE PARM(X,P,H,PHI,Q,R)
      DIMENSION X(8),P(8,8),H(8),PHI(8,8),Q(8,8)
      DO 10 I=1,8
      X(I)=0.
      H(I)=0.
      DO 10 J=1,8
      P(I,J)=0.
      PHI(I,J)=0.
   10 Q(I,J)=0.
C
C     INITIAL CCNDITIONS
C
C
C     SYSTEM MODEL
C
      H(1)=-1.
      H(2)=-1.
      H(4)=-1.
      H(7)=1.
      X(6)=-6.374784E-10
      PHI(6,6)=0.990054
      PHI(7,7)=1.
      PHI(7,6)=1.19E9
      PHI(2,2)=0.996197
      PHI(3,3)=0.996197
      PHI(2,3)=0.087129
      PHI(3,2)=-0.087129
      PHI(4,4)=0.9849
      PHI(5,5)=0.9849
      PHI(4,5)=0.173123
      PHI(5,4)=-0.173123
      R=0.
      Q(2,2)=0.100770
```

```
      Q(3,3)=Q(2,2)
      Q(4,4)=0.122090
      Q(5,5)=Q(4,4)
      Q(7,7)=.158
      Q(6,6)=1.519825E-21
      P(6,6)=7.678408E-20
      Q(1,1)=54.1612281
      PHI(1,1)=0.7497616
      P(1,1)=123.696
      P(5,5)=122.09
      P(4,4)=122.09
      P(3,3)=100.77
      P(2,2)=100.77
      RETURN
      END
//
```